APPLICATION OF SAR TECHNIQUES IN AN ULTRASOUND TESTBED

A THESIS SUBMITTED TO
THE GRADUATE SCHOOL OF NATURAL AND APPLIED SCIENCES
OF
MIDDLE EAST TECHNICAL UNIVERSITY

BY

GÜVEN SOLAK

IN PARTIAL FULFILLMENT OF THE REQUIREMENTS
FOR
THE DEGREE OF MASTER OF SCIENCE
IN
ELECTRICAL AND ELECTRONICS ENGINEERING

DECEMBER 2008

Approval of the thesis:

APPLICATION OF SAR TECHNIQUES IN AN ULTRASOUND TESTBED

submitted by **GÜVEN SOLAK** in partial fulfillment of the requirements for the degree of Master of Science in **Electrical and Electronics Engineering Department**, **Middle East Technical University** by,

Prof. Dr. Canan ÖZGEN _____
Dean, Graduate School of **Natural and Applied Sciences**

Prof. Dr. İsmet ERKMEN _____
Head of Department, **Electrical and Electronics Engineering**

Prof. Dr. Engin TUNCER _____
Supervisor, **Electrical and Electronics Engineering Dept., METU**

Examining Committee Members

Assoc. Prof. Dr. Özlem Aydın ÇİVİ _____
Electrical and Electronics Engineering Dept., METU

Prof. Dr. Engin TUNCER _____
Electrical and Electronics Engineering Dept., METU

Assist. Prof. Dr. Çağatay CANDAN _____
Electrical and Electronics Engineering Dept., METU

Assist. Prof. Dr. Afşar SARANLI _____
Electrical and Electronics Engineering Dept., METU

Güney ÖZKAYA (M.Sc.) _____
Senior Expert Engineer, ASELSAN

Date: (05.12.2008)

I hereby declare that all information in this document has been obtained and presented in accordance with academic rules and ethical conduct. I also declare that, as required by these rules and conduct, I have fully cited and referenced all material and results that are not original to this work.

Name, Last name : Güven Solak

Signature :

ABSTRACT

APPLICATION OF SAR TECHNIQUES IN AN ULTRASOUND TESTBED

SOLAK, Güven

M.Sc., Department of Electrical and Electronics Engineering

Supervisor: Prof. Dr. Engin TUNCER

December 2008, 101 pages

In this thesis, an ultrasound testbed is designed in order to practice the Synthetic Aperture Radar (SAR) techniques. The thesis work is built on the fundamentals of SAR theory. In this respect, four different methods for the reconstruction of SAR image are considered. The ultrasonic testbed is composed of a mobile vehicle where the ultrasound transmitter and receiver are mounted. An analog circuit is designed in order to condition the transmitted and received signals. The receiving signal is processed in a personal computer using MATLAB routines. A GUI is designed for user friendly operation. Different experiments are done with the designed system. The theoretical and practical results for SAR imaging are compared. It is shown that the designed system functions properly with a good approximation to the theoretical results. The deviations from the theoretical

results are caused by the idealistic assumptions as well as the distortions introduced by the practical system. More specifically, some of the distortions are generated by the nonuniform velocity of the moving platform, the phase distortion due to the analog filters and imperfect filtering during down-conversion. While the sources of distortions certainly affect the SAR system response, the implemented system is valuable for the practical analysis of SAR system performance.

Keywords: SAR, ultrasound, imaging, reconstruction

ÖZ

SAR TEKNİKLERİNİN ULTRASONİK TEST ORTAMINDA UYGULANMASI

SOLAK, Güven
Yüksek Lisans, Elektrik ve Elektronik Mühendisliği Bölümü
Tez Yöneticisi: Prof. Dr. Engin TUNCER

Aralık 2008, 101 sayfa

Bu tez çalışmasında, yapay açıklıklı radar (SAR) tekniklerinin sınanması için bir ultrasonik test ortamı tasarlanmıştır. Çalışma, SAR teorisinin temel ilkeleri üzerine kurulmuştur. Buna yönelik olarak dört farklı yeniden oluşturma algoritması kullanılmıştır. Test ortamı, ultrasonik verici ve alıcının yer aldığı hareketli bir araçtan oluşmaktadır. Ultrasonik verici ve alıcıyla bilgisayar arasındaki arayüzü sağlamak üzere bir analog devre tasarlanmıştır. İşaret işleme çalışmaları, MATLAB programı kullanılarak bir bilgisayar içerisinde gerçekleştirilmektedir. Kullanım kolaylığı sağlamak amacıyla bir kullanıcı arayüzü yazılımı tasarlanmıştır. Tasarlanan sistemle çeşitli deneyler yapılmıştır. SAR görüntü oluşturma konusunda, teorik ve pratik sonuçlar karşılaştırılmıştır.

Tasarlanan sistemin teorik sonuçlara yakın performansla çalıştığı gösterilmiştir. Teoriden sapmalar, teorinin kendisinin idealize edilmiş olmasından ve tasarlanan sistemin bir takım hatalara neden olmasından kaynaklanmaktadır. Hataların bir kısmı kullanılan aracın hızındaki değişimlerden, kullanılan analog filtrelerin işaret fazlarında bozulmaya yol açmasından ve frekans düşürme işlemi sırasındaki filtrelemeden kaynaklanmaktadır. Bahsedilen hata kaynakları sistem performansını doğrudan etkilese de, tasarlanan sistem SAR sistem performans analizine yönelik uygulamalar için yararlıdır.

Anahtar Kelimeler: SAR, ultrasonik, görüntüleme, yeniden oluşturma

ACKNOWLEDGMENTS

I would like to express my deepest sense of gratitude to my supervisor Prof. Dr. Engin TUNCER for his guidance and invaluable ideas.

I am deeply grateful to ASELSAN Inc. for providing tools and other facilities throughout this study.

I would like to forward my appreciation to all my friends and colleagues who contributed to my thesis with their continuous encouragement.

I would also like to thank my parents, Fatma and Sefer SOLAK and my brother, Serhat SOLAK for giving me encouragement during this thesis and all kind of supports during my whole education.

Finally, I have very special thanks for my lovely wife İlksen, for her endless love and patience during this thesis.

TABLE OF CONTENTS

LIST OF TABLES

LIST OF FIGURES

LIST OF ABBREVIATIONS

SAR	Synthetic Aperture Radar
I/O	Input/Output
PC	Personal Computer
DSP	Digital Signal Processing
IC	Integrated Circuit
ADC	Analog to Digital Converter
DAC	Digital to Analog Converter
TDC	Time Domain Correlation
US	Ultrasound
GUI	Graphical User Interface

CHAPTER 1

INTRODUCTION

Synthetic Aperture Radar is a well-known imaging technique for producing high spatial resolution representation of the reflectivity of Earth's surface. These high resolution images are obtained by illuminating the target region with radar signal radiation and processing the received echo [12]. In many environmental monitoring applications (topographic imaging of the surface of planets, underground resources exploration, mine detection, ground moving target detection and tracking), high resolution imaging capability which is independent of weather conditions is required [2]. As a complementary to optical imaging systems, Synthetic Aperture Radar (SAR) systems have the ability to view at night and through clouds [3]; SAR imaging method is independent of all natural processes.

The wide use of SAR in remote sensing applications is based on three main advantages [13]:

- Carrying its own illumination, radar can work well in darkness.
- The electromagnetic waves of common radar frequencies pass through clouds and precipitation without deterioration.
- Different scattering properties of materials to the radar energy provide a complementary and sometimes better discrimination of surface features than optical sensors.

SAR systems are based on the idea of synthesizing the effect of a large-aperture physical radar antenna, which is too difficult or impossible to construct [1]. There are many types of SAR systems classified according to radar look direction, sensor position, radar and target movement. Some of them are [13]:

Stripmap SAR: The antenna pointing direction is held constant while radar platform moves. Radar beam sweeps along the ground at a uniform rate.

Spotlight SAR: The antenna points to a spot on the ground in the center of the target area as the radar moves. This can be achieved by steering the beam gradually backwards as the radar passes the scene. The resolution is improved compared to Stripmap SAR but the final image is not continuous. Because the antenna must ultimately be steered forward again resulting gaps in the reconstructed image.

Scan SAR: This type of SAR is similar to Stripmap SAR. The only difference is that the antenna scans the range several times during a synthetic aperture.

Circular SAR: In this type of SAR system, the trajectory of the radar is not linear, while the radar look angle is perpendicular to moving direction as in Stripmap SAR. Radar carrying platform rotates around a spot in the ground.

Inverse SAR: The case that radar is stationary while the target is moving is called as the Inverse SAR.

Bistatic SAR: The SAR system in which the transmitter and receiver are located at different positions is the Bistatic SAR. In general the transmitter and receiver are approximately at the same position, which is referred as Monostatic SAR.

In this thesis, Monostatic Stripmap SAR will be implemented. The Stripmap SAR system requires a constant and known-speed mobile platform on top of which the radar is settled. In order to apply the theory, a low cost ultrasound testbed is designed and evaluated using SAR techniques. Using an ultrasound transmitter and receiver keeps the complete system to work in low frequencies, e.g., 40 kHz. This relatively low frequency of the system reduces the amount of processed data which results as lower computational cost. The system uses the analog front end of

an ordinary PC as an analog-to-digital and digital-to-analog converter. The ultrasound SAR system also requires analog circuits including analog multipliers, amplifiers, filters, sine-wave generator and power circuits. 40 kHz centered signal is generated and sampled using PC analog front end with the help of analog circuitry which is designed according to the technique known as 'heterodyning' [15]. The system structure mimics a real life high speed microwave SAR system with down-conversion and up-conversion processes performed in analog circuitry.

Using this testbed, many SAR techniques can be studied in a laboratory using a regular PC. One of the primary aims of this work is to evaluate the validity and usability of the testbed as an inexpensive and practical alternative to a real SAR system or simulation environments.

The organization of this thesis is as follows. In Chapter 2, Basics of SAR Theory are reviewed. Before examining Multidimensional SAR Systems, the related one dimensional applications, range and cross-range imaging problems are mentioned. The solution to Multidimensional SAR problem will be built on the results of one dimensional applications.

In Chapter 3, current SAR reconstruction algorithms are discussed in detail. Spatial Frequency Interpolation, Range Stacking, Time Domain Correlation and Backprojection algorithms are examined. Digital Spotlighting algorithm which is optionally used to focus on the target area is discussed.

Chapter 4 covers full design description of the ultrasound experimental setup used for Stripmap SAR applications. The design specifications and hardware resources are presented. The last section of the chapter includes the software which is composed of toolboxes with different functioning. Graphical user interface links the toolboxes to allow quick changes in the experiment parameters.

In Chapter 5, the used SAR techniques for identifying the location of the objects in the imaging scene are analyzed in several experimental scenarios. The steps of the reconstruction process are examined one by one in detail. The performance of the experimental setup is evaluated using spatial resolution characteristics.

Finally Chapter 6 concludes the thesis by summarizing the results of the study and highlighting the contributions made.

CHAPTER 2

BASICS OF SAR

2.1 1-D IMAGING PROBLEMS

2.1.1 RANGE IMAGING PROBLEM

The purpose of the range imaging problem is to identify the location of targets in a 1-D scene as seen in Figure2-1. The reflectivity of the targets may be varied (σ_n). The radar and the targets are located on the same line. When p(t) is the transmitted radar signal from the radar, the received echo from the target area is;

$$s(t) = \sum_n \sigma_n p(t - 2\frac{x_n}{c}) \tag{2.1}$$

In practice, the target reflectivity σ_n varies with the radar frequency ω and the target coordinates. The small frequency dependency will be neglected here. The amplitude function $\frac{1}{x_n}$, which is related to the wave divergence [11], is absorbed in σ_n.

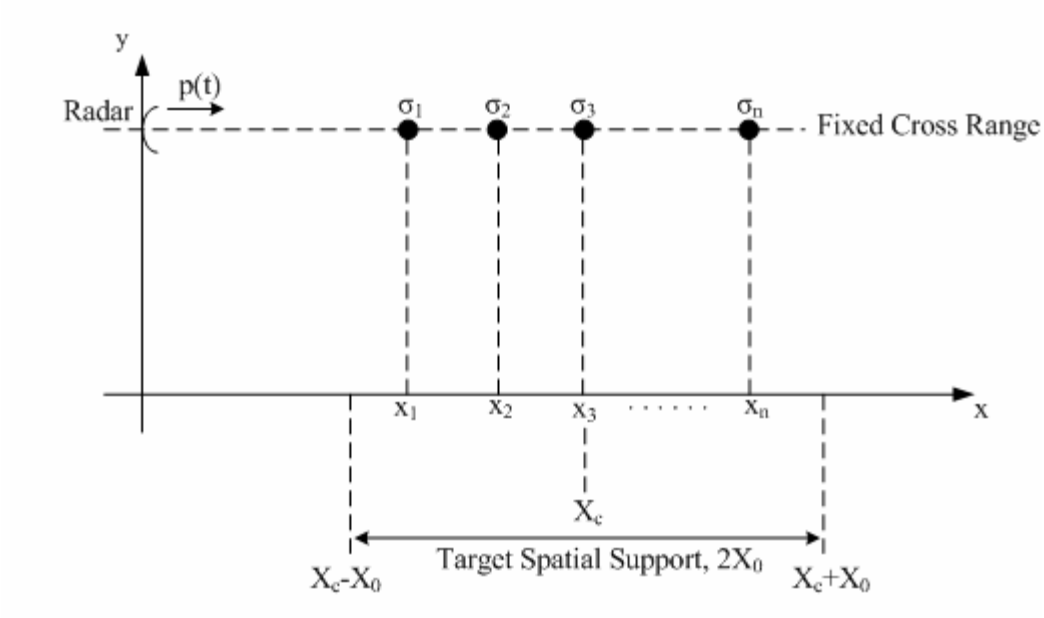

Figure2-1 Range Imaging Geometry [1]

If one intends to measure the range distance to the center X_c, rather than the x=0 point; then he should use x_n+X_c value as the distance to x=0 point.

Hence s(t) takes the form:

$$s(t) = \sum_n \sigma_n p(t - 2\frac{(x_n + X_c)}{c}) \tag{2.2}$$

The Fourier transform of the received signal s(t) is;

$$S(\omega) = P(\omega)\sum_n \sigma_n \exp(-j\omega 2\frac{(x_n + X_c)}{c}) . \tag{2.3}$$

Because p(t) is a band-limited signal, it is not possible to divide echoed signal spectrum to transmitted signal spectrum to find x_n values. In order to find a solution for x_n, the method called 'Matched Filtering' can be used [1].

Matched Filtering method is based on the idea of correlating the received signal with the transmitted signal. It will be more useful to use a shifted version of the transmitted signal in the correlation process to obtain a solution that takes into consideration the center of the target area X_c.

This shifted version of the transmitted signal or reference echo signal is taken to be,

$$s_0(t) = p(t - 2\frac{X_c}{c}), \tag{2.4}$$

and the baseband version,

$$s_{0b}(t) = s_0(t)\exp(-j\omega_c t) = p(t - 2\frac{X_c}{c})\exp(-j\omega_c t) \tag{2.5}$$

where ω_c is the carrier frequency of p(t). The Fourier transform of the baseband reference echo signal is,

$$S_{0b}(\omega) = S_0(\omega + \omega_c) = P(\omega + \omega_c)\exp(-j(\omega + \omega_c)2\frac{X_c}{c}) \tag{2.6}$$

Similarly the baseband version of the received signal s(t) is,

$$s_b(t) = s(t)\exp(-j\omega_c t) = \sum_n \sigma_n p(t - 2\frac{(x_n + X_c)}{c})\exp(-j\omega_c t), \tag{2.7}$$

and the frequency spectrum,

$$S_b(\omega) = S(\omega + \omega_c) = P(\omega + \omega_c)\sum_n \sigma_n \exp(-j(\omega + \omega_c)2\frac{(x_n + X_c)}{c}). \tag{2.8}$$

Therefore the matched filtered signal in time domain is,

$$s_{Mb}(t) = s_b(t) * s_{0b}(-t) = F^{-1}_{(\omega)}\left[S_b(\omega)S^*_{0b}(\omega)\right], \tag{2.9}$$

and the frequency spectrum,

$$\begin{aligned} S_{Mb}(\omega) &= S_b(\omega)S^*_{0b}(\omega) \\ &= P(\omega + \omega_c)\sum_n \sigma_n \exp(-j(\omega + \omega_c)2\frac{(x_n + X_c)}{c}) \\ &\qquad P^*(\omega + \omega_c)\exp(+j(\omega + \omega_c)2\frac{X_c}{c}) \end{aligned}$$

$$= \left|P(\omega+\omega_c)\right|^2 \sum_n \sigma_n \exp(-j(\omega+\omega_c)2\frac{x_n}{c}) . \tag{2.10}$$

In general p(t) is a linear frequency modulated (chirp) signal;

$$p(t) = a(t)\exp(j\beta t + j\alpha t^2) , \tag{2.11}$$

where $a(t) = 1$ for $0 \le t \le T_p$ and zero otherwise.

The instantaneous frequency of the chirp for $0 \le t \le T_p$ is;

$$\frac{d}{dt}(\beta t + \alpha t^2) = \beta + 2\alpha t . \tag{2.12}$$

The carrier frequency stands at the middle point of the frequency interval of

$$[\ \beta,\ \beta + 2\alpha T_p\ ].$$

$$\omega_c = \beta + \alpha T_p \tag{2.13}$$

If $2\omega_0$ is the baseband bandwidth of the transmitted signal p(t) then,

$$\alpha T_p = \omega_0 . \tag{2.14}$$

The baseband version of the transmitted signal p(t) is,

$$\begin{aligned} p_b(t) &= p(t)\exp(-j\omega_c t) = a(t)\exp(j(\beta-\omega_c)t + j\alpha t^2) \\ &= a(t)\exp(-j\omega_0 t + j\alpha t^2) \end{aligned} \tag{2.15}$$

It is necessary to examine the spectrum of this baseband chirp signal in order to better understand the matched filtered signal spectrum of (2.10).

Define $c(t) = a_c(t)\exp(j\alpha t^2)$, (2.16)

$a_c(t) = 1$ for $-T_p/2 \le t \le T_p/2$ and zero otherwise.

The spectrum of c(t) is given as, [14]

$$C(\omega)=\exp(-j\frac{\omega^2 T_p}{4\omega_0})\sqrt{\frac{\pi T_p}{2\omega_0}}\left\{K\left[\frac{1}{2}\sqrt{\frac{T_p}{\omega_0}}(\omega_0-\omega)\right]+K\left[\frac{1}{2\pi}\sqrt{\frac{\omega_0}{T_p}}(\omega_0+\omega)\right]\right\}$$

where $K(x)=M(x)+jS(x)$,

$$M(x)=\frac{2}{\sqrt{2\pi}}\int_0^x\cos(t^2)dt,\quad S(x)=\frac{2}{\sqrt{2\pi}}\int_0^x\sin(t^2)dt\,. \tag{2.17}$$

Merging expression 2.15 and 2.16;

$$\begin{aligned}p_b(t)&=c(t-T_p/2)\exp(-j\alpha(t-T_p/2)^2)\exp(-j\omega_0 t)\exp(j\alpha t^2)\\&=c(t-T_p/2)\exp(-j\omega_0 T_p/4)\end{aligned} \tag{2.18}$$

and the Fourier domain representation will be:

$$P(\omega+\omega_c)=P_b(\omega)=C(\omega)\exp(-j\omega T_p/2)\exp(-j\omega_0 T_p/4) \tag{2.19}$$

$$\left|P(\omega+\omega_c)\right|^2=\left|P_b(\omega)\right|^2=\left|C(\omega)\right|^2 \tag{2.20}$$

For the values given below;

$$T_p=3ms,\ f_c=40kHz$$

$\left|P_b(\omega)\right|^2$ and $F_{(\omega)}^{-1}\left\{\left|P_b(\omega)\right|^2\right\}$ can be seen in Figure2-2 and Figure2-3 respectively.

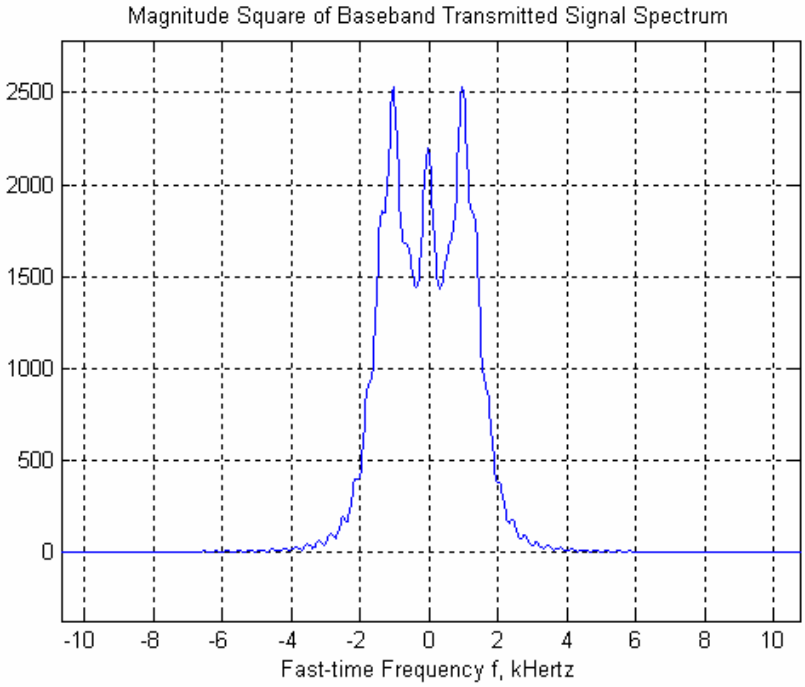

Figure2-2 Magnitude Square of Baseband Transmitted Signal Spectrum

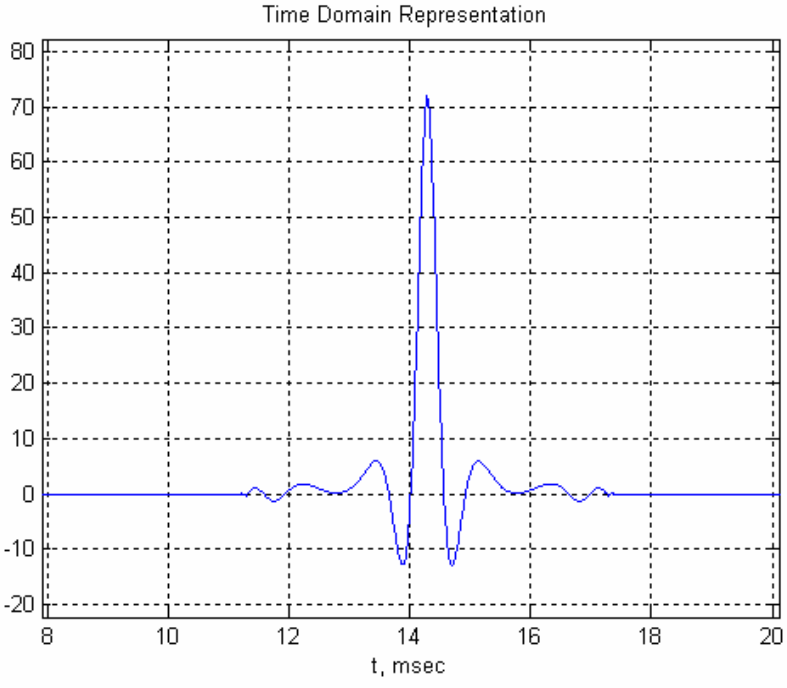

Figure2-3 Time Domain Representation

$F_{(\omega)}^{-1}\left\{\left|P_b(\omega)\right|^2\right\}$ seems like a sinc function. This is not a surprised result in the sense that, $\left|P_b(\omega)\right|^2$, which is seen in Figure2-2 has approximately a rectangular shape. Hence let us call $F_{(\omega)}^{-1}\left\{\left|P_b(\omega)\right|^2\right\}$ as point spread function of the range imaging system;

$$psf_t(t) = F_{(\omega)}^{-1}\left\{\left|P_b(\omega)\right|^2\right\}. \tag{2.21}$$

Rewrite expression (2.10) as,

$$S_{Mb}(\omega) = \left|P_b(\omega)\right|^2 \sum_n \sigma_n \exp(-j\omega t_n)\exp(-j\omega_c t_n) \tag{2.22}$$

where t_n represents the time delay caused by the n^{th} target;

$$t_n = 2x_n / c\,. \tag{2.23}$$

After inverse Fourier transformation;

$$s_{Mb}(t) = \sum_n \sigma_n psf_t(t - t_n)\exp(-j\omega_c t_n)\,. \tag{2.24}$$

Expression (2.24) can be rewritten using range domain instead of time domain by taking,

$$t = 2x / c\,. \tag{2.25}$$

The output is the target reflectivity function that we need to obtain;

$$f(x) = s_{Mb}(2x/c) = \sum_n \sigma_n psf(x - x_n)\exp(-j\omega_c t_n) \tag{2.26}$$

The complete range imaging reconstruction scenario can be seen in Figure2-4.

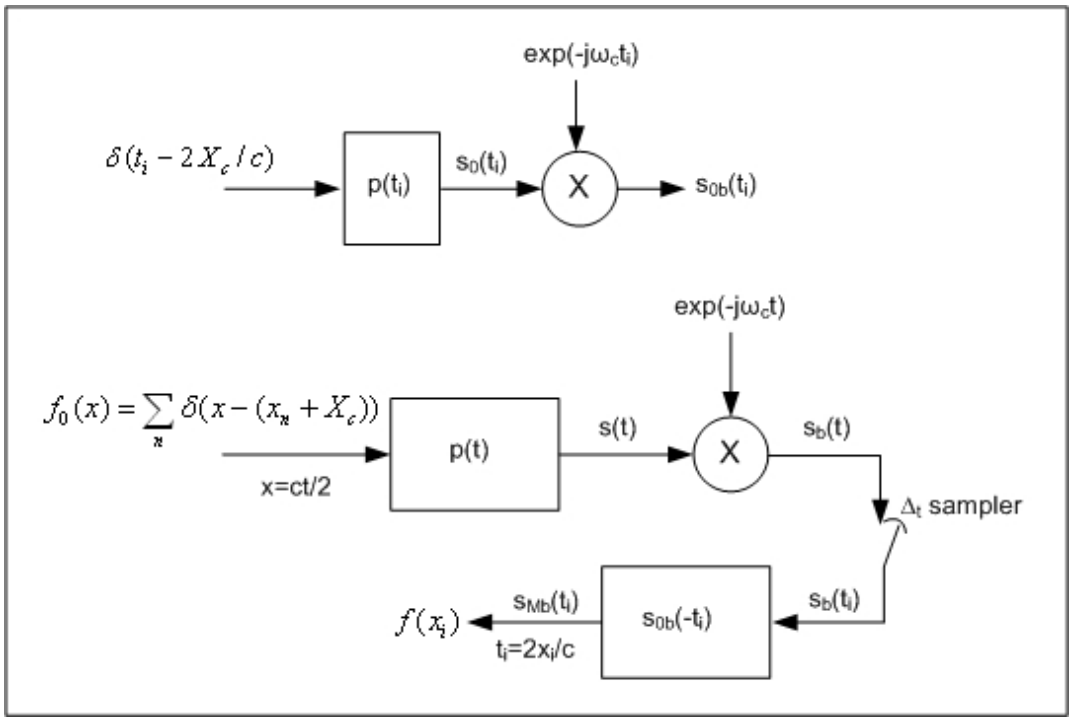

Figure2-4 Block Diagram of Range Imaging System [1]

Sampling Rate

In order to use a minimum sampling rate, it is preferred to work with the baseband received signal $s_b(t)$ having a $2\omega_0$ bandwidth ($\pm\omega_0$). The echoed signal s(t) should be converted into baseband at the hardware. This signal is then suitable for A/D conversion.

From Nyquist sampling rate theorem, the sampling interval should be

$$\Delta_t \le \frac{2\pi}{2\omega_0} = \frac{\pi}{\omega_0}. \tag{2.27}$$

Range Resolution

From Figure2-2 and Figure2-3, it can be seen that $psf_t(t)$ is a sinc like function. If $|P_b(\omega)|^2$ were a perfect rectangle, e.g. $|P_b(\omega)| = 1$ for $-\omega_0<\omega<\omega_0$, then

$$psf_t(t) = \Omega \operatorname{sinc}\left(\frac{1}{2\pi}\Omega t\right) \tag{2.28}$$

where $\Omega = 2\omega_0$ is the bandwidth of $\left|P_b(\omega)\right|^2$.

If we look at the range domain,

$$psf(x) = \Omega \operatorname{sinc}\left(\frac{1}{2\pi}\Omega\frac{2x}{c}\right) = \Omega \operatorname{sinc}\left(\frac{1}{2\pi}\frac{4\omega_0}{c}x\right). \tag{2.29}$$

Then the range resolution will be,

$$\Delta_x = \frac{2\pi}{4\omega_0 / c} = \frac{c\pi}{2\omega_0}. \tag{2.30}$$

2.1.2 CROSS-RANGE IMAGING PROBLEM

The purpose of cross-range imaging system is to identify the location and the reflectivity of the objects in a fixed and known range. In this case radar movement along the synthetic aperture is required as seen in Figure2-5.

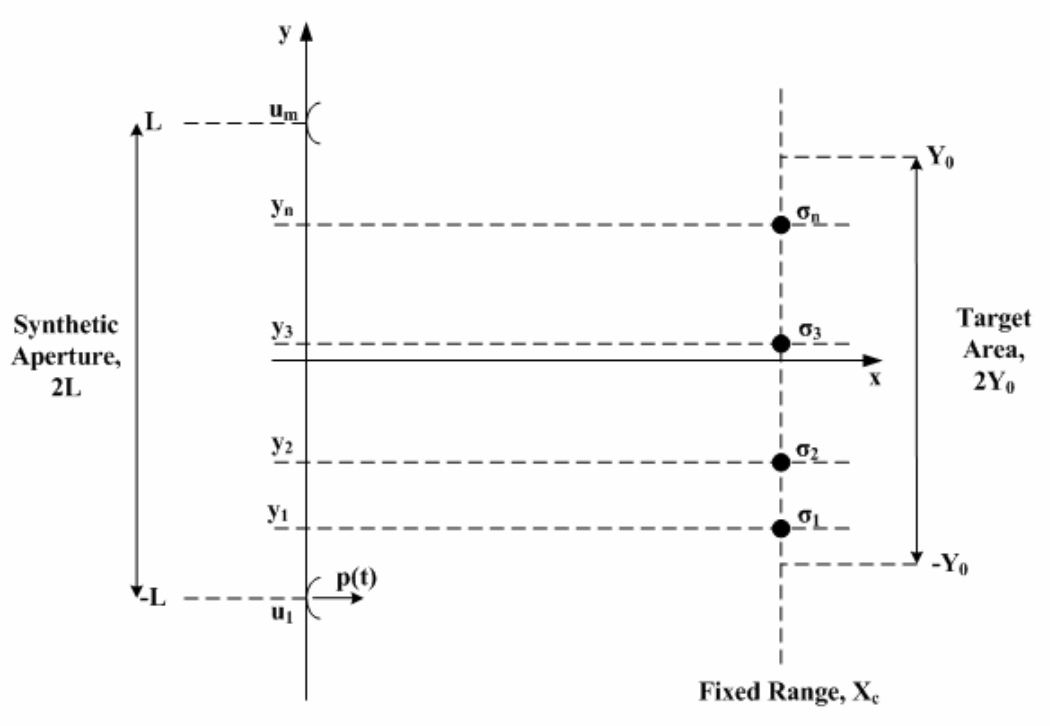

Figure2-5 Cross-Range Imaging Geometry [1]

First, define an ideal target function in the cross range domain,

$$f_0(y) = \sum_n \sigma_n \delta(y - y_n), \tag{2.31}$$

and its Fourier transform,

$$F_0(k_y) = \sum_n \sigma_n \exp(-jk_y y_n) \tag{2.32}$$

where σ_n is the frequency independent target reflectivity and y_n is the cross-range coordinate of the n^{th} target. The objective will be to obtain a result as close as to the ideal function.

In order to solve cross-range imaging problem, there is no need to use wide-bandwidth radar signal [1]. Using a pure sinusoid, $p(t) = \exp(j\omega t)$, 1-D cross-range image can be formed.

The echoed signal from the n targets in the target area is;

$$s(t,u) = \sum_n \sigma_n p\left[t - 2\frac{\sqrt{x_n{}^2 + (y_n - u)^2}}{c} \right], \qquad (x_n = X_c)$$

$$= \exp(j\omega t)\sum_n \sigma_n \exp\left[- j2k\sqrt{X_c{}^2 + (y_n - u)^2} \right] \tag{2.33}$$

where $k = \frac{\omega}{c}$ is the wavenumber, u is the position of the radar.

It is obvious that baseband echoed signal does not depend on t, depends on only u. By using (2.33), the baseband echo can be written as;

$$s_b(t,u) = s(t,u)\exp(-j\omega t) = \sum_n \sigma_n \exp\left[- j2k\sqrt{X_c{}^2 + (y_n - u)^2} \right].$$

$$\Rightarrow s(u) = \sum_n \sigma_n \exp\left[- j2k\sqrt{X_c{}^2 + (y_n - u)^2} \right] \tag{2.34}$$

By defining the reference echoed signal as echoed signal from a unit reflector in the midpoint of the target area, e.g $y_n = 0$;

$$s_0(t,u) = p\left[t - 2\frac{\sqrt{X_c{}^2 + u^2}}{c} \right], \tag{2.35}$$

and in the frequency domain;

$$s_0(\omega,u) = \exp\left[- j\omega 2\frac{\sqrt{X_c{}^2 + u^2}}{c} \right] = \exp\left[- j2k\sqrt{X_c{}^2 + u^2} \right]. \tag{2.36}$$

Expression (2.36) depends on only u; ω variable was taken to be constant. Hence rewrite (2.36) as:

$$s_0(u) = \exp\left[- j2k\sqrt{X_c{}^2 + u^2} \right] \tag{2.37}$$

The Matched filtered signal is defined as;

$$s_M(u) = s(u) \ * \ s_0^*(-u)\,, \tag{2.38}$$

and in the Fourier domain;

$$S_M(k_u) = S(k_u)S_0^*(k_u)\,. \tag{2.39}$$

Define range and cross-range domain variables as;

$$k_x = \sqrt{4k^2 - k_u^2}\,, \quad k_y = k_u\,. \tag{2.40}$$

The Fourier domain representations of $s(u)$ and $s_0(u)$ are given below [1];

$$S(k_u) = \exp(-j\pi/4)\sum_n \sigma_n I_n(k_y)\exp\left(-jk_x X_c - jk_y y_n\right) \tag{2.41}$$

where

$$I_n(k_u) = \begin{cases} 1, & if\ k_u \in \left[2k\sin\left(\theta_n(L)\right),\ 2k\sin\left(\theta_n(-L)\right)\right] \\ 0, & otherwise \end{cases}, \tag{2.42}$$

$$\theta_n(u) = \arctan\left\{\frac{y_n - u}{X_c}\right\} \tag{2.43}$$

and L is the synthetic aperture half length, e.g. $u \in \left[-L,\ L\right]$,

$$S_0(k_u) = \begin{cases} \exp(-j\pi/4)\exp\left(-jk_x X_c\right), & if\ k_u \in \left[-2k,\ 2k\right] \\ 0, & otherwise \end{cases} \tag{2.44}$$

Therefore the matched filtered echoed signal spectrum can be found using expressions (2.39), (2.40), (2.41) and (2.44) as:

$$S_M(k_y) = \exp(-j\pi/4)\sum_n \sigma_n I_n(k_y)\exp\left(-jk_x X_c - jk_y y_n\right)$$
$$\exp(+j\pi/4) I_n(k_y)\exp\left(+jk_x X_c\right)$$

$$S_M(k_y) = \sum_n \sigma_n I_n(k_y)\exp\left(-jk_y y_n\right) \tag{2.45}$$

The inverse Fourier transform of (2.45) will give the final target reflectivity,

$$s_M(y) = \sum_n \sigma_n i_n(y - y_n) \tag{2.46}$$

where

$$i_n(y) = \Omega_n \exp(j\Omega_{nc} y)\text{sinc}\left(\frac{1}{2\pi}\Omega_n y\right) \quad [1]$$

and

$$\Omega_n = 2k\sin(\theta_n(-L)) - 2k\sin(\theta_n(-L))$$

$$\Omega_{nc} \approx 2k\sin(\theta_n(0))$$

The complete cross-range imaging system is given in Figure2-6.

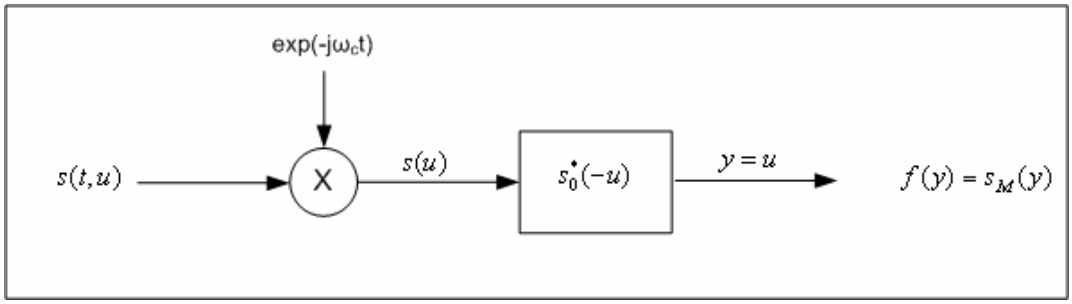

Figure2-6 Block Diagram of Cross-Range Imaging System [1]

The cross-range reconstructed image which is obtained by processing the real data echoed from the two objects in the target area recorded by the experimental setup designed in this thesis work is shown in Figure2-7.

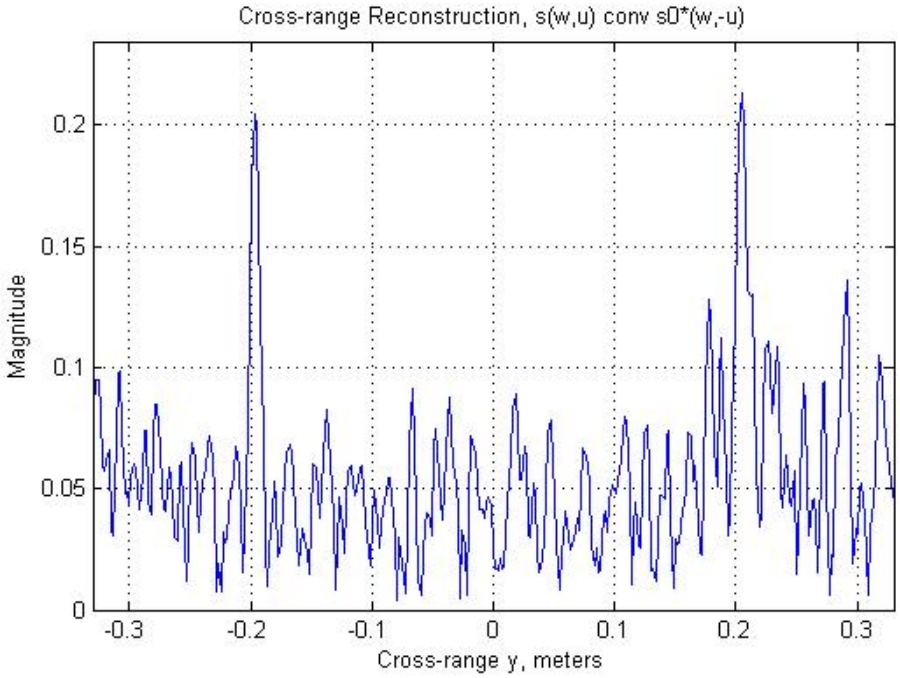

Figure2-7 Reconstructed Cross-Range Target Area

2.2 MULTIDIMENSIONAL SAR PROBLEM

The general Synthetic Aperture Radar (SAR) problem aims to obtain the reflection properties of a surface. Radar looks the target area by an angle from high altitudes. Therefore the study of Multidimensional SAR imaging should take into consideration three dimensions while combining the results of 1-D imaging problems. The procedure will be similar; surface reflectivity function will be obtained using the mathematical relationship between transmitted and received signals.

There are many types of Multidimensional SAR problems according to the movement of the radar and the radar look direction.

In this thesis Stripmap (or side-looking) SAR geometry, which is seen Figure2-8 will be studied. The details of the designed experimental setup will be given in Chapter 4. The application of SAR theory to the setup is given in Appendix A.

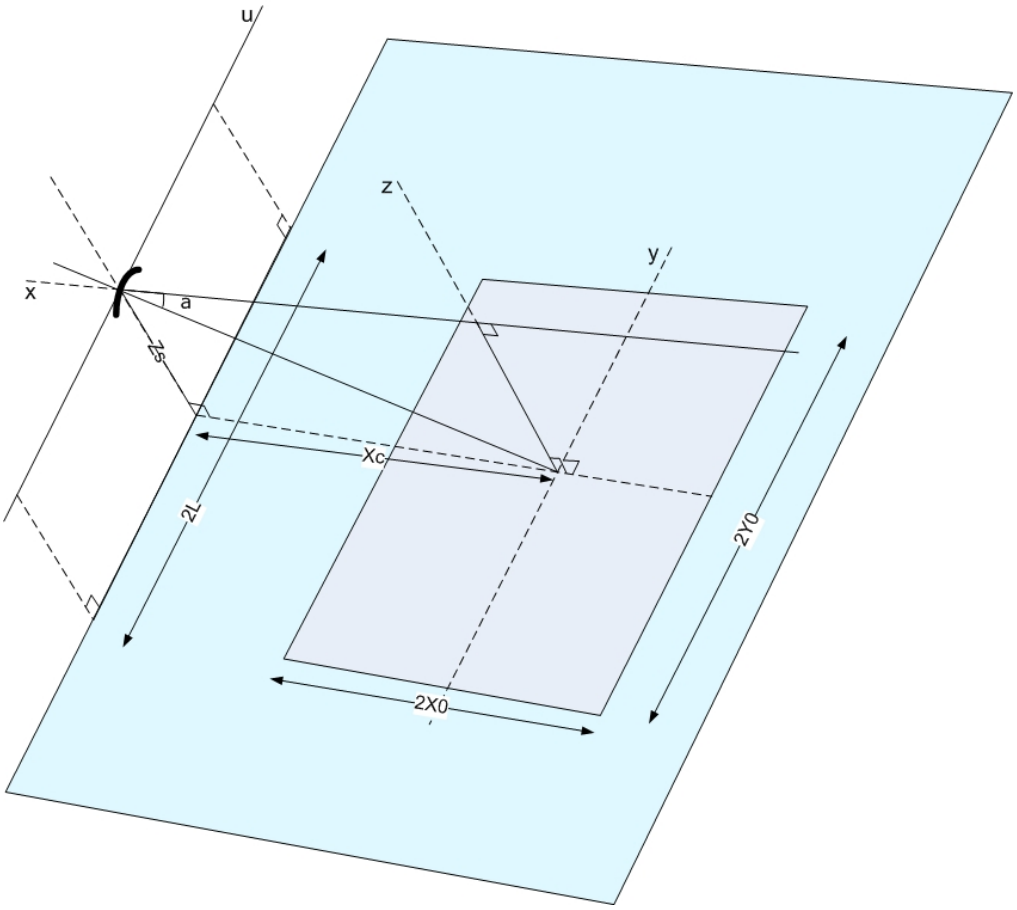

Figure2-8 Stripmap SAR Geometry, 3-D

In the figure, radar is mounted on a moving platform. The moving flight direction of the radar (u-axis) is referred as the azimuth or along-track direction. The used radar is assumed to be omni-directional point radar which does not exist in reality. In fact real beam angle properties of the sensors will be taken into consideration in the implementation of the algorithms.

The case that the center of radar path is aligned with center of target area (u=y) is referred as broadside target area. The application studied here will be for broadside target area.

x-axis is called as the range domain, the center of which is referred as X_c. Y_0 is the half size of the desired target area in cross-range domain. L is the half size of synthetic aperture where the radar moves along. Y_0 will be taken to be equal to L for the sake of simplicity in the application.

The object of SAR signal processing is to form a target region reflectivity function in the multidimensional spatial range, cross-range and altitude domains (x,y,z). In order to simplify the theory, the altitude is selected to be fixed, and $x_s = \sqrt{x^2 + Z_s^{\,2}}$ is referred as slant range.

In order to form an image, intensity measurements must be taken in two orthogonal directions [13]. In SAR theory, one dimension is parallel to the radar beam, as discussed in range imaging system, Section 2.2. The time delay of the received echo is proportional to the distance along the beam to the scatterer. Slant range to the ground range conversion is performed during the processing. The second dimension of the image is given with the movement of the radar itself. The radar system emits pulses of the electromagnetic (or accoustic) energy and receives the echoes to process.

When p(t) is the transmitted signal and s(t,u) is the received signal echoed from the target region;

$$s(t,u) = \sum_n \sigma_n p(t - t_n) \tag{2.47}$$

where,

$$t_n = \frac{2\sqrt{x_{sn}^2 + (y_n - u)^2}}{2}, \tag{2.48}$$

$$x_{sn} = \sqrt{(x_n + X_c)^2 + Z_s{}^2}\,, \tag{2.49}$$

(x_n+X_c,y_n) is the 2-D target coordinates of the n_{th} target, $(X_c,0)$ is the center of target region which can be seen in Figure2-8 and u is the position of the radar. As in the case of 1-D imaging problems, the amplitude term related to wave divergence [11] is absorbed in reflectivity constant σ_n in the above model.

It can be seen that, echoed signal is a function of both t and u. t represents fast time domain while u represents slow time domain. (u changes slowly compared to t as the radar carrying vehicle moves with constant low speeds compared to speed of sound.) The Fourier transform representation of slow time domain u is called as 'slow time Doppler domain', and notated as k_u.

Linear frequency modulated (chirp) signal is used as transmitted radar signal similar to range imaging problem given in equations (2.11) - (2.13).

$$p(t) = a(t)\exp(j\beta t + j\alpha t^2)\,, \tag{2.50}$$

where $a(t) = 1$ for $0 \le t \le T_p$ and zero otherwise.

Baseband received signal is,

$$s_b(t,u) = s(t,u)\exp(-j\omega_c t) \tag{2.51}$$

where ω_c is the carrier frequency of p(t),

$\omega_c = \beta + \omega_0$ and $\omega_0 = \alpha T_p$.

From expressions (2.47) and (2.51), baseband received signal is

$$s_b(t,u) = \sum_n \sigma_n p(t - t_n)\exp(-j\omega_c t)\,. \tag{2.52}$$

The fast time Fourier (ω,u) domain representation of received signal is

$$S(\omega,u) = F_{(t)}\{s(t,u)\} = P(\omega)\sum_n \sigma_n \exp(-j\omega t_n)\,, \tag{2.53}$$

and the corresponding baseband spectrum,

$$S_b(\omega,u) = F_{(t)}\{s_b(t,u)\} = P(\omega+\omega_c)\sum_n \sigma_n \exp\big(-j(\omega+\omega_c)t_n\big). \tag{2.54}$$

Define the reference echoed signal as;

$$s_0(t) = p(t-t_c) \tag{2.55}$$

where,

$$t_c = \frac{2x_{sc}}{c} \tag{2.56}$$

and

$x_{sc}^2 = X_c^{\,2} + Z_s^{\,2}$, $(x_n = 0, y_n = u)$.

Fast time Fourier domain representation is

$$S_0(\omega) = P(\omega)\exp(-j\omega t_c), \tag{2.57}$$

and the baseband version becomes

$$S_{0b}(\omega) = S_0(\omega+\omega_c) = P(\omega+\omega_c)\exp\big(-j(\omega+\omega_c)t_c\big) \tag{2.58}$$

The next step will be fast time matched filtering of the baseband received signal to the defined reference echo. The matched filtered signal will be

$$\begin{aligned} S_M(\omega,u) &= S_b(\omega,u)S_{0b}^*(\omega) \\ &= \sum_n \sigma_n P(\omega+\omega_c)\exp\big(-j(\omega+\omega_c)t_n\big)P^*(\omega+\omega_c)\exp\big(+j(\omega+\omega_c)t_c\big) \\ &= \big|P(\omega+\omega_c)\big|^2 \exp\big(+j(\omega+\omega_c)t_c\big)\sum_n \sigma_n \exp\big(-j(\omega+\omega_c)t_n\big) \end{aligned} \tag{2.59}$$

Define wavenumber sequence and wavenumber carrier as;

$$k = \frac{\omega}{c}, \quad k_c = \frac{\omega_c}{c}.$$

Wavenumber sequence centered at carrier is;

$$k_{\omega c} = k + k_c = \frac{\omega+\omega_c}{c}.$$

Rewrite expression (2.59) using (2.48) and inserting wavenumber into equation:

$$S_M(\omega,u) = \left|P(\omega+\omega_c)\right|^2 \exp\left(j(\omega+\omega_c)t_c\right). \sum_n \sigma_n \exp\left(-j2k_{\omega c}\sqrt{x_{sn}^2+(y_n-u)^2}\right) \tag{2.60}$$

Slow time domain representation of the fast time matched filtered signal $S_M(\omega,u)$ [1] is;

$$S_M(\omega,k_u) = \left|P(\omega+\omega_c)\right|^2 \exp\left(j(\omega+\omega_c)t_c\right)\exp(-j\pi/4) \sum_n \sigma_n I_n(\omega,k_u)\exp\left(-j\sqrt{4k_{\omega c}^2-k_u^2}\,x_{sn}-jk_u y_n\right) \tag{2.61}$$

where;

$$I_n(\omega,k_u) = \begin{cases} 1, & if\ k_u \in \left[2k_{\omega c}\sin\left(\theta_{sn}(L)\right),\ 2k_{\omega c}\sin\left(\theta_{sn}(-L)\right)\right] \\ 0, & otherwise \end{cases} \tag{2.62}$$

$$\theta_{sn}(u) = \arctan\left\{\frac{y_n-u}{x_{sn}}\right\}, \tag{2.63}$$

and L is the synthetic aperture half length, e.g. $u \in \left[-L,\ L\right]$.

Rewrite 2.2.15 using expression 2.1.1.15,

$$S_M(\omega,k_u) = \left|P_b(\omega)\right|^2 \exp\left(j(\omega+\omega_c)t_c\right)\exp(-j\pi/4) \sum_n \sigma_n I_n(\omega,k_u)\exp\left(-j\sqrt{4k_{\omega c}^2-k_u^2}\,x_{sn}-jk_u y_n\right) \tag{2.64}$$

where,

$P_b(\omega) = P(\omega+\omega_c)$ is the baseband transmitted signal with $2\omega_0$ bandwidth, e.g. $\omega \in \left[-\omega_0,\ \omega_0\right]$.

Define the range and cross-range domain frequency representations as;

$$k_x(\omega,k_u) = \sqrt{4k_{\omega c}^2-k_u^2}, \quad k_y(\omega,k_u) = k_u. \tag{2.65}$$

One more step is required for the fast time matched filtered signal spectrum;

$$(\omega+\omega_c)t_c = 2\frac{(\omega+\omega_c)}{c}x_{sc} = 2k_{\omega c}x_{sc}\,.$$

If we combine (2.64) and (2.65),

$$S_M\left(k_x(\omega,k_u),k_y(\omega,k_u)\right) = \left|P_b(\omega)\right|^2 \exp\left(j2k_{\omega c}x_{sc}\right)\exp(-j\pi/4) \sum_n \sigma_n I_n(\omega,k_y)\exp\left(-jk_x x_{sn} - jk_y y_n\right) \tag{2.66}$$

At this point, a different matched filter, namely 2-D matched filter, will be used to discard unnecessary parts of the fast time matched filtered signal.

$$S_0(\omega) = \exp\left(-j\pi/4\right)\exp\left(j2k_{\omega c}x_{sc}\right) \tag{2.67}$$

2-D matched filtered signal spectrum is;

$$F_{SM}\left(k_x(\omega,k_u),k_y(\omega,k_u)\right) = S_M\left(k_x(\omega,k_u),k_y(\omega,k_u)\right)S_0^*(w) = \left|P_b(\omega)\right|^2\sum_n \sigma_n I_n(\omega,k_y)\exp\left(-jk_x x_{sn} - jk_y y_n\right). \tag{2.68}$$

Target reflectivity function is the spatial domain (x,y) representation of the matched filtered signal as given in the following,

$$f(x,y) = F_{k_x,k_y}^{-1}\left\{F_{SM}\left(k_x(\omega,k_u),k_y(\omega,k_u)\right)\right\}. \tag{2.69}$$

It will be necessary to analyze the spectral support of 2D matched filtered signal spectrum, $F_{SM}\left(k_x,k_y\right)$, to find a solution for target reflectivity function .

Both $\left|P_b(\omega)\right|^2$ and $I_n(\omega,k_u)$ can be approximated by a rectangular shape. $\left|P_b(\omega)\right|^2$ is examined in Figure2-2.

For $I_n(\omega, k_u)$, using expression (2.62) and Figure2-9, the spectral support for k_u can be found out to be changed for different targets. But this result is because of the fact that the used radar is assumed to be an omni-directional point radar.

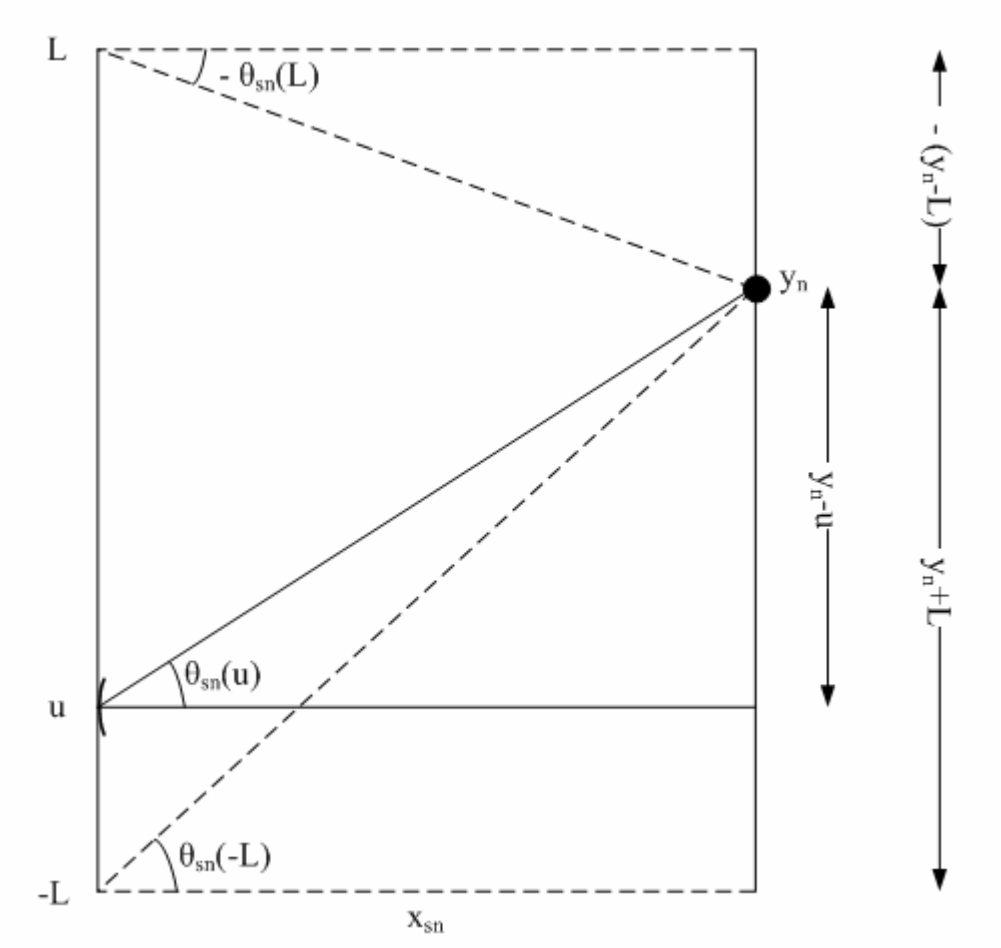

Figure2-9 Aperture Angle

In the application of this thesis work, the ultrasound transmitter and receiver cannot totally be considered as perfect point radar. If the radiation pattern shown in Figure4-4 in Chapter 4 is examined, it can be understood that the power of sensors are concentrated on a limited region, $\pm\varphi_d$. (e.g. $\varphi_d=\pi/6$)

Therefore the expression for $I_n(\omega, k_u)$ is approximated as,

$$I_n(\omega, k_u) = \begin{cases} 1, & if\ k_u \in [-2k_{\omega c} \sin\varphi_d,\ 2k_{\omega c} \sin\varphi_d] \\ 0, & otherwise \end{cases}$$

where φ_d is the beam angle of the radar.

Hence the spectral support of $|P_b(\omega)|^2 I_n(\omega, k_u)$ for both ω and k_u domains can be displayed as in Figure2-10.

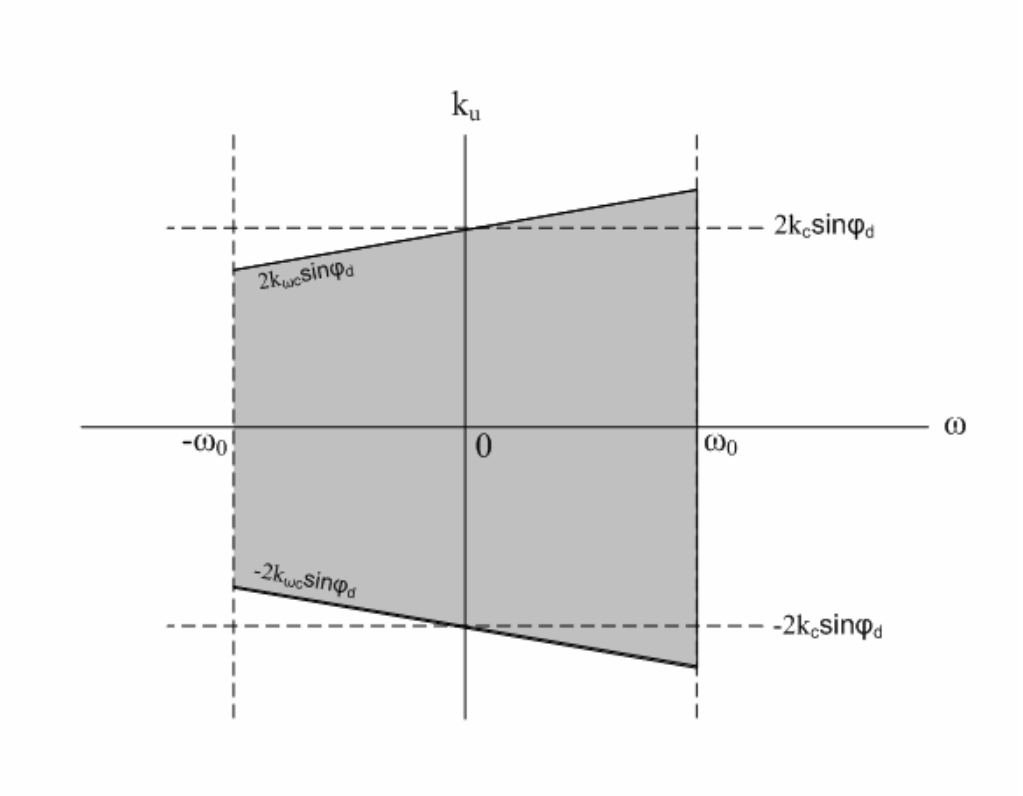

Figure2-10 Spectral Support in k_u-ω Domain

Wavenumber centered at carrier is,

$$k_{\omega c} = k + k_c = \frac{\omega + \omega_c}{c}.$$

Therefore using a narrowband system, $\frac{\omega_c + \omega_0}{\omega_c} \approx 1 \approx \frac{\omega_c - \omega_0}{\omega_c}$, the support region in k_u-ω domain can be handled as a rectangle. As the bandwidth of the system increases, the support region becomes a trapezoid.

In the real application of this thesis work, $\frac{\omega_c + \omega_0}{\omega_c} = \frac{40 + 2}{40}$. This value is close enough to 1 to treat the support region as a rectangle.

After the mapping to spatial k_x - k_y domain, the spectral support of the target region is given Figure2-11.

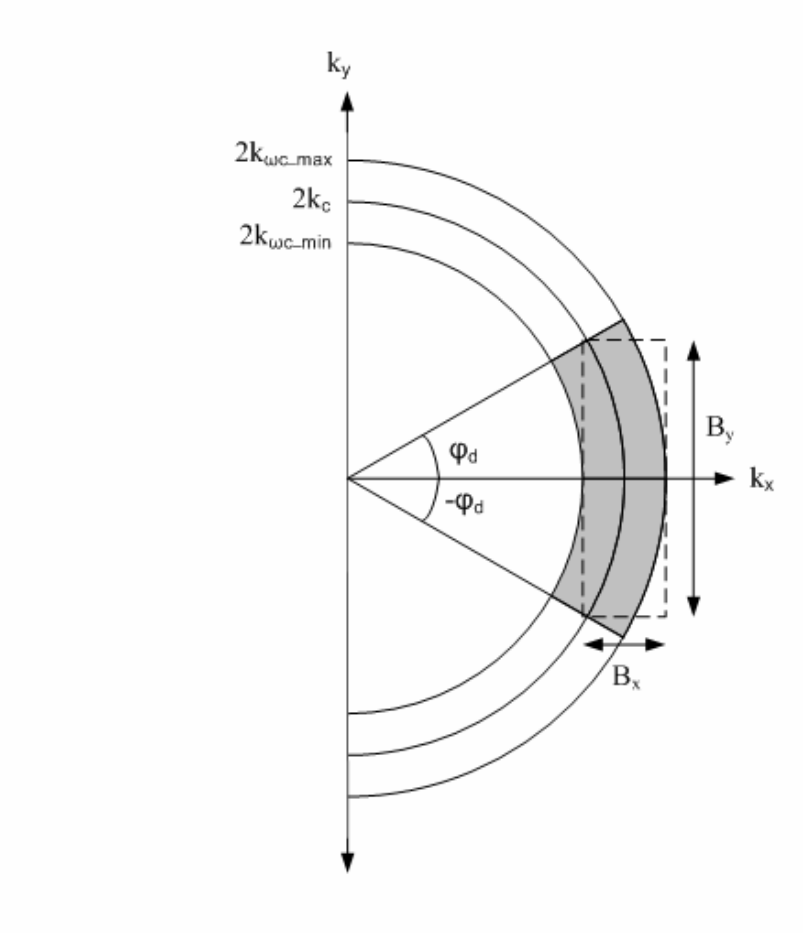

Figure2-11 Spectral Support in k_x - k_y Domain [1]

In Figure2-11, the variables are given as,

$$k_{\omega c\_\min} = k_c - \frac{\omega_0}{c}, \quad k_{\omega c\_\max} = k_c + \frac{\omega_0}{c}. \tag{2.70}$$

$$B_x = 2k_{\omega c\_\max} - 2k_{\omega c\_\min} = \frac{4\omega_0}{c} \tag{2.71}$$

$$B_y = 4k_c \sin\varphi_d \tag{2.72}$$

The inverse Fourier Transform of this approximately rectangular shape is basically separable sinc functions in x, y domains, namely,

$$F_{k_x,k_y}^{-1}\left\{\left|P_b(\omega)\right|^2 I_n(\omega,k_u)\right\} \quad (\text{for} \quad k_x(\omega,k_u)=\sqrt{4k_{\omega c}^2-k_u^2}, \quad k_y(\omega,k_u)=k_u)$$

$$= B_x \text{sinc}\left(\frac{1}{2\pi}B_x x\right) B_y \text{sinc}\left(\frac{1}{2\pi}B_y y\right) \tag{2.73}$$

In expression (2.73), a constant coefficient may be added to the right hand side of the equality which comes from $\left|P_b(\omega)\right|^2$. Here $\left|P_b(\omega)\right|^2 = 1, \ \ (\text{for} -\omega_0 \le \omega \le \omega_0)$.

Therefore, when we consider expression (2.68) and (2.69) again;

$$F_{SM}\left(k_x(\omega,k_u),k_y(\omega,k_u)\right) = \left|P_b(\omega)\right|^2 \sum_n \sigma_n I_n(\omega,k_y)\exp\left(-jk_x x_{sn} - jk_y y_n\right)$$

$$f(x,y) = F_{k_x,k_y}^{-1}\left\{F_{SM}\left(k_x(\omega,k_u),k_y(\omega,k_u)\right)\right\}$$

$$= B_x B_y \sum_n \sigma_n \ \text{sinc}\left(\frac{1}{2\pi}B_x(x-x_{sn})\right)\text{sinc}\left(\frac{1}{2\pi}B_y(y-y_n)\right). \tag{2.74}$$

The targets are seen at (x_{sn}, y_n) points in the (x_s, y) coordinate system. This slant range target positions should be mapped to (x,y) coordinate system using expression (2.49) with the following mapping;

$$x_n = \sqrt{x_{sn}^2 - Z_s^{\ 2}} - X_c. \tag{2.75}$$

Fast Time Sampling Rate

The same discussion in section 2.1.1 of range imaging problem is valid for fast time sampling rate of multidimensional SAR problem. From Nyquist sampling rate theorem, the sampling interval should be

$$\Delta_t \le \frac{2\pi}{2\omega_0} = \frac{\pi}{\omega_0}. \tag{2.76}$$

Time Gating

It has a critical importance to determine the time interval of sampling to increase the system performance. The sampling interval directly relates to the system geometry and duration of the transmitted pulse.

The recording operation should be started before initial portion of the echoed signal reaches the receiver. The minimum time that the signal arrives to the receiver should be taken as the starting time of sampling.

The recording operation should be stopped after the echoed signal from the distant point of the target region arrives at the receiver completely. The following values are used to restrict the time interval of sampling.

$$T_{start} = \frac{2r_{\min}}{c} = \frac{2\sqrt{(X_c - X_0)^2 + Z_s{}^2}}{c}$$

$$T_{final} = \frac{2r_{\max}}{c} + T_p = \frac{2\sqrt{(X_c + X_0)^2 + (Y_0 + L)^2 + Z_s{}^2}}{c} + T_p$$

Hence fast time gate is,

$t \in [\ T_{start}, T_{final}\ ]$.

Slow Time Sampling Rate

Slow time sampling rate is the number of points in the u domain that radar sends and receives signal.

2-D matched filtered signal spectrum in k_u domain is found to be limited in:

$k_u \in [-2k_{\omega c} \sin\varphi_d,\ 2k_{\omega c} \sin\varphi_d]$

Then sampling without aliasing requires that,

$$\Delta_u \le \frac{2\pi}{4k_{\omega c} \sin\varphi_d}.$$

Using the maximum value for $k_{\omega c}$ to limit the sampling interval more;

$$\Delta_u \le \frac{2\pi}{4\left(k_c + \frac{\omega_0}{c}\right)\sin\varphi_d} \text{ is obtained.} \qquad (2.77)$$

For typical values of;

$\varphi_d = \pi/6$, $f_c = 40kHz$, $f_0 = 2kHz$

$\Delta_u \le 4.05mm$

Spatial Resolution

There are different methods to find the spatial resolution characteristics of the system. Rayleigh criterion is an important tool that establishes a standard to characterize the Spatial Resolution of an imaging system (the minimum resolvable detail, or how much two points can be close to each other before they become indistinguishable).

The criterion is satisfied when the central maximum of one imaged point falls below the first minimum of the other. The spatial resolution of 1-D sinc function magnitude given in Figure2-12 is the distance between the central maximum point and the finite zero-crossing.

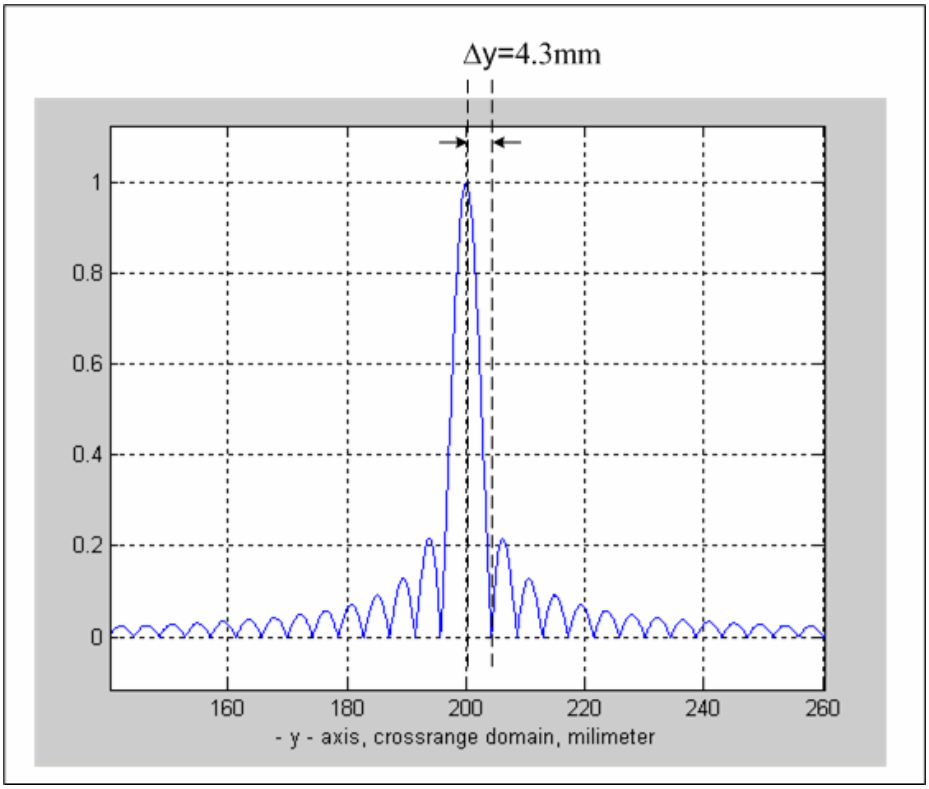

Figure2-12 Sinc Function Magnitude

The range and cross range resolution values can be found using the target reflectivity function given in expression 2.2.28.

$$\Delta_x = \frac{2\pi}{B_x}\frac{1}{\cos\alpha}, \tag{2.78}$$

where,

$$\cos\alpha = \frac{X_c}{\sqrt{X_c^2 + Z_s^2}}.$$

The term $\cos\alpha$ comes from the fact that, we work on slant range. The theoretical resolution value we have found discarding $\cos\alpha$ is range resolution in the slant range domain.

Using (2.71) and (2.78), range resolution is found to be as;

$$\Delta_x = \frac{2\pi}{4\omega_0 / c} \frac{\sqrt{X_c^2 + Z_s^2}}{X_c} = \frac{\pi c \sqrt{X_c^2 + Z_s^2}}{2\omega_0 X_c}, \tag{2.79}$$

and using (2.72) cross-range resolution is,

$$\Delta_y = \frac{2\pi}{B_y} = \frac{2\pi}{4k_c \sin\varphi_d} = \frac{\pi c}{2\omega_c \sin\varphi_d}. \tag{2.80}$$

For typical values of;

$\varphi_d = \pi/6, \quad f_c = 40k\ Hz, \quad f_0 = 2k\ Hz, \quad X_c = 1.04m, \quad Z_s = 0.78m$

$\Delta_x = 5.3cm, \quad \Delta_y = 4.3mm$ is found.

The created 2-D sinc function using the same theoretical resolution values is shown in Figure2-13.

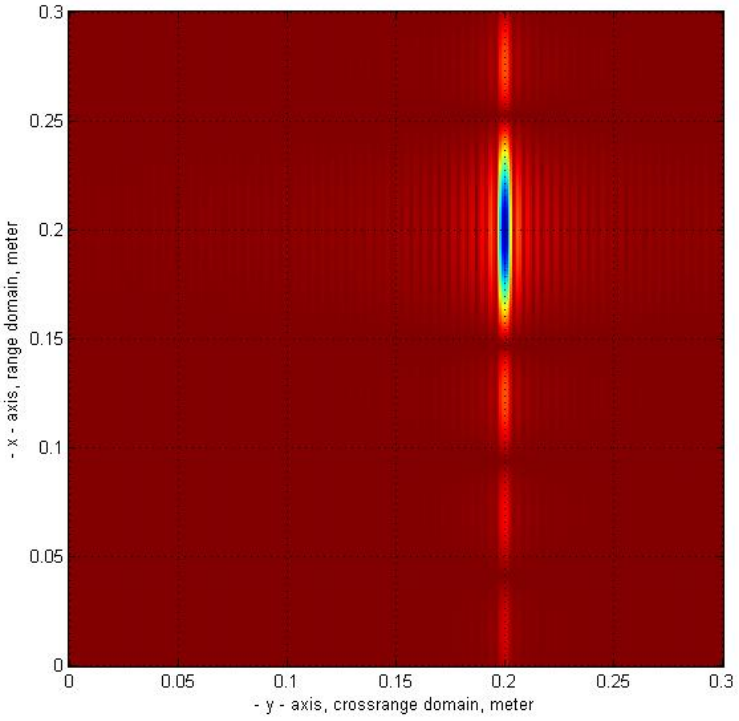

Figure2-13 Simulation for 2-D Sinc Function, Δx=5.3cm Δy=4.3mm (4kHz bandwidth chirp is used)

Note that the use of a single frequency transmitted signal does not allow us to resolve the targets in x direction. In Figure2-11, the spectral support of the matched filtered SAR signal in k_x-k_y domain is shown for the case that the bandwidth of the transmitted signal is $2\omega_0$. For a pure sinosid transmitted signal, the length of the x-direction edge of the rectangle, B_x, will be zero. This result indicates the necessity to use a wideband transmitted signal for range imaging applications.

CHAPTER 3

SAR ALGORITHMS

3.1 INTRODUCTION

SAR Imaging approach discussed in Chapter 2 can be implemented using various algorithms. The origin of these methods is based on wave equation inversion theory [6] which is used at 1960s by SAR researchers for imaging [7, 8]. Because of the practical limitations of that time, SAR researchers used an approximation (Fresnel) for reconstruction [1]. Also Plane wave approximation based reconstruction algorithms were used to simplify the theory and reduce the computational cost.

Today using powerful digital computers and developed digital signal processing algorithms, there is no need to use Fresnel approximation for reconstruction [1]. In this chapter, those methods that do not use Fresnel and plane wave approximation will be examined.

3.2 SPATIAL FREQUENCY INTERPOLATION

The SAR reconstruction discussed in previous chapter requires the mapping of measurement Fourier domain (ω, k_u) to target Fourier domain (k_x, k_y). The measurement domain parameters include evenly spaced samples while corresponding target domain samples include unevenly spaced samples due to nonlinearity in the mapping.

If we assume that there are M samples in the synthetic aperture with Δ_u sampling spaces, then in the Fourier domain [1], the sampling interval is,

$$\Delta k_u = \frac{2\pi}{2L} = \frac{2\pi}{M\Delta_u},$$

where L is synthetic aperture half length.

The mapping of $k_u \to k_y$ is evenly spaced since $k_u = k_y$. But the mapping to k_x domain is unevenly spaced.

$k_x = \sqrt{4k^2 - k_u^2}$. ($k = \frac{\omega}{c}$ is the wave number)

For discrete values of m, n;

$$k_{ymn} = k_{um} = m\Delta k_u$$

$$k_{xmn} = \sqrt{4k_n^2 - k_{um}^2}$$

$$k_n = n\Delta_k = \frac{n\Delta_\omega}{c} \tag{3.1}$$

If we call the nonlinear transformation as g_m:

$$k_x = g_m(\omega) = \sqrt{4k^2 - k_{um}^2}$$

Hence;

$k_{xmn} = g_m(n\Delta_\omega)$.

The mapping structure is given in Figure3-1.

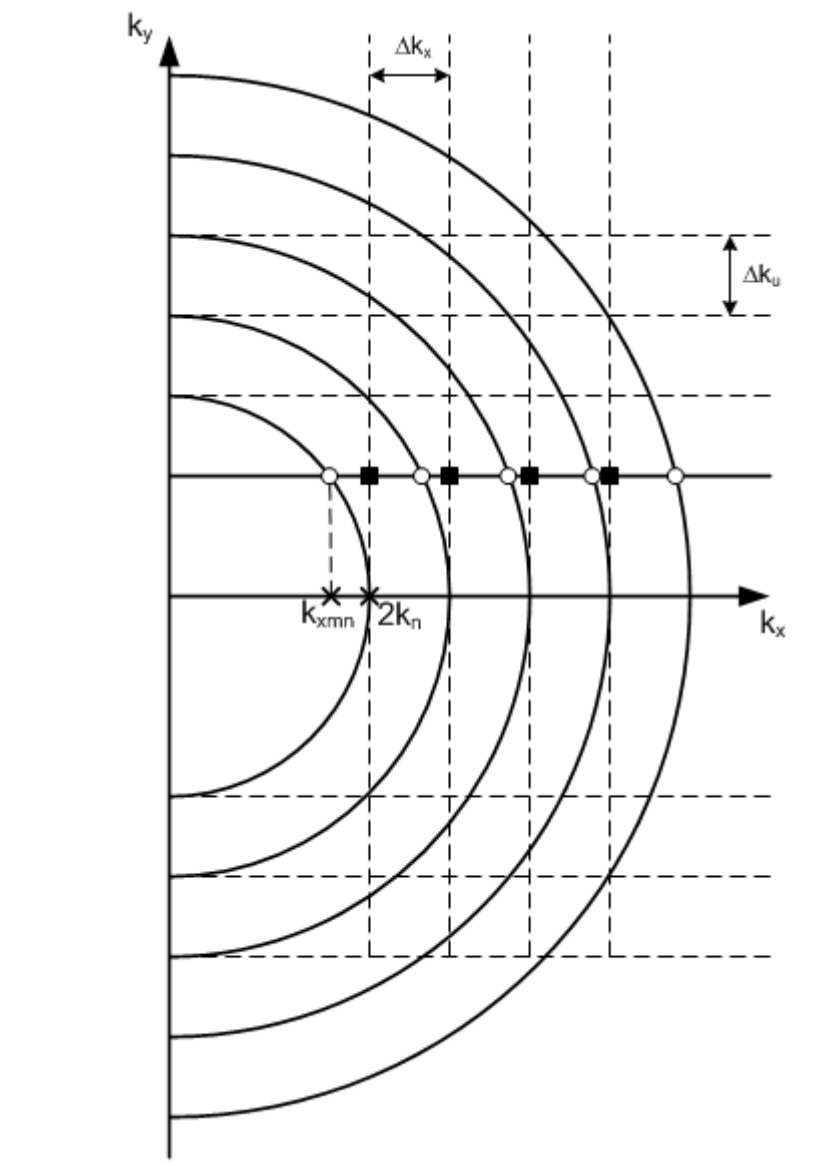

Figure3-1 Spatial Frequency Mapping [1]

The interpolation equation for this geometry can be approximated as [9]:

$$F(k_x, k_{ymn}) \approx \sum_{|k_x - k_{xmn}| \le N_s \Delta k_x} J_m(n\Delta_\omega) F(k_{xmn}, k_{ymn}) h_\omega(k_x - k_{xmn}) \tag{3.2}$$

where,

$$J_m(\omega) = \frac{dg_m(\omega)}{d\omega} = \frac{4k}{c\sqrt{4k^2 - k_{um}^2}}$$

$$h_\omega(k_x) == \begin{cases} h(k_x)\omega(k_x), & for\ |k_x| \le N_s \Delta k_x \\ 0, & otherwise \end{cases}$$

$$h(k_x) = \mathrm{sinc}\left(\frac{k_x}{\Delta k_x}\right)$$

$$\omega(k_x) = \begin{cases} 0.54 + 0.46\cos\left(\frac{\pi k_x}{N_s \Delta k_x}\right), & for\ |k_x| \le N_s \Delta k_x \\ 0, & otherwise \end{cases}$$

Spatial Frequency Interpolation algorithm is summarized in Figure3-2.

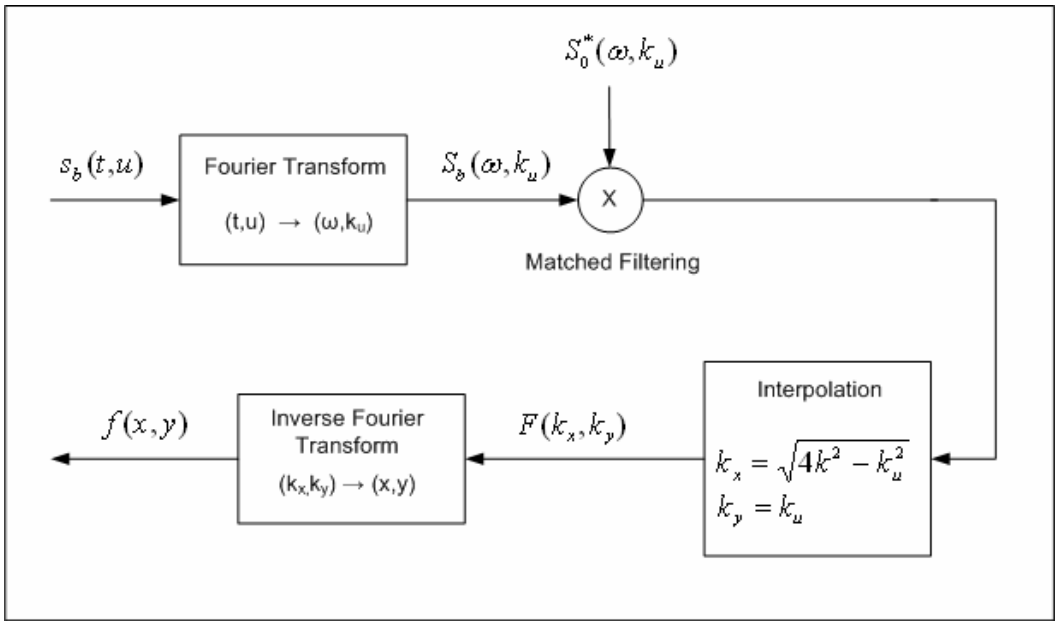

Figure3-2 Spatial Frequency Interpolation Algorithm [1]

3.3 RANGE STACKING

Range stacking algorithm is based on the idea of transforming ω-u domain integration to x-y domain.

Inverse Fourier integral given below,

$$f(x,y) = \iint_{k_x\, k_y} F(k_x, k_y)\exp(jk_x x_s + jk_y y)dk_x dk_y \tag{3.3}$$

where

$$x_s = \sqrt{(x + X_c)^2 + Z_z^2}$$

can be rewritten as [1];

$$f(x,y) = \iint_{k_u\, \omega} F_{SM}(\omega, k_u)\exp(jk_x(\omega, k_u)x_s + jk_u y)J(\omega, k_u)d\omega dk_u$$

where,

$$J(\omega, k_u) = \frac{4k}{c\sqrt{4k_{\omega c}^2 - k_u^2}}.$$

The effect of slowly fluctuating Jacobian term is negligible in the reconstruction. Discarding the Jacobian term and solving the integration for each range bin x_i, separately, the following can be written,

$$f(x_i, y) = \iint_{k_u\, \omega} F_{SM}(\omega, k_u)\exp(jk_x(\omega, k_u)x_{si} + jk_u y)d\omega dk_u \tag{3.4}$$

where

$$x_{si}^2 = (x_i + X_c)^2 + Z_s{}^2.$$

Defining the reference signal as;

$$s_{0i}(t,u) = p(t - \frac{2\sqrt{x_{si}^2 + u^2}}{c}), \tag{3.5}$$

then the baseband version will be

$$s_{0ib}(t,u) = p(t - \frac{2\sqrt{x_{si}^2 + u^2}}{c}) \exp(-j\omega_c t). \tag{3.6}$$

After 2-D Fourier transformation, using the Fourier transformation of expression (2.15), defined baseband reference signal for each range bin is obtained as;

$$S_{0ib}(\omega, k_u) = P_b(\omega) \exp(-jk_x x_{si}). \tag{3.7}$$

Using expression (2.54) for $S_b(\omega, u)$, the baseband echoed signal spectrum is found as:

$$S_b(\omega, k_u) = P_b(\omega) \sum_n \sigma_n I_n(\omega, k_u) \exp(-jk_x(\omega, k_u) x_{sn}) \exp(-jk_u y_n) \tag{3.8}$$

Merging (3.4), (3.7), (3.8); the range stacking algorithm is formed as:

$$f(x_i, y) = \int_{k_u} \left[\int_{\omega} S_{0ib}^*(\omega, k_u) S_b(\omega, k_u) d\omega \right] \exp(jk_u y) dk_u \tag{3.9}$$

The algorithm is summarized in Figure3-3.

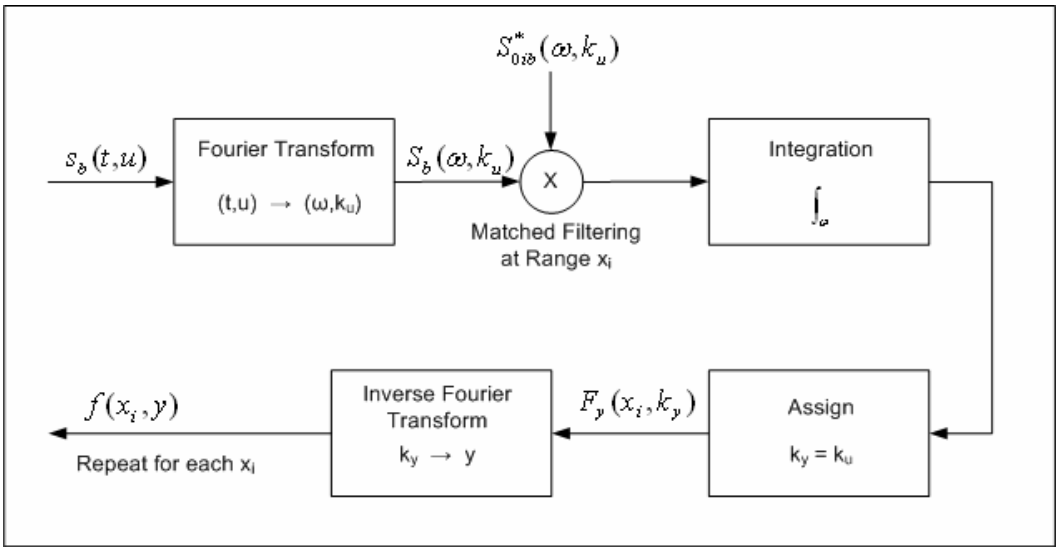

Figure3-3 Range Stacking Algorithm [1]

3.4 TIME DOMAIN CORRELATION

Time Domain Correlation algorithm is based on correlation implementation of the matched filtering [1].

The imaging equation for TDC is [1];

$$f(x_i, y_j) = \int_u \int_t s_b(t,u) p_b^*\left[t - t_{ij}(u)\right] dt du \tag{3.10}$$

where

$$t_{ij}(u) = \frac{2\sqrt{x_{si}^2 + (y_j - u)^2}}{c}$$

and

$s_b(t,u)$ is the baseband received signal given in expression (2.51).

Hence, the reconstruction process will be performed for discrete values of the spatial (x,y) domain. This way of reconstruction needs an interpolator to find the required time instants of baseband transmitted signal, $p_b(t)$.

TDC algorithm can be developed one more step further to take into consideration the limitation on $t_{ij}(u)$ value. We have mentioned before in the Multidimensional SAR Problem section that the used radar in this study can be supposed to have a limited beam-width, $\pm\varphi_d$. This limited beam-width (BWD) ensures the following inequality of time grids,

$$t_{ij}(u) = \frac{2\sqrt{x_{si}^2 + (y_j - u)^2}}{c}, \quad \text{if } \left|y_j - u\right| \le BWD \tag{3.11}$$

where

$BWD = x_{si} \tan(\varphi_d)$

and

$$x_{si} = \sqrt{(x_i + X_c)^2 + Z_s{}^2} \ .$$

TDC reconstruction equation (3.10) can also be written as below from Parseval's theorem [1]:

$$f(x_i, y_j) = \int_u \int_\omega S_b(\omega, u) P_b^*(\omega) \exp(j\omega t_{ij}(u)) d\omega du \tag{3.12}$$

By using expression (3.12) for TDC reconstruction, it is no more required to use an interpolator to find the $t - t_{ij}(u)$ time instants of the baseband transmitted signal, namely $p_b(t)$, given in expression (3.10).

TDC algorithm via expression (3.12) can be summarized as in Figure3-4.

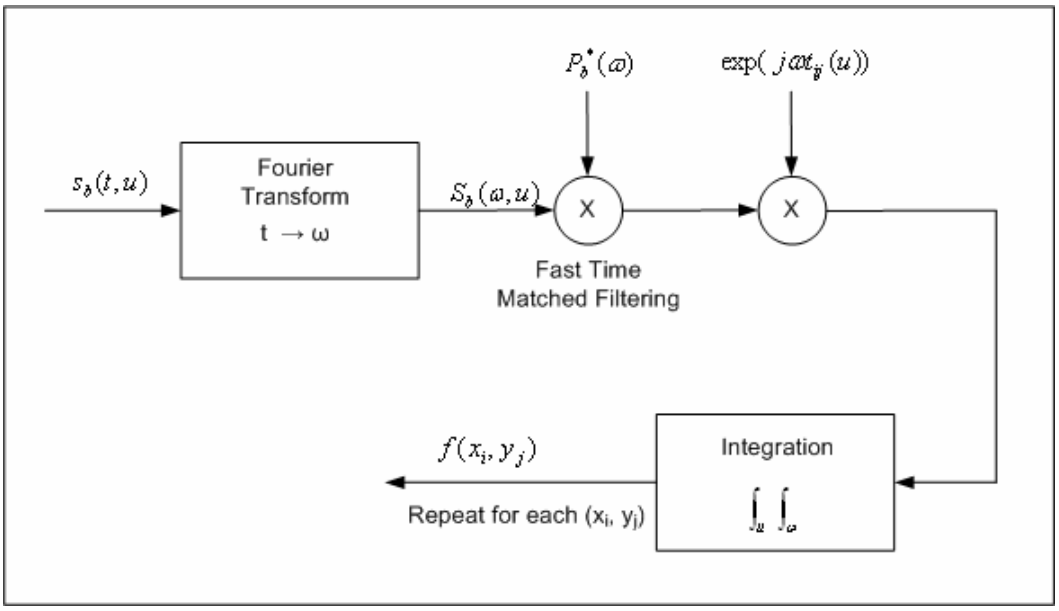

Figure3-4 TDC Algorithm

Because of the 2-D discrete summing process, TDC algorithm is computationally very complex. Also while using equation (3.10) in the implementation; a sufficiently accurate interpolator will be required to obtain $p_b^*\left[t - t_{ij}(u)\right]$ values.

3.5 BACKPROJECTION

Backprojection algorithm has a very similar implementation to Time Domain Correlation algorithm. In Backprojection algorithm, matched filtered echoed signal is used in TDC reconstruction equation (3.12).

If we denote the fast time matched filtered echoed signal as,

$$s_{BP}(t,u) = s_b(t,u) * p_b^*(-t), \tag{3.13}$$

then in the frequency domain, it will be represented as,

$$s_{BP}(\omega,u) = s_b(\omega,u)P_b^*(\omega). \tag{3.14}$$

If we rewrite expression (3.12) using (3.14); then

$$\begin{aligned} f(x_i, y_j) &= \int_u \int_\omega s_{BP}(\omega,u)\exp(j\omega t_{ij}(u))d\omega du \\ &= \int_u s_{BP}(t_{ij}(u),u)du. \end{aligned} \tag{3.15}$$

The limitation given in expression (3.11) can be used in Backprojection algorithm in a similar way to discard the SAR imaging information coming further than the beam-width.

One of the important problems about this method is the interpolator requirement to obtain $s_{BP}(t_{ij}(u))$ values. This problem is overcome by upsampling the matched filtered echoed signal with high ratios in the application.

Backprojection algorithm is summarized in Figure3-5.

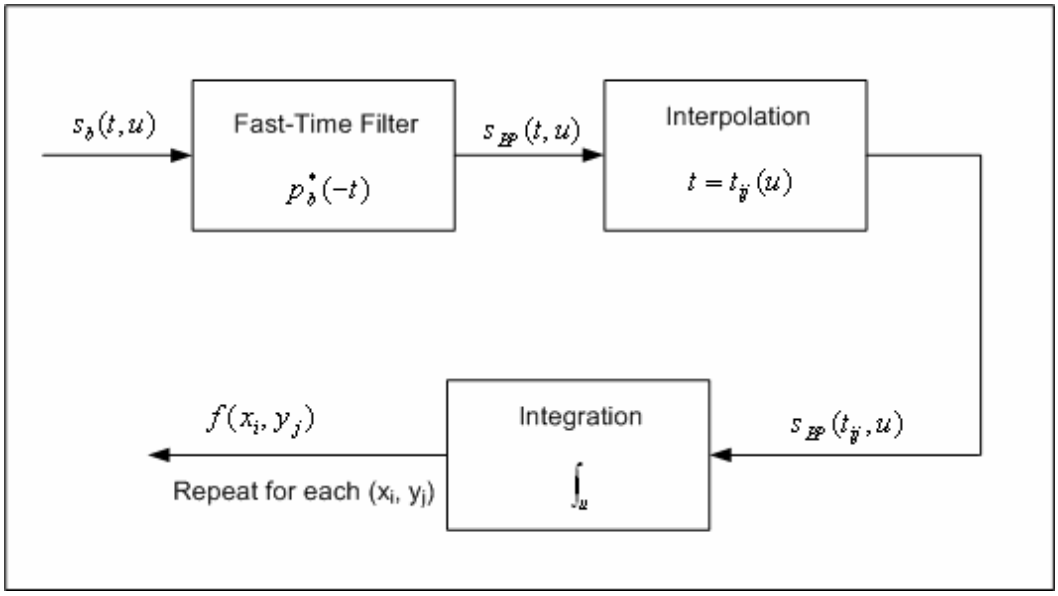

Figure3-5 Backprojection Algorithm [1]

3.6 DIGITAL SPOTLIGTHING

Digital Spotlighting Algorithm is an important tool to extract the SAR signature of a specific target area. It can be used with all of the SAR reconstruction algorithms given in previous parts in this Chapter.

Digital Spotlighting algorithm is based on polar format processing which is an old radar signal processing tool for reconstruction using approximations.

Digital Spotlight filter can be applied to splitted subapertures of the target region separately. Digital Spotlight filter is defined [1] in (t, k_u) domain via

$$W_{di}(t,k_u)=\begin{cases}1, & for \left|\frac{ct}{2}\cos(\varphi+\theta_{ci})-X_c\right|<X_0 \ \ and \ \left|\frac{ct}{2}\sin(\varphi+\theta_{ci})-Y_i\right|<Y_0\\ 0, & otherwise\end{cases} \tag{3.16}$$

where

$$\varphi=\arcsin\left(\frac{k_u}{2k_c}\right), \quad \theta_{ci}=\arctan\left(\frac{Y_i}{\sqrt{X_c^2+Z_s^2}}\right)$$

(X_c, Y_i) is the mid-point of each subaperture.

The Digital Spotlighting algorithm for subaperture processing is summarized in Figure3-6. In the figure the used reference signal is [1],

$c_0(\omega,u)=\exp\left[\ -j2k\sqrt{X_{cs}^2+u^2}+j2k\sqrt{X_{cs}^2+Y_i^2}\ \right]$.

$S_M(\omega,u)$ is the matched filtered signal spectrum given in (2.59).

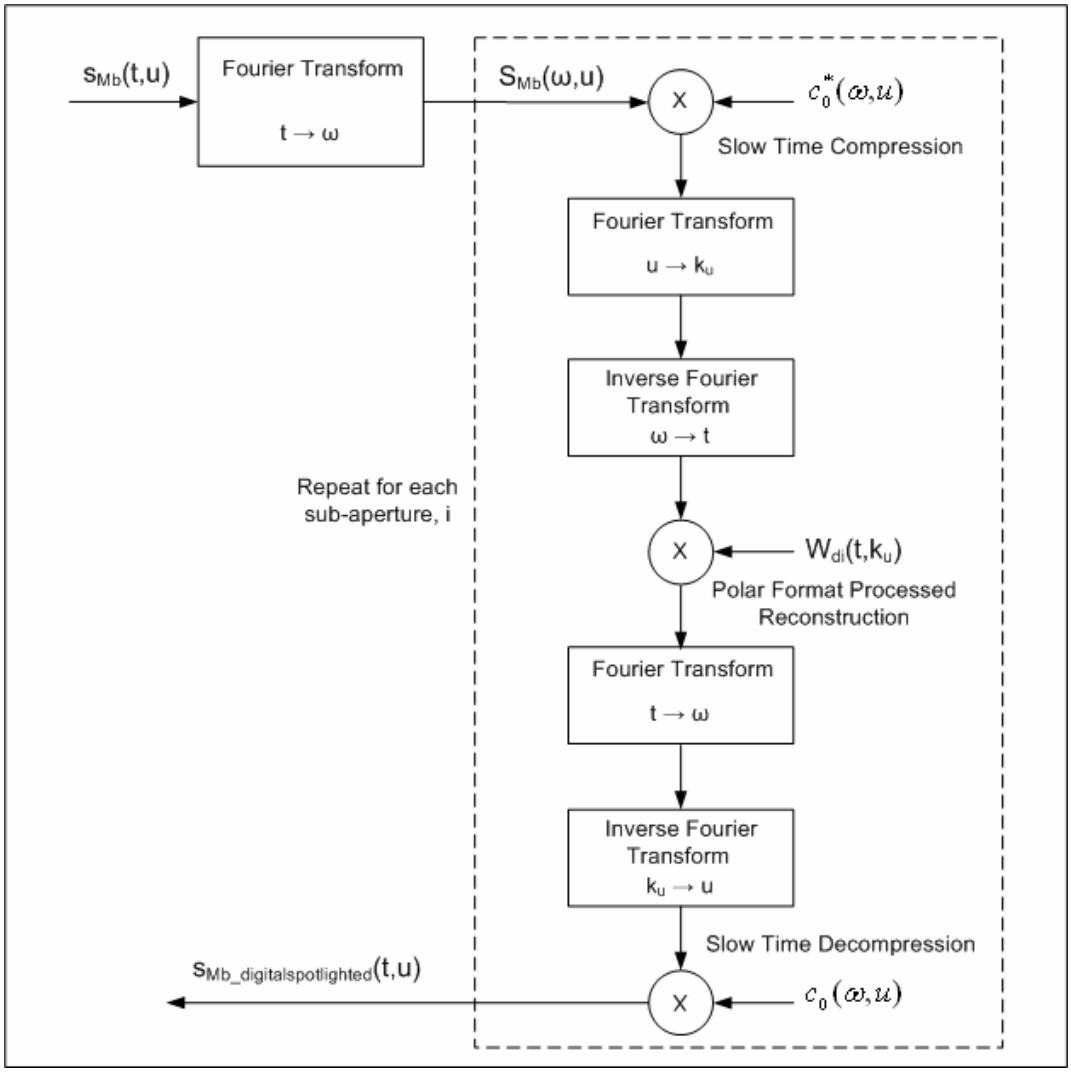

Figure3-6 Digital Spotlighting Algorithm

CHAPTER 4

EXPERIMENTAL SAR SETUP

4.1 PARTS OF THE HARDWARE

The hardware of the ultrasound testbed for evaluating SAR techniques is composed of the mobile platform, the ultrasound transmitter and receiver, the analog circuitry to drive the transmitter and to acquire data from the receiver, and an ordinary PC having 16 bits, 96 kSamples/sec Analog I/O (sound card.) The signal processing operations are realized after the data acquisition process by using MATLAB.

The actual geometry and the working system are shown in Figure4-1.

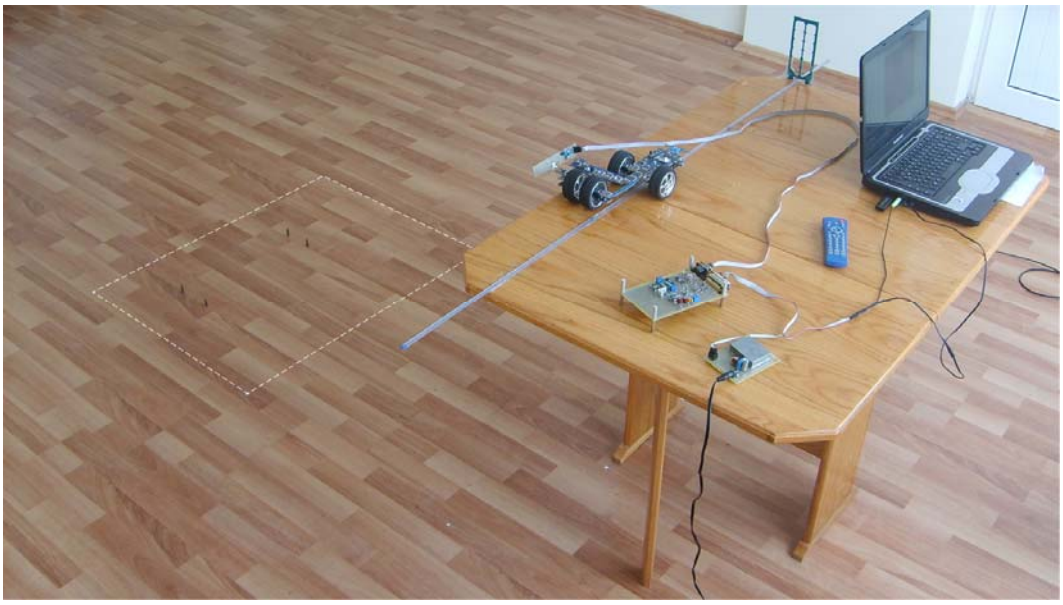

Figure4-1 Experimental SAR Setup

4.2 THE MOBILE PLATFORM AS A MOVING VEHICLE

In order to apply Stripmap SAR geometry, a moving vehicle carrying the radar is needed. In Stripmap SAR (or side-looking SAR) system, the radar maintains the same broadside radiation pattern for all fixed points in the linear route of the vehicle. Therefore the illuminated cross-range area is shifted from one data transmission-reception to the other.

The linearity of the route and the speed of the vehicle can play a critical role under certain circumstances. If the speed of the vehicle is not fixed and changes slowly, the replacement of the vehicle for different time intervals will not be the same, e.g. synthetic aperture sample spacing of SAR signal Δ_u will be a function of varying speed. Because Δ_u is assumed to be fixed in the calculations, the quality of final reconstructed image reduces.

A software programmable product, namely Viper [4], is used as a moving platform. This programmable robot is made up of a motherboard where the software embeddable IC is located, and the peripheral components that make Viper an infrared controllable moving platform. The used language to program Viper is BASIC. The programmed speed of Viper while carrying the ultrasound transmitter and receiver is nearly 3.5cm/sec. Figure4-2 shows the photo of Viper with ultrasound transmitter and receiver is mounted on the vehicle.

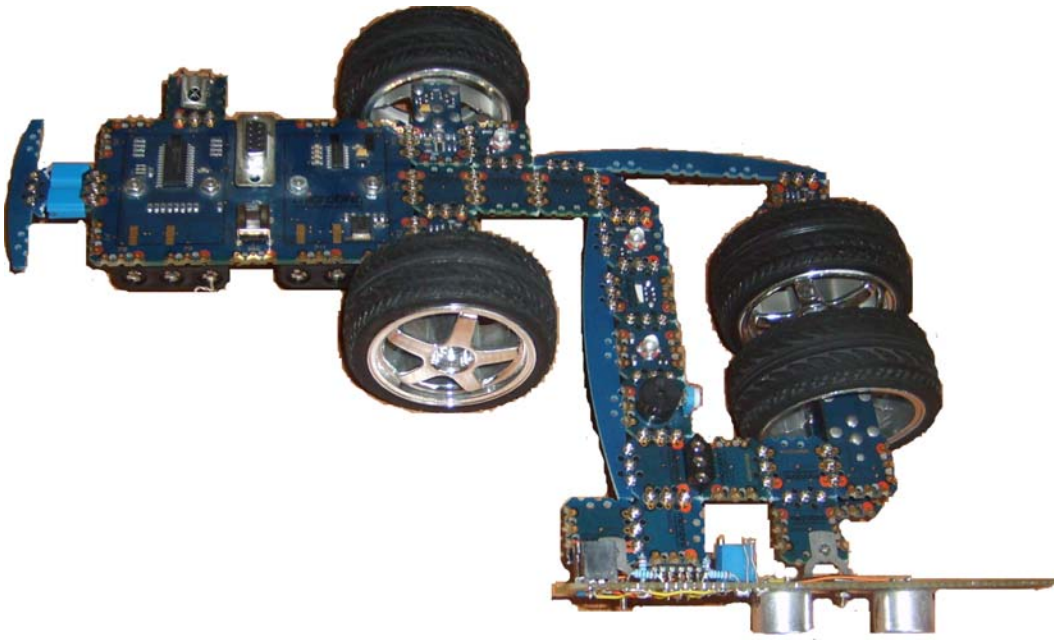

Figure4-2 Ultrasonic Circuitry Mounted Mobile Platform

4.3 THE ANALOG CIRCUITRY FOR DATA TRANSMISSION AND RECEPTION

Data transmission and reception process requires a kind of analog circuitry given in Figure4-3. The used ultrasonic transmitter and receiver have a center frequency of nearly 40kHz [5]. In Figure4-4, the bandwidth, center frequency and beam angle characteristics of ultrasonic transmitter and receiver are shown. These

properties are crucial in the reconstruction algorithms. For beam angle of the transmitter and receiver, the angle that causes 6 db power reduction compared to center power is taken to be as the beam angle.

In this study the following values are used for beam angle, center frequency and bandwidth.

$\varphi_d = \pi / 6, \quad f_c = 40kHz, \quad f_0 = 2kHz$

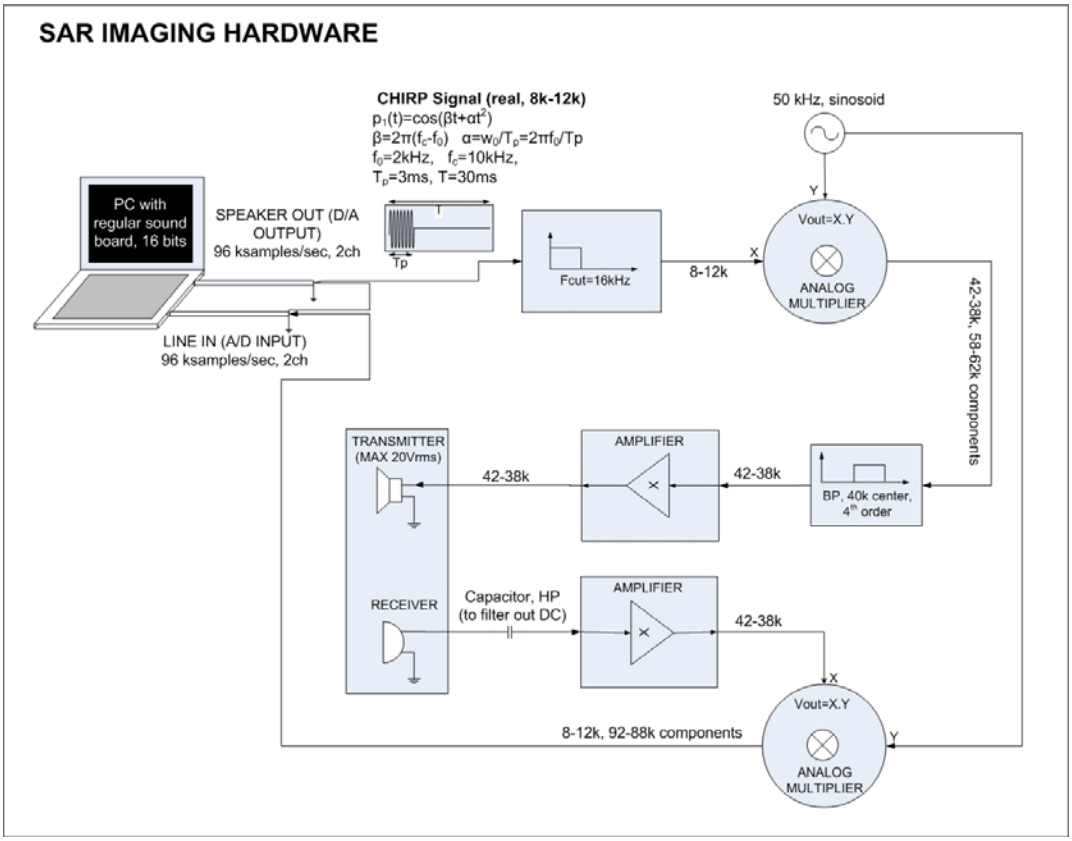

Figure4-3 Analog Circuitry for SAR Imaging

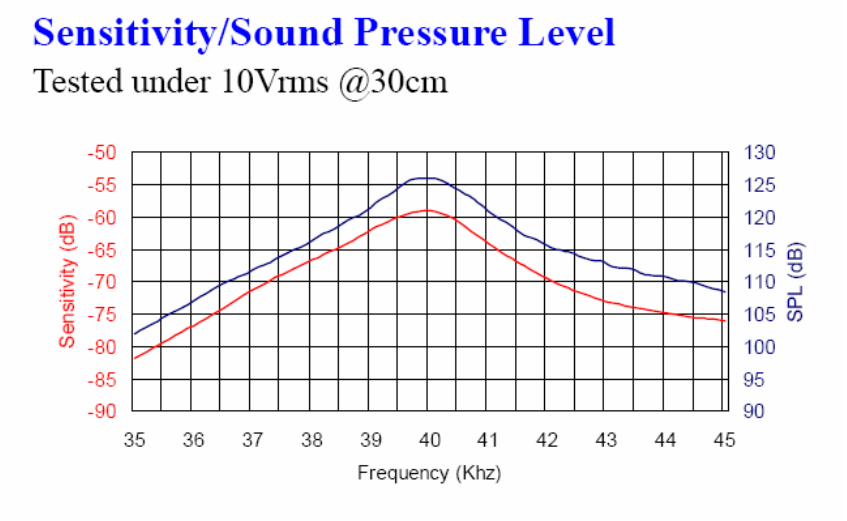

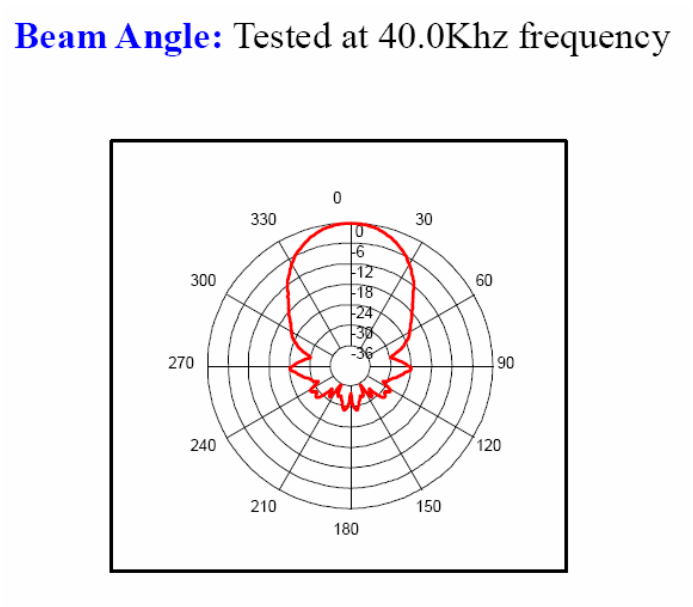

Figure4-4 Center Frequency, Bandwidth and Beam Angle of the Used Transmitter

In order to generate the waveform having the required center frequency of 40kHz, 96kSample/sec DAC of PC analog front end can be insufficient and can result significant harmonic distortion in the desired output waveform because of the practical limitations of a sharp reconstruction filter. This fact explains why it is necessary to use a mixer signal of 50 kHz to drive the transmitter.

10 kHz centered chirp signal is created digitally in PC, and driven using PC analog interface. The 16 kHz cut-off reconstruction filter is used to smooth the output waveform. The filtered signal is then multiplied with the 50 kHz sinusoid which results 40 kHz and 60 kHz centered components (The constant phase of the 50 kHz sinusoid is added to 40 and 60 kHz components). The ultrasound transmitter transmits the 40 kHz centered component while blocks 60 kHz centered one.

Similar procedure is followed after reception of the echoed signal. 40 kHz centered echoed signal coming from the target region is received by the ultrasound receiver. After filtering out DC components using a capacitor as a high pass filter, the received signal is amplified approximately 1000 times. This amplified signal is multiplied with the same 50 kHz sinusoid used before to downconvert the signal. This multiplication cancels out the constant phase in the received signal which was added before transmission by the 50 kHz mixer. 10 kHz and 90 kHz centered signals are inputs to PC analog interface where 90 kHz component is filtered by the anti-aliasing analog filter. Finally 10 kHz signal is sampled using the 96 kSample/sec ADC of PC.

The hardware allows two channel recording which enables both transmitted raw signal and received echoed signal to be acquired synchronously.

Finally the designed analog circuitry is made up of;

- 2 amplifiers
- 1 4^{th} order low-pass filter (Butterworth)
- 1 4^{th} order bandpass filter (Butterworth)
- 2 analog multipliers (**MPY 634**)
- 50 kHz sinusoid generator.

The designed amplifiers, filters and sinusoid generator require operational amplifiers. For these purposes, low noise, wide bandwidth operational amplifier, **AD8512**, is used in the circuits.

4.4 SAR PROCESSING SOFTWARE

The software used in the system is composed of MATLAB functions designed for realizing several tasks given in Figure4-5. Using the software, the linear frequency modulated pulses (chirps) can be generated (**Create Output**). When this output is applied to the system, both transmitted and received signals can be recorded using **Record** toolbox. It is also possible to reload previously recorded data.

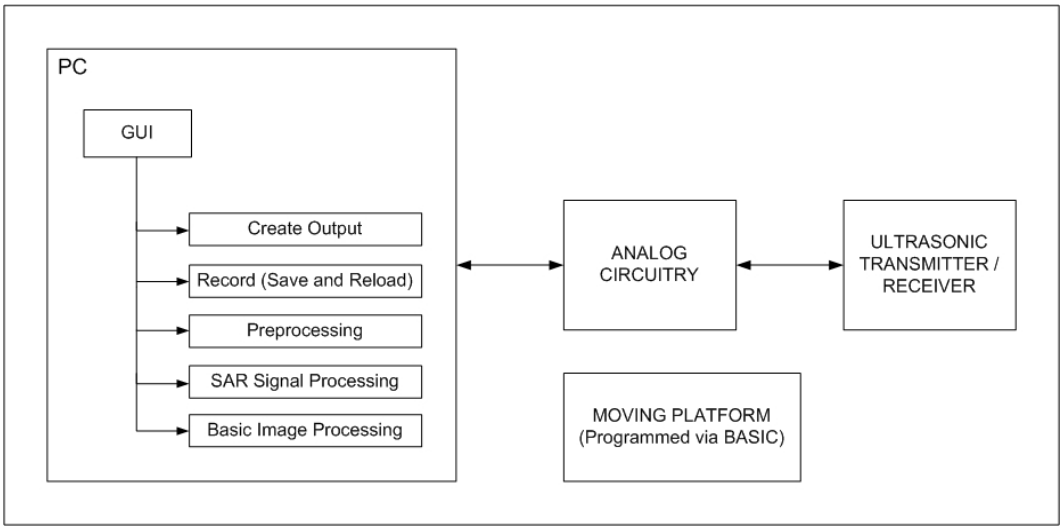

Figure4-5 General Structure of SAR Processing System

Preprocessing toolbox stands for reshaping the data before proceeding to SAR processing. This toolbox takes the raw data composed of transmitted and received signals, finds the beginning and end points of the required time interval for SAR

Processing according to geometry (Time Gating), down-sample the data to reduce the computational cost and convert one dimensional data (t domain; sequence) to two dimensional (t,u domain; matrix) data which will be used in SAR Signal Processing.

SAR Signal Processing toolbox allows the user to select which algorithm is going to be used in the reconstruction step. Also it is possible to apply digital spotlighting filter to focus the targets.

The last part is **Basic Image Processing** toolbox which enables target signatures to become clear while prevents the noisy background to be seen for visual purposes. It uses a kind of center of mass algorithm to find the place where the target signature clouds indicate. Colormap view is used to visualize the obtained results.

All toolboxes are linked by a graphical user interface (MATLAB GUI) which is shown in Figure4-6.

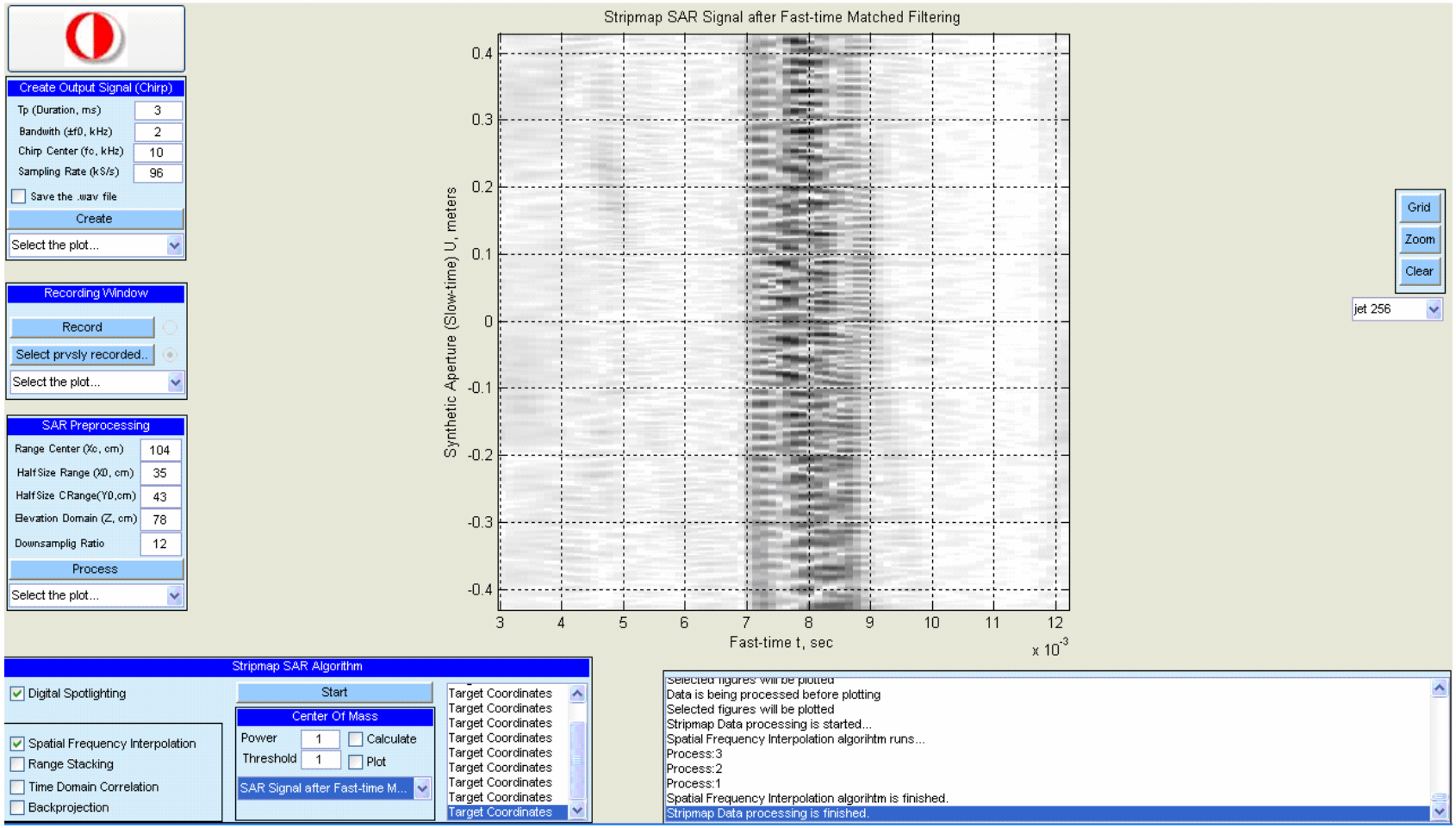

Figure4-6 Graphical User Interface

CHAPTER 5

EXPERIMENTAL RESULTS OF THE ULTRASONIC SAR SYSTEM

5.1 INTRODUCTION

The designed setup is used to obtain the target reflectivity function of the ground. The ultrasonic testbed shown in Figure4-1 gives a chance to apply many SAR techniques to deal with Stripmap SAR problem. In this study Spatial Frequency Interpolation, Range Stacking, Time Domain Correlation and Backprojection Stripmap SAR reconstruction algorithms are applied to the raw SAR data to form the final image. All of the four methods can be used with an important SAR technique, namely Digital Spotlighting, to spotlight a limited target region.

The effect of targets inside and outside the target region to the reconstructed image is analyzed for different algorithms. The processing time as well as resulting images from each of the four algorithms are examined. The range and cross range resolution values are evaluated using the setup. The bandwidth of the used sensor affects the resolution of the reconstructed image range domain. This effect is investigated using another chirp signal having different bandwidth.

5.2 TRANSMITTED AND RECEIVED SIGNAL

The chirp signal is created using PC analog interface with the following parameters:

$$p_{out}(t) = \cos\left(\beta t + \alpha t^2\right)$$

$$\beta = 2\pi\left(f_c^{'} - f_0\right), \quad \alpha = \frac{2\pi f_0}{T_p}$$

$$f_c^{'} = 10k\ Hz, \quad f_0 = 2k\ Hz, \quad T_p = 3m\sec$$

The created chirp signal and the signal spectrum are given Figure5-1 and Figure5-2 respectively.

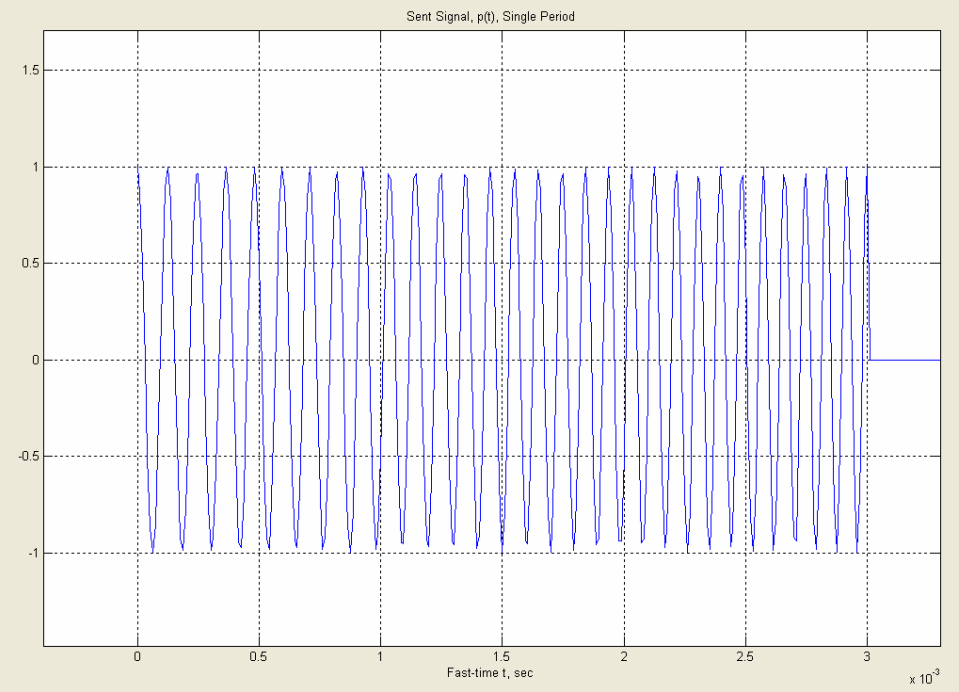

Figure5-1 Output Waveform Created using PC Analog Interface

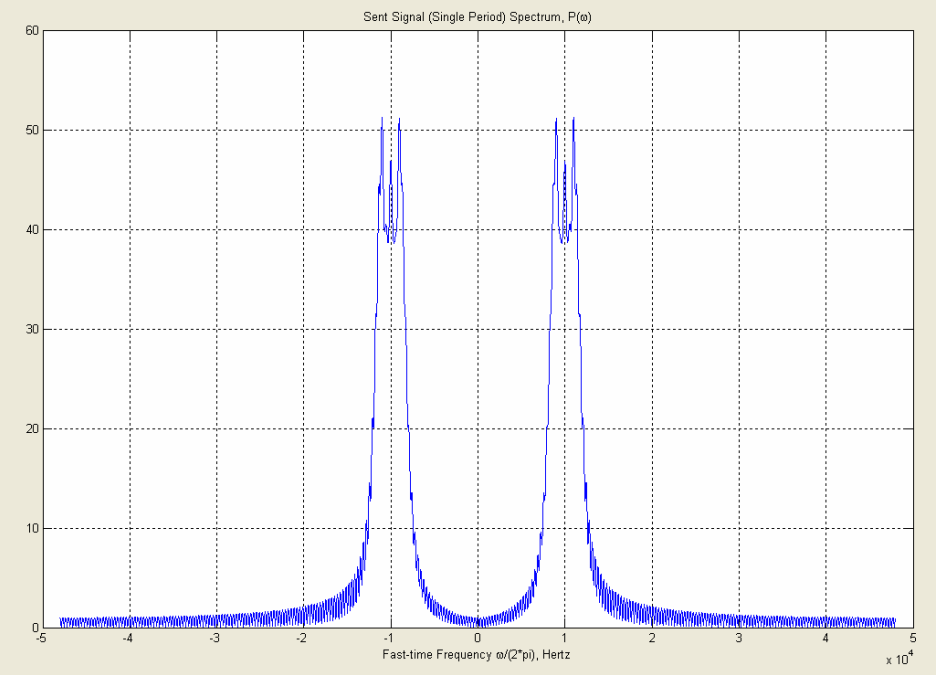

Figure5-2 Output Waveform Spectrum

The output waveform, after mixing with the $fm = 50kHz$ sinusoid, is transmitted to the target area via ultrasound transmitter as in Figure4-3. The transmitted signal hits the target region, comes back to the ultrasound transceiver, and is down-converted to output waveform frequency using exactly the same mixer signal. Both the output waveform and received echo signal are recorded together synchronously to be used in SAR signal processing. The transmitted and received signal in time domain and in Fourier domain for two data transmission and reception moments is shown in Figure5-3 and Figure5-4 respectively. While the radar carrying platform moves, it is assumed that the vehicle stops, the data transmission and reception process are performed and the vehicle moves to the next transceiving position (stop-and-go assumption [1]).

In Figure5-3, the larger amplitudes of the echoed signal correspond to higher reflectivity parts of the target region. The large amplitudes just after transmission

of the output waveform (approximately $t \in [31\,m\,\text{sec},\ 33\,m\,\text{sec}]$) exist because of the fact that ultrasound transmitter affects receiver during transmission. The very far away larger amplitudes of the received echo signal include the reflections of the objects outside the target region which should be discarded in SAR signal processing algorithms (Time Gating).

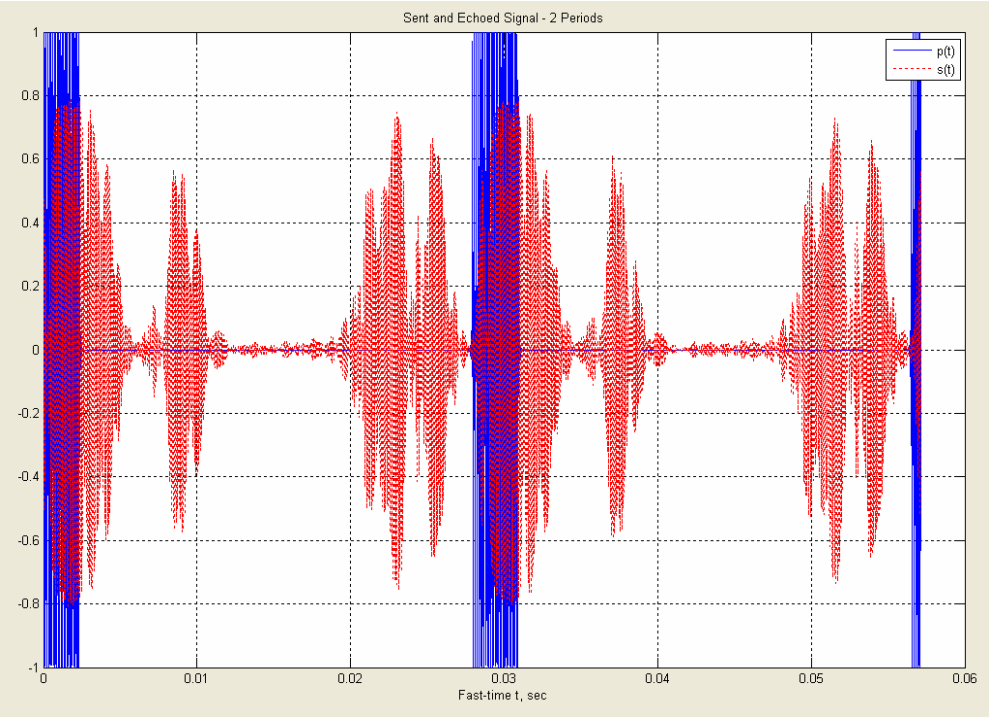

Figure5-3 Transmitted and Received Signal in Time Domain (PC record)

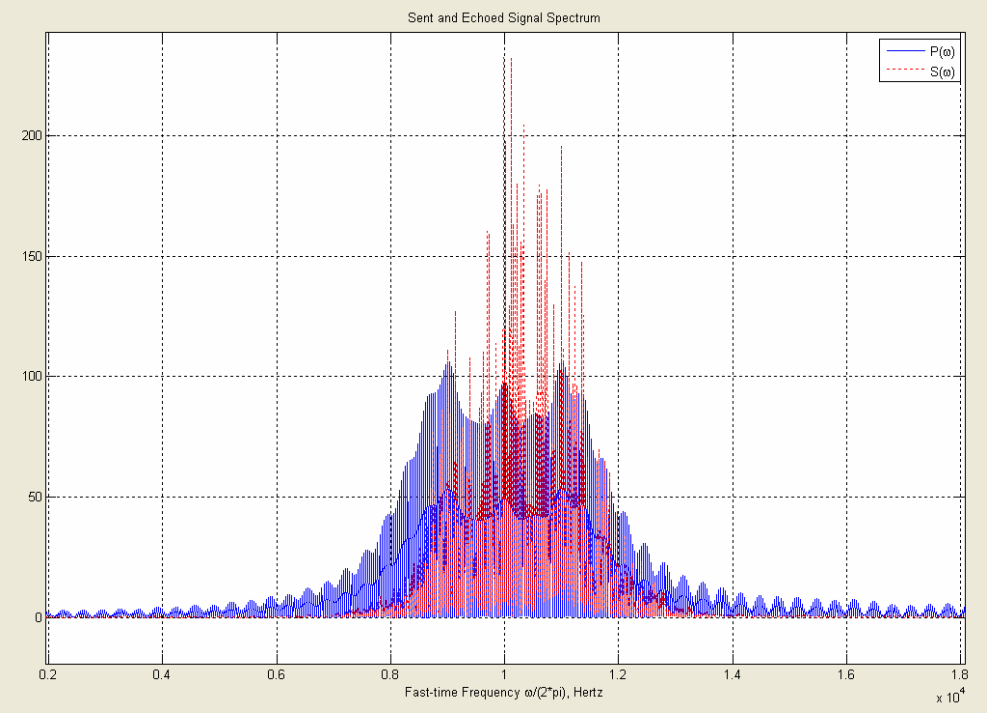

Figure5-4 Transmitted and Received Signal Spectrum (PC record)

One of the important practical problems of SAR preprocessing is the difficulty to find the $t = 0$ instant. From Figure5-3, the beginning nonzero part of the transmitted signal (blue one) should be the $t = 0$ instant that we look for. But if we concentrate on the zoomed version of $t = 0$ neighborhood shown in Figure5-5, it is not possible to determine which point belongs to $t = 0$ instant. In order to overcome this problem, the digitally created input waveform in PC is shifted and amplitude modulated to coincide with the recorded real transmitted signal (Figure5-6). Using the t=0 instant of the simulated signal, starting point of the time axis of the SAR system can be found.

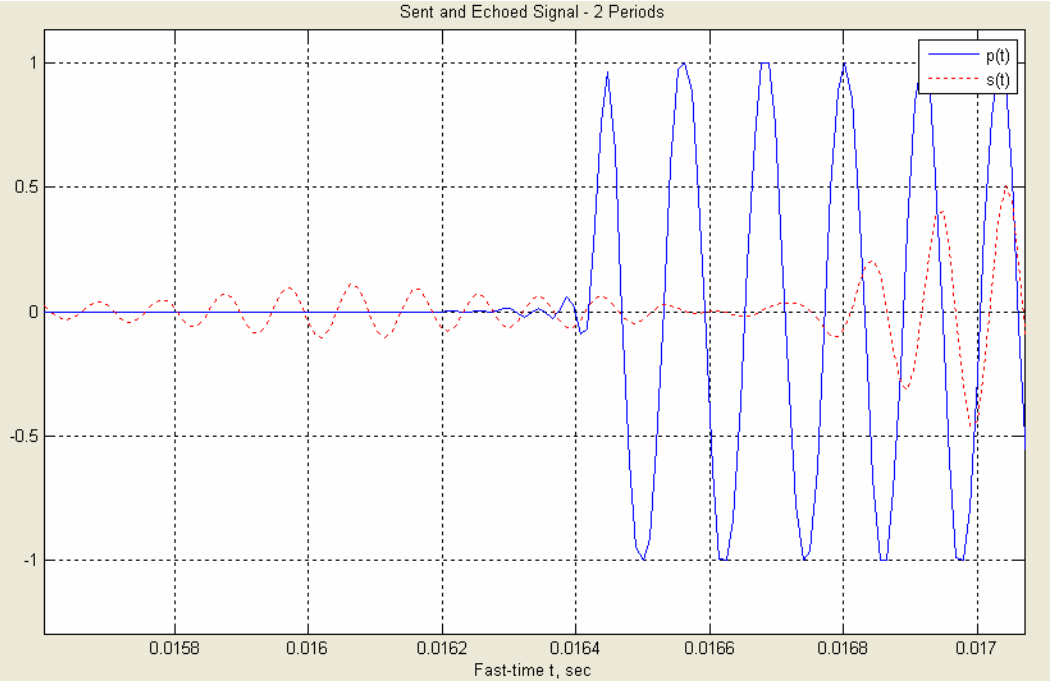

Figure5-5 Transmitted and Received Signal, t=0 instant

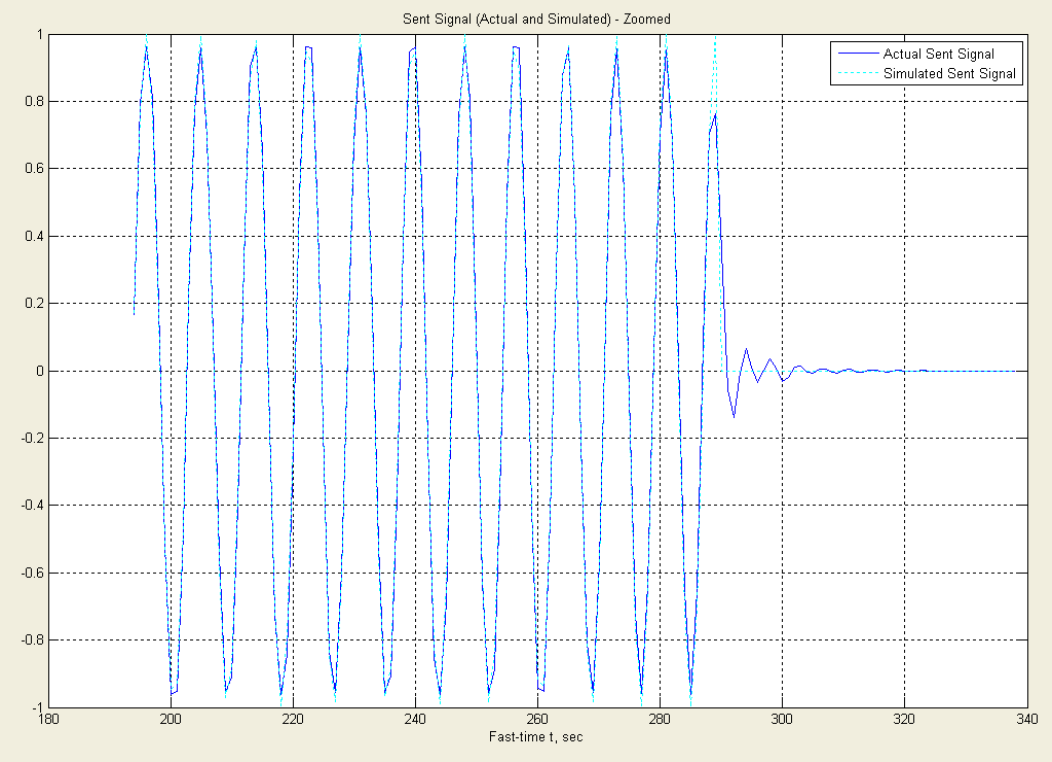

Figure5-6 Sent Signal (Actual and Simulated)

While processing the SAR signature mentioned in Chapter 2, baseband echoed signal is used in the algorithms. The expression below, for a specific radar position, is plotted in Figure5-7.

$$s_b(t,u) = \sum_n \sigma_n \exp\left(j\omega_0(t-t_n) - j\alpha(t-t_n)^2\right)\exp\left(-j\omega_c t_n\right)$$

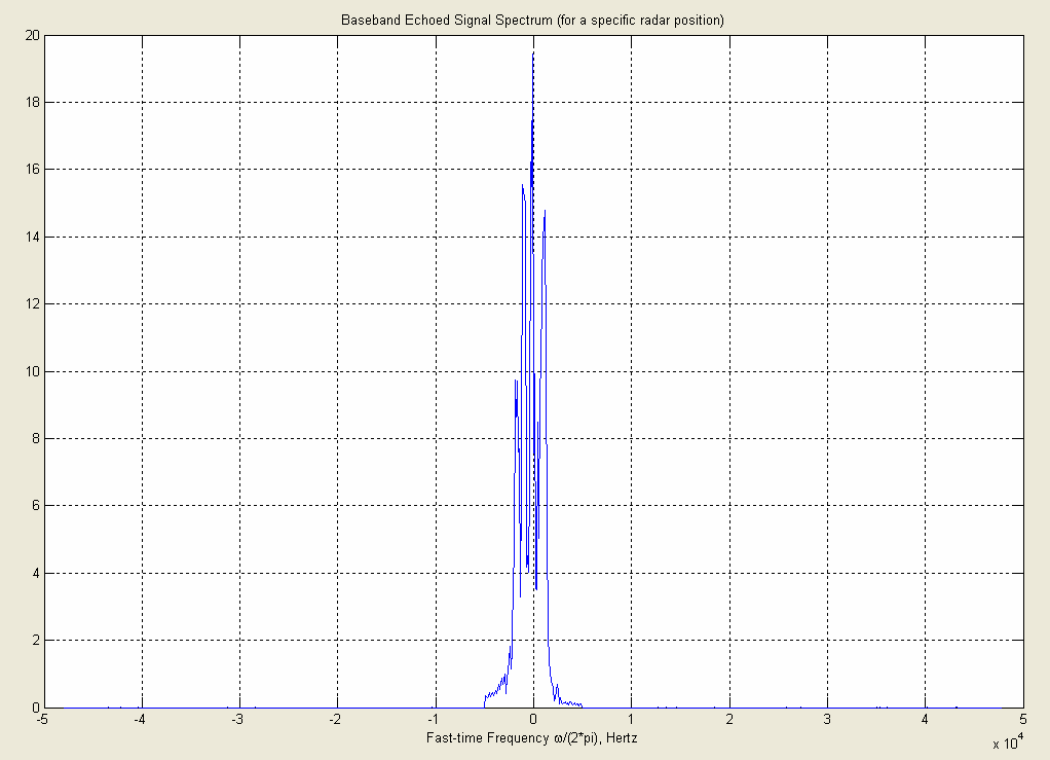

Figure5-7 Baseband Received Signal Spectrum

5.3 SAR PROCESSING

SAR processing part includes the application of the procedures mentioned in Multidimensional SAR Problem (Section 2.2.) and SAR Algorithms (Chapter 3). Many experiments are done using the experimental setup. The results for the reconstruction algorithms and the effect of digital spotlighting technique on these algorithms are analyzed in this section.

Real target scene is shown in Figure5-8. The letter "M" part in the left hand side of the figure is the concentrated target region that the radar moves Z_s meter (≈0.78m) above left to right. The extra target in the right hand side part symbolizes the targets out of the scene. The corruption effect caused by this extra target will also be seen in the obtained target reflectivity function at the end.

The used objects in the study, screwdriver pins, can be seen in Figure5-9. They are made up of Aluminum, which is satisfactorily good at sound reflectivity.

Figure5-8 Target Region

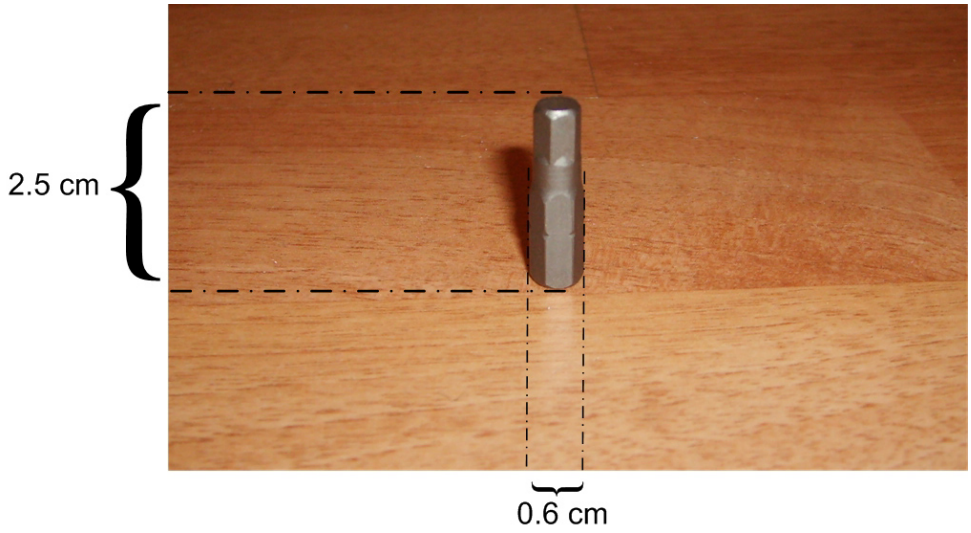

Figure5-9 Used Objects

Magnitude plot of measured baseband SAR signal for above target region is shown Figure5-10. The theoretical expression for this baseband echoed signal can be found using expression (2.50) and (2.52) as;

$$s_b(t,u) = \sum_n \sigma_n \exp\left(j\omega_0(t-t_n) - j\alpha(t-t_n)^2\right)\exp\left(-j\omega_c t_n\right).$$

The x-axis in the graph represents the fast time t in seconds while y-axis represents the slow time u in meters.

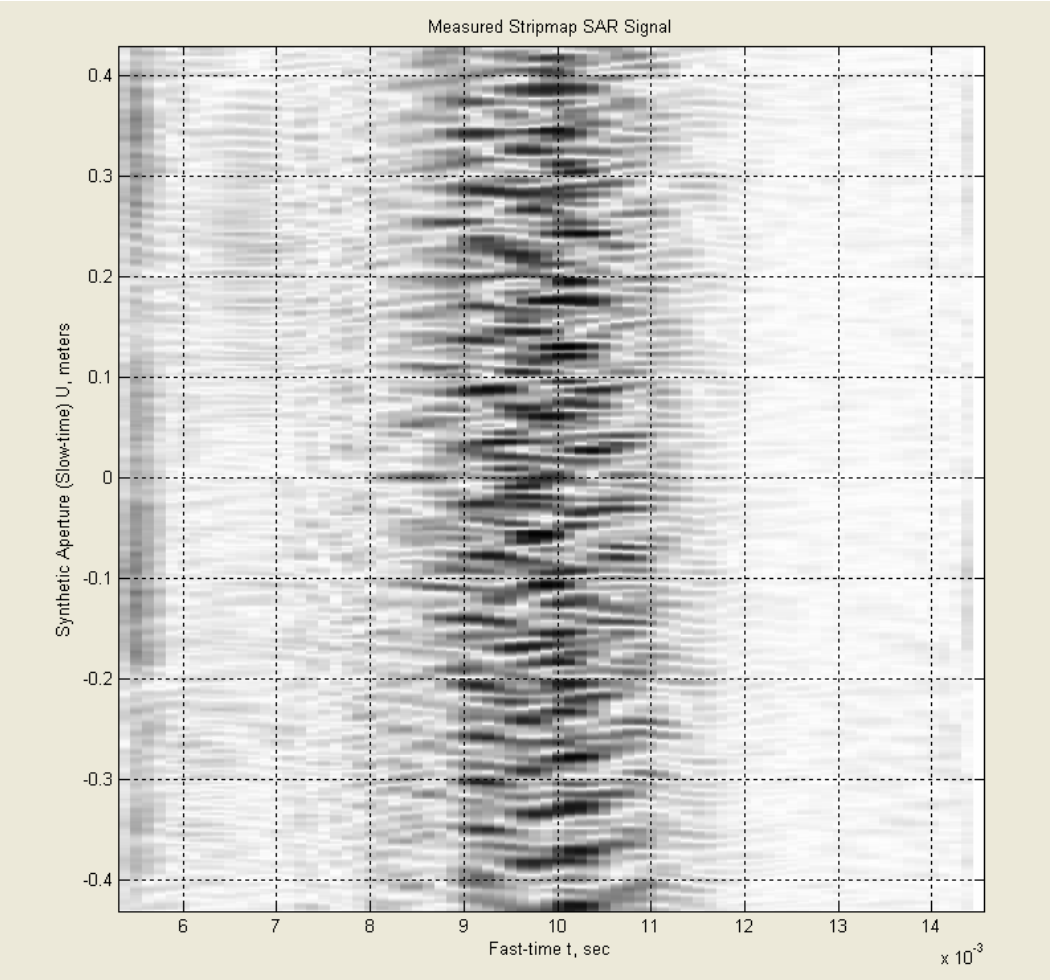

Figure5-10 Measured Baseband SAR Signal

Next step is the fast time matched filtering process of the baseband echoed signal. The theoretical expression for matched filtered baseband echoed signal can be obtained from (2.21), (2.57) and (2.63) as:

$$s_m(t,u) = \sum_n \sigma_n psf\left(t - \left(t_n(u) - t_c\right)\right)\exp\left(-j\omega_c\left(t_n(u) - t_c\right)\right).$$

The magnitude plot of the obtained result from the experimental setup is shown in Figure5-11.

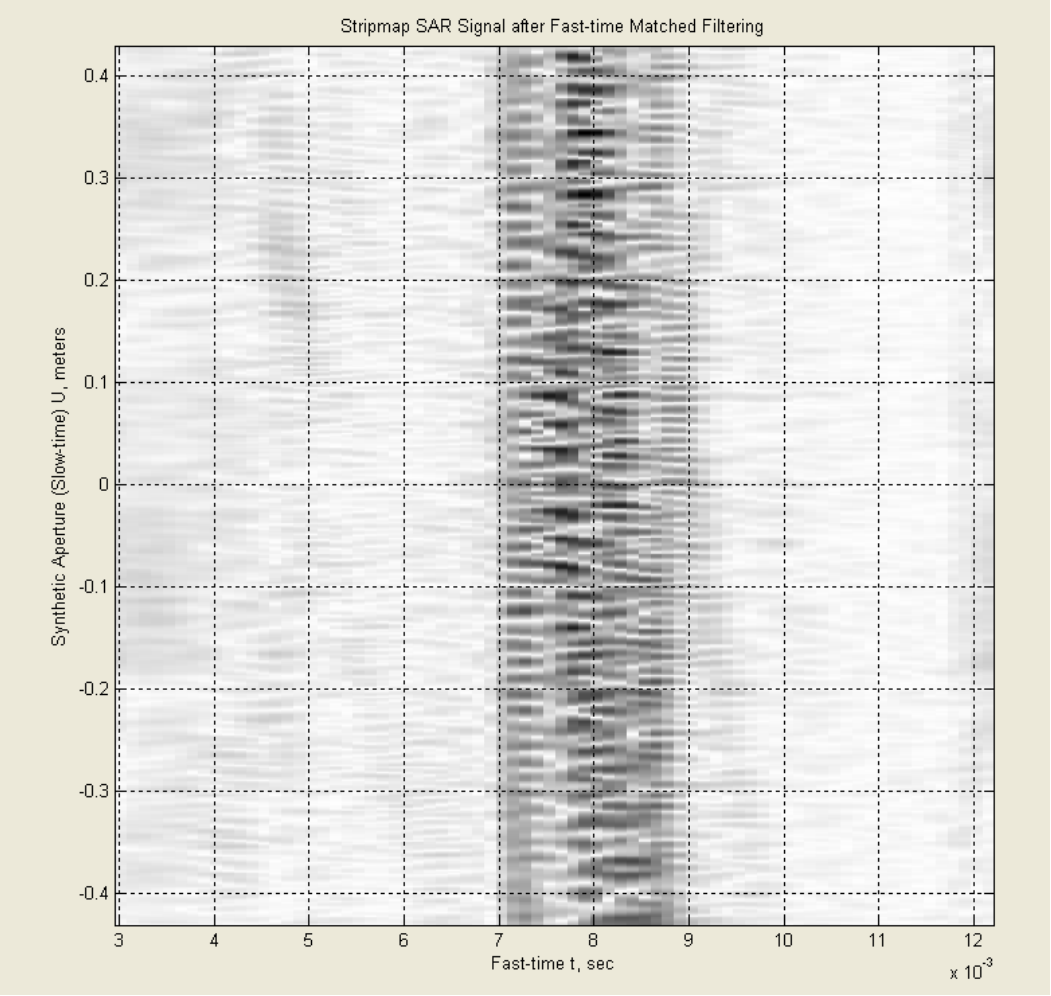

Figure5-11 Fast-time Matched Filtered SAR Signal

Fast time matched filtered SAR signal can be digital spotlighted to concentrate on a limited region. If digital spotlighting technique is applied to the signal, (t,u) domain SAR signal will be as in Figure5-12. The echo from outside of the target region is filtered by using digital spotlighting filter in the (t,k_u) domain.

Corresponding (ω,k_u) domain digital spotlighted SAR signal spectrum is shown in Figure5-13. Carrier frequency centered spectrum is shown rather than baseband spectrum to see the effects of analog filters and ultrasound transmitter/receiver. Theoretically we expect to see an f_c=40 kHz centered signal at ω coordinate axis.

The reason we see most of the power below carrier is caused by the overall effect of the shifted center frequency of used analog filters and ultrasound transceivers.

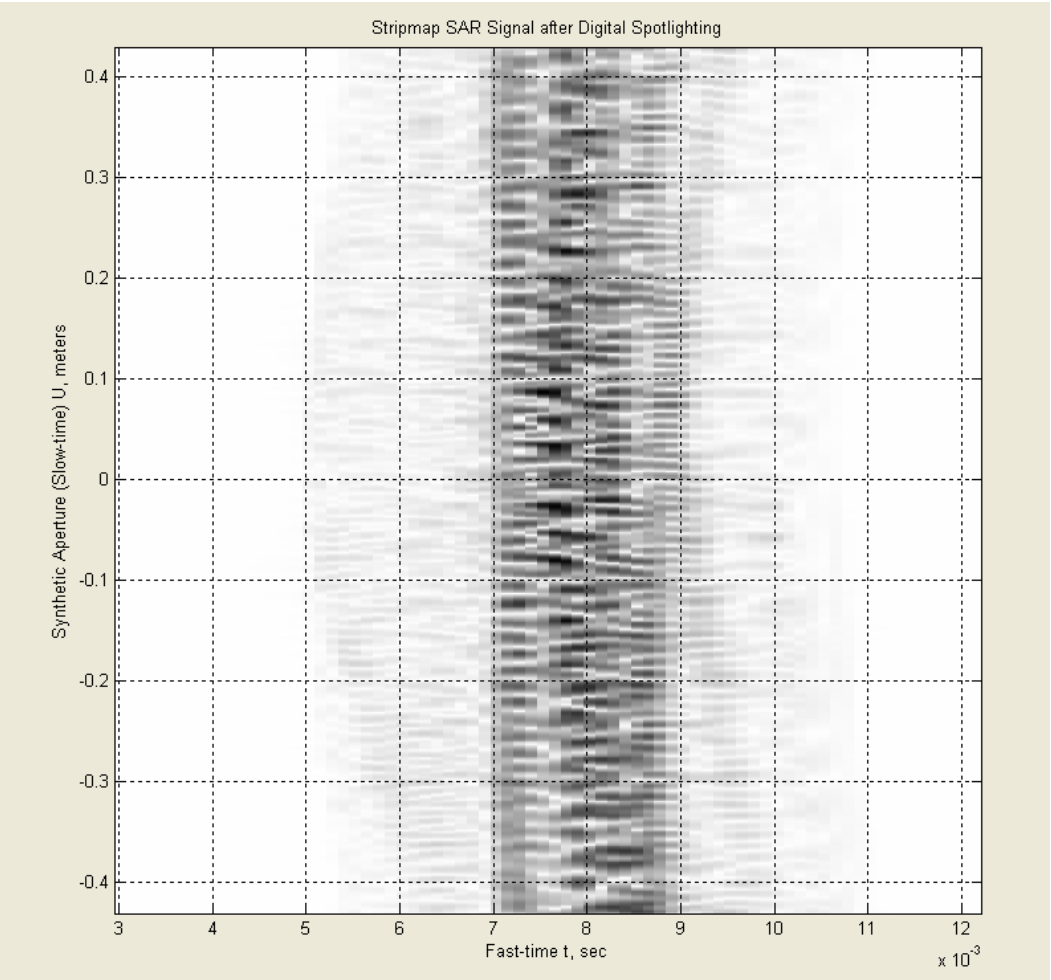

Figure5-12 Digital Spotlighted SAR Signal

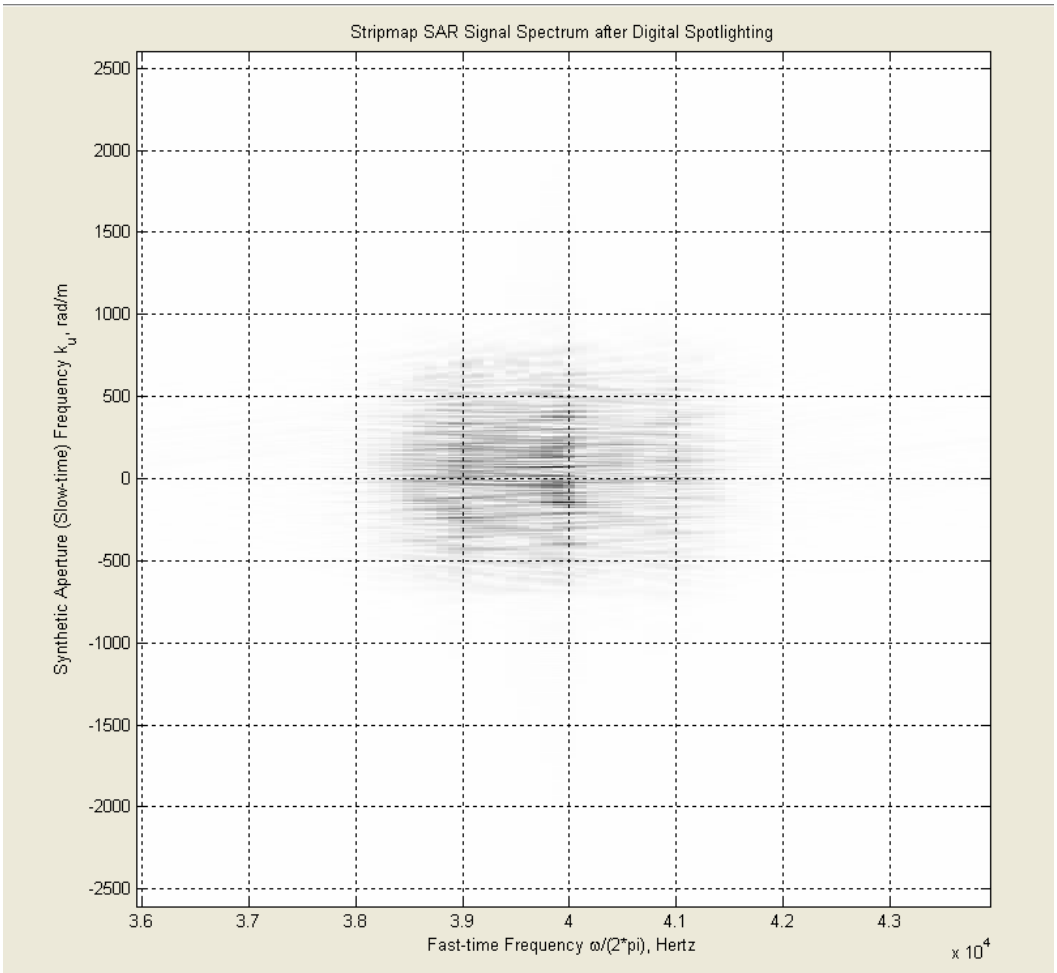

Figure5-13 Digital Spotlighted SAR Signal Spectrum

In Figure5-14 to Figure5-21, final target reflectivity functions obtained by using different algorithms with or without digital spotlighting the target area are shown. The theoretical expression for target reflectivity function $f(x,y)$ is repeated below:

$$F_{SM}\left(k_x(\omega,k_u),k_y(\omega,k_u)\right)=\left|P_b(\omega)\right|^2\sum_n \sigma_n I_n(\omega,k_y)\exp\left(-jk_x x_{sn}-jk_y y_n\right)$$

$$f(x,y)=F_{k_x,k_y}^{-1}\left\{F_{SM}\left(k_x(\omega,k_u),k_y(\omega,k_u)\right)\right\}$$

$$= B_x B_y \sum_n \sigma_n \operatorname{sinc}\left(\frac{1}{2\pi} B_x (x - x_{sn})\right) \operatorname{sinc}\left(\frac{1}{2\pi} B_y (y - y_n)\right)$$

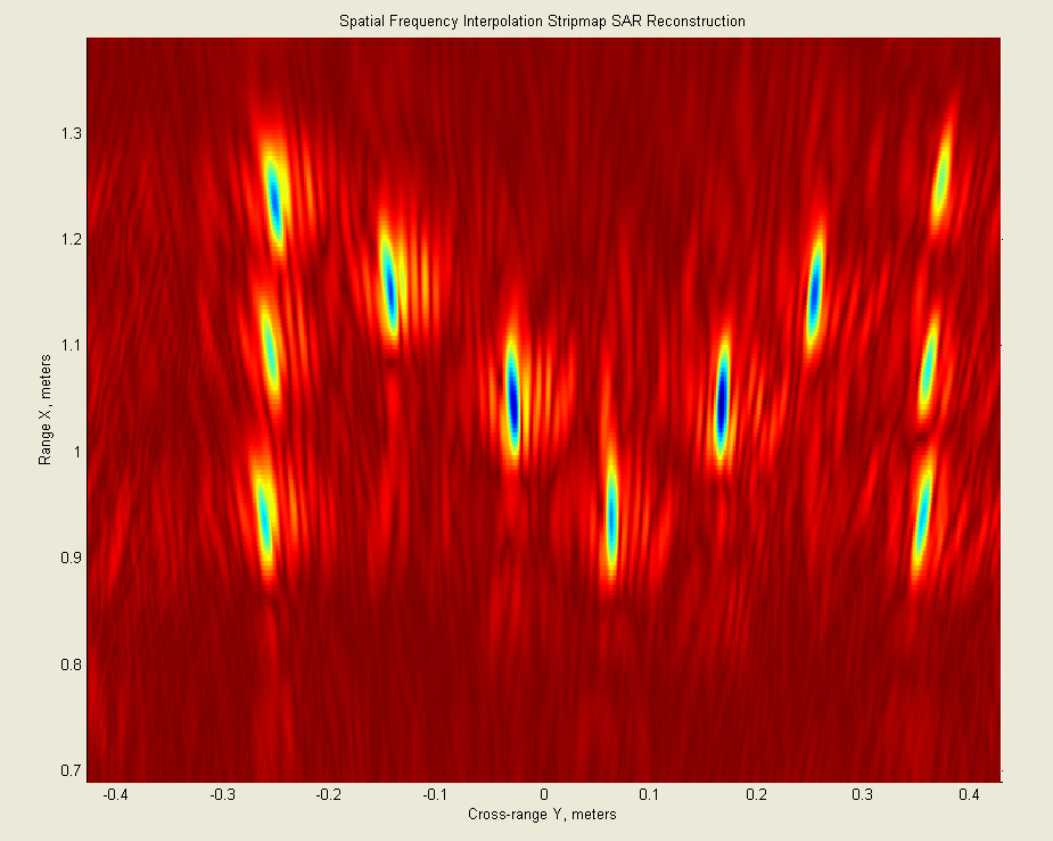

Figure5-14 Spatial Frequency Interpolation Stripmap SAR Reconstruction (Digitally Spotlighted)

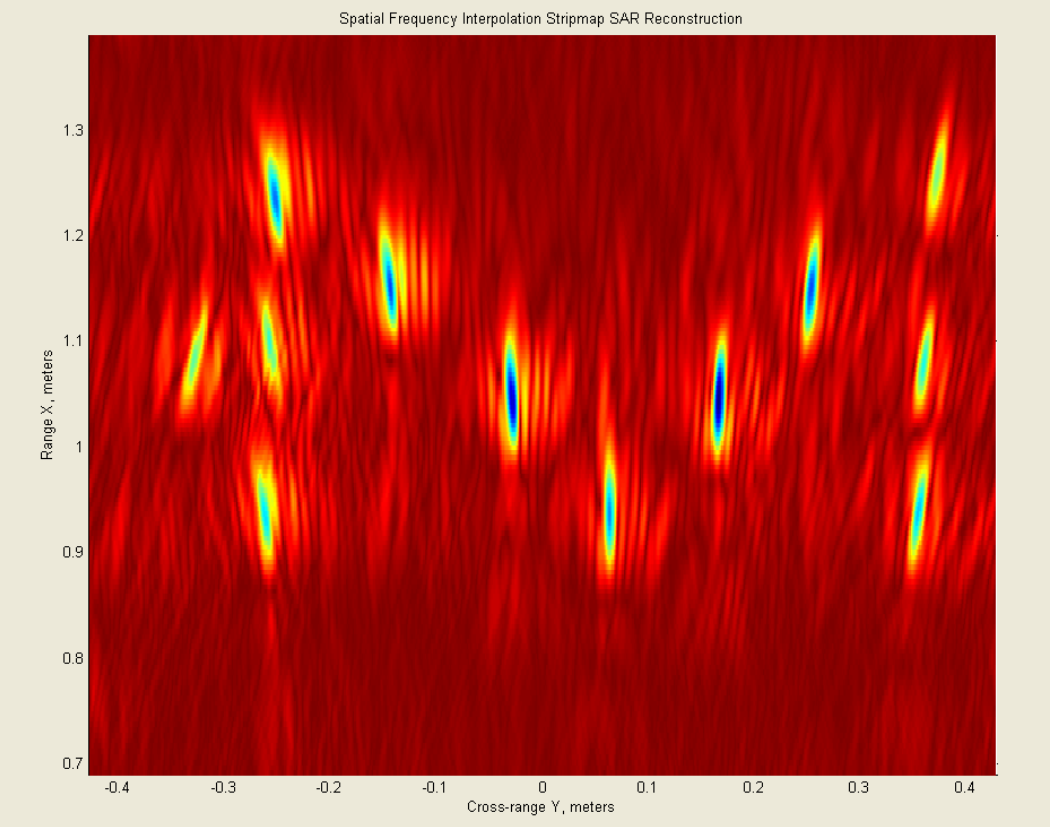

Figure5-15 Spatial Frequency Interpolation Stripmap SAR Reconstruction (No Digital Spotlight Filter)

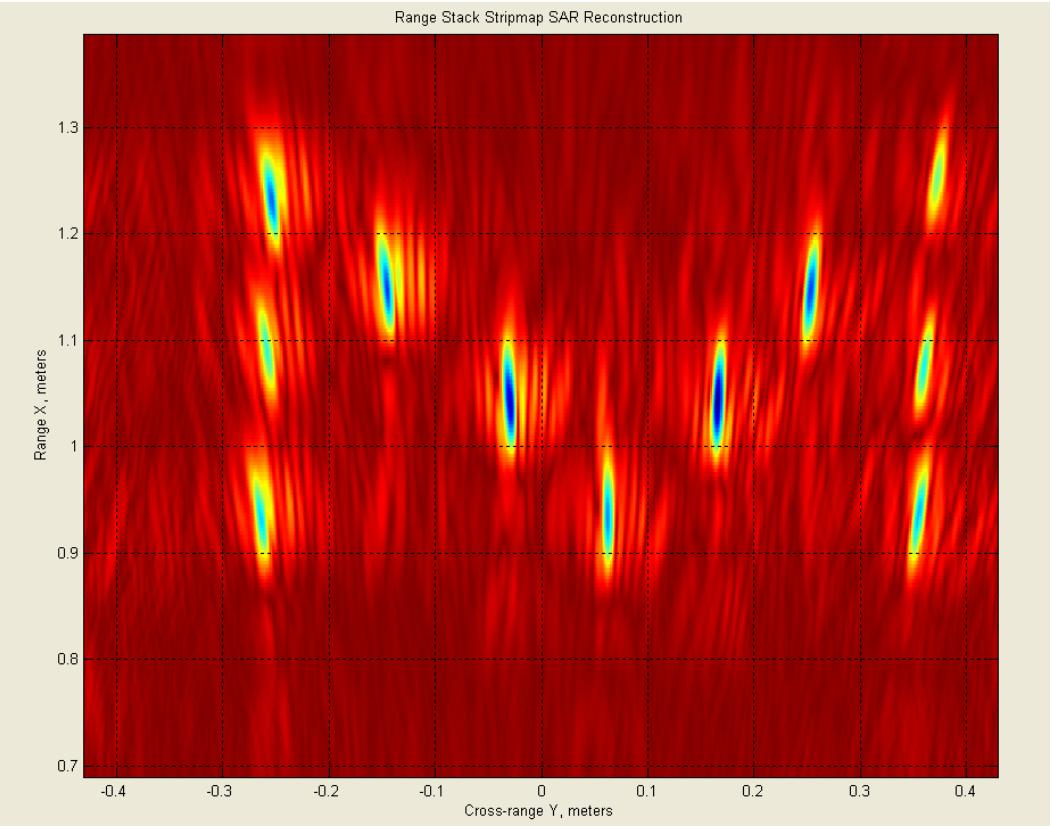

Figure5-16 Range Stacking Stripmap SAR Reconstruction (Digitally Spotlighted)

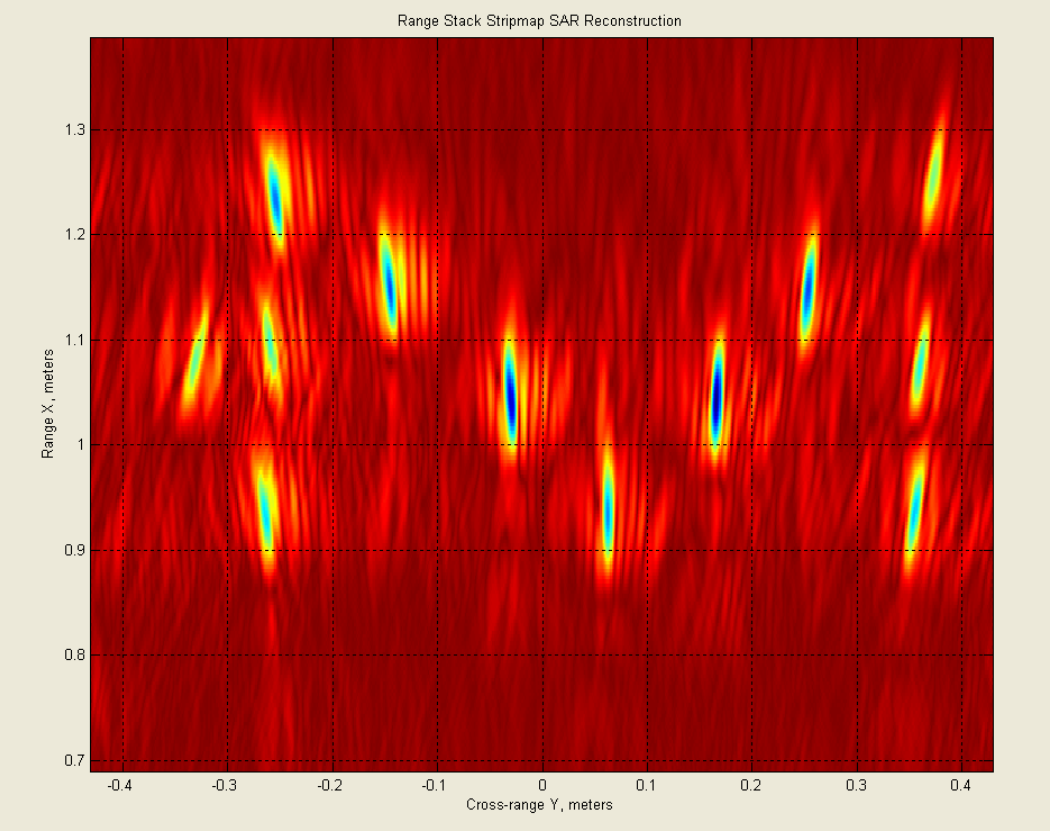

Figure5-17 Range Stacking Stripmap SAR Reconstruction (No Digital Spotlight Filter)

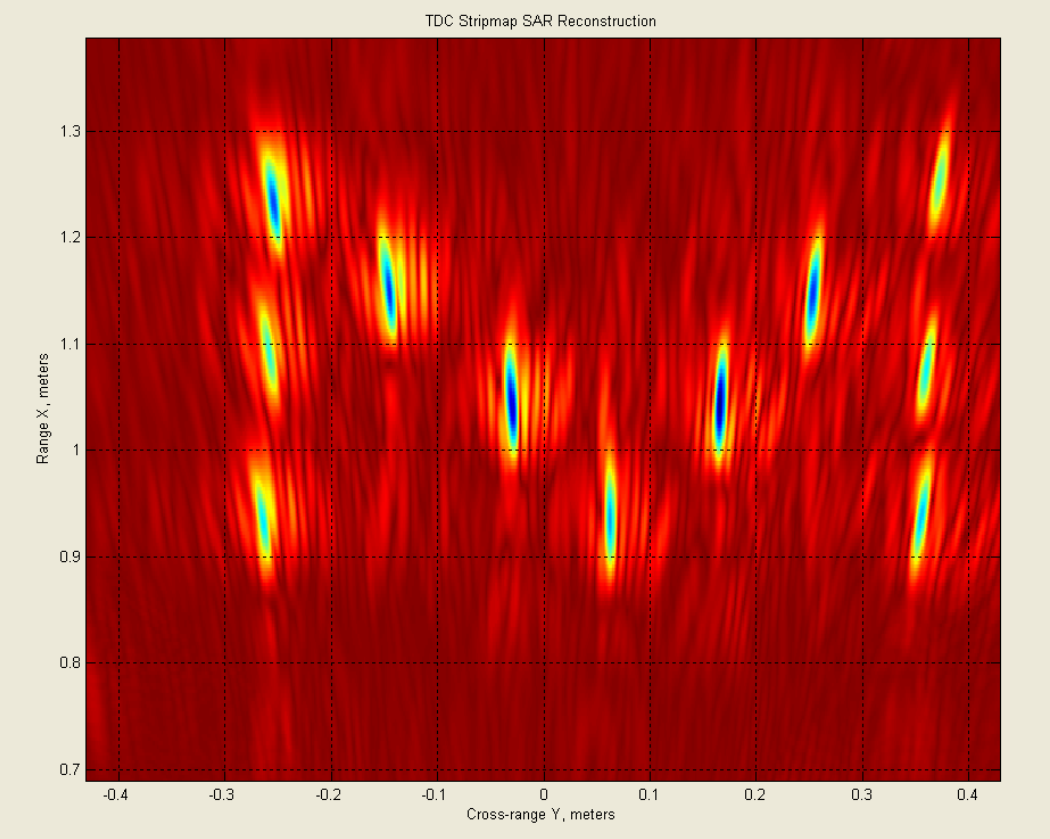

Figure5-18 Time Domain Correlation Stripmap SAR Reconstruction (Digitally Spotlighted)

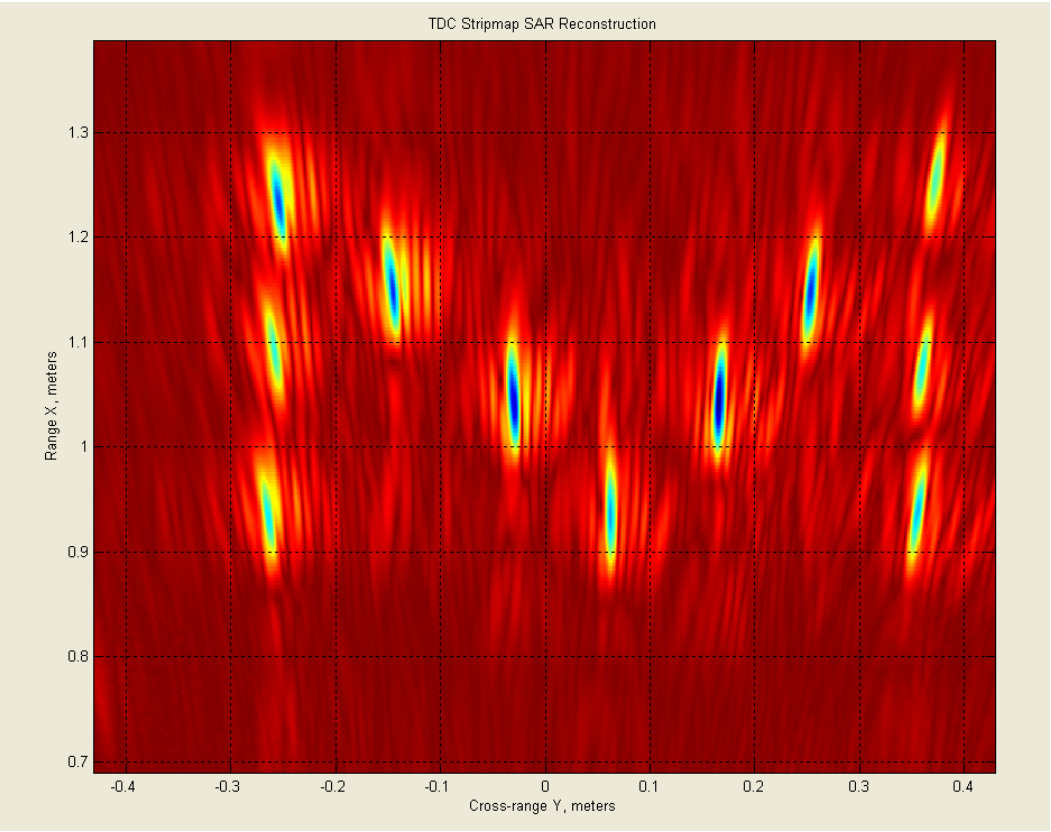

Figure5-19 Time Domain Correlation Stripmap SAR Reconstruction (No Digital Spotlight Filter)

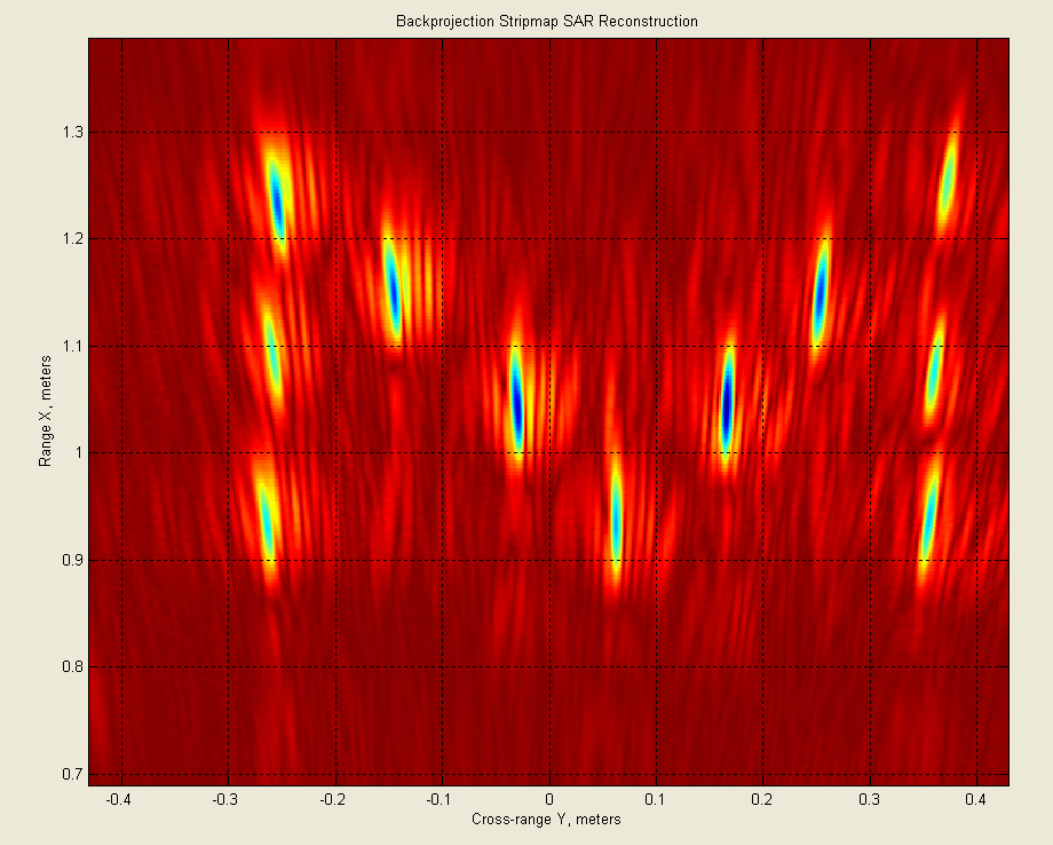

Figure5-20 Backprojection Stripmap SAR Reconstruction (Digitally Spotlighted)

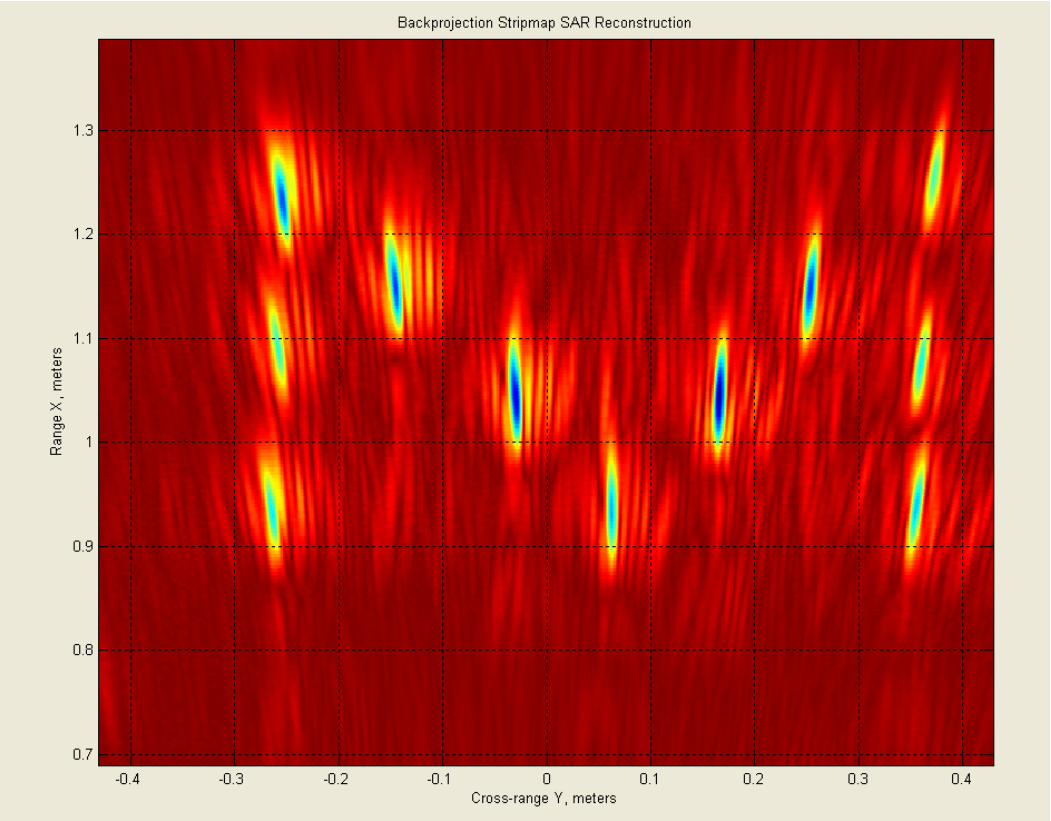

Figure5-21 Backprojection Stripmap SAR Reconstruction (No Digital Spotlight Filter)

Comments on Target Reflectivity Function

If Digitally Spotlighting Filter is used, it can be seen from the plots (Figure5-14, Figure5-16, Figure5-18, Figure5-20) that target reflectivity functions for all used reconstruction algorithms are very similar to each other. This is an expected result in the sense that all used algorithms utilize SAR Wavefront Reconstruction [10] method which is outlined in Chapter 2. SAR Wavefront Reconstruction theory does not put limitations on the target size, frequency and range.

Spatial Frequency Interpolation algorithm requires a sufficiently accurate interpolator to map (ω, k_u) domain into (k_x, k_y) domain. The assumptions to make

the interpolation step easier (e.g. $|k_u << k|$, $2\omega_0 < \omega_c \Rightarrow k_x \approx 2k$) or using inaccurate interpolators result degradations in the target reflectivity function.

Range Stacking algorithm has an ability to form the target reflectivity function at individual range bins x_i. At the end, the target reflectivity values for range bin x_i's are joined together to form the overall reflectivity of the target area. Dependent on the used interpolator in Spatial Frequency Interpolation, Range Stacking algorithm can be more time consuming as in this case. Range Stacking algorithm does not require interpolation so no truncation errors are expected.

Time Domain Correlation algorithm forms the target reflectivity function at individual (x_i, y_j) coordinates. The Fourier domain representation (expression 3.4.3) of TDC algorithm is used in the software. This method is similar to (ω, k_u) domain range stacking reconstruction method mentioned before. But TDC is a very time consuming way of reconstruction.

Backprojection algorithm reaches the same result in time domain. Backprojection method forms the target reflectivity function at individual (x_i, y_j) coordinates like TDC. This method also requires $t_{ij}(u)$ (expression 3.4.2) instants of the matched filtered signal, which can be obtained by interpolation. As in the Spatial Frequency Interpolation algorithm, the success of Backprojection algorithm depends on the accuracy of the interpolation process.

If no Digital Spotlighting Filter is used, the effect of right hand side positioned target seen in Figure5-8 can be seen in the final reconstructed image.

In Figure5-15 and Figure5-17 the reflectivity function of the target region when no digital spotlighting filter is used is shown for Spatial Frequency Interpolation and Range Stacking algorithms. The right hand side target outside the target region seen in Figure5-8 shifts $2Y_0$ left and falls inside the target region in the final

reflectivity scene. This fact can be understood by looking over the reconstruction equation of range stacking with the addition of this extra target. It is stated before (expression 3.4) that:

$$f(x_i, y) = \iint_{k_u\,\omega} F_{SM}(\omega, k_u)\exp\left(jk_x(\omega, k_u)x_{si} + jk_u y\right)d\omega dk_u$$

$$F_{SM}\left(k_x(\omega, k_u), k_y(\omega, k_u)\right) = \left|P_b(\omega)\right|^2 \sum_n \sigma_n I_n(\omega, k_y)\exp\left(-jk_x x_{sn} - jk_y y_n\right)$$

Hence;

$$f(x_i, y) = \iint_{k_u\,\omega} \left|P_b(\omega)\right|^2 \sum_n \sigma_n I_n(\omega, k_u)\exp\left(-jk_x(\omega, k_u)x_{sn} - jk_u y_n\right) \exp\left(jk_x(\omega, k_u)x_{si} + jk_u y\right)d\omega dk_u \quad (5.1)$$

Rewrite (5.1) as;

$$f(x_i, y) = \iint_{k_u\,\omega} \left|P_b(\omega)\right|^2 \sum_n \sigma_n I_n(\omega, k_u)\exp\left(jk_x(\omega, k_u)(x_{si} - x_{sn})\right) \exp\left(jk_u(y - y_n)\right)d\omega dk_u . \quad (5.2)$$

Let us suppose that the target region includes no targets within the interval $x \in [\ X_c - X_0,\ X_c + X_0\ ]$, $y \in [\ -Y_0,\ Y_0\ ]$. The only target is located at $(x_k, y_k + 2Y_0)$ which is the coordinate of the right hand side target outside the region seen in Figure5-8.

Then expression (5.2) becomes,

$$f(x_i, y) = \iint_{k_u\,\omega} \left|P_b(\omega)\right|^2 \sigma_k I_k(\omega, k_u)\exp\left(jk_x(\omega, k_u)(x_{si} - x_{sk})\right) \exp\left(jk_u(y - y_k)\exp\left(-jk_u(2Y_0)\right)\right)d\omega dk_u . \quad (5.3)$$

Sample spacing of SAR signal in slow time (u) domain is;

$$\Delta k_u = \frac{2\pi}{2Y_0} \quad , \qquad (Y_0 = L) .$$

$$k_u = h\,.\,\Delta k_u \quad , \qquad (\text{h is an integer constant changing from } -\frac{m}{2} \text{ to } \frac{m}{2})$$

m is the number of positions that radar makes data transmissions.

Hence,

$$\exp\left(-jk_u(2Y_0)\right)=\exp\left(-jh.\Delta k_u(2Y_0)\right)=\exp\left(-jh2\pi\right)=1 \tag{5.4}$$

From expression (5.3) and (5.4) the following is obtained,

$$f(x_i,y)=\iint_{k_u\,\omega}\left|P_b(\omega)\right|^2\sigma_k I_k(\omega,k_u)\exp\left(jk_x(\omega,k_u)(x_{si}-x_{sk})\right)$$
$$\exp\left(jk_u(y-y_k)\right)d\omega dk_u . \tag{5.5}$$

Expression (5.5) verifies the obtained target reflectivity image shown in Figure5-15 and Figure5-17. The target outside the scene comes across to $2Y_0$ left and is seen as an inside object with new coordinates of (x_k,y_k). This means that all the reflections from the outside objects which pass the time gate will be seen inside the target region in the final reconstructed image if no digital spotlighting filter is used.

A useful precaution to restrict the distance between radar position and cross-range bin y_j on which corresponding image point will be constructed can be used with Time Domain Correlation and Backprojection algorithms.

If we reconsider expression (3.12):

$$f(x_i,y_j)=\int_u\int_\omega s_b(\omega,u)P_b^*(\omega)\exp(j\omega t_{ij}(u))d\omega du$$

The integration should be calculated for u values that satisfy:

$$\left|y_j-u\right|\le BWD,\qquad BWD=x_{si}\tan(\varphi_d) \tag{5.6}$$

The condition given by (5.6) prevents the targets outside the region to be seen inside the target area in the final reconstructed image. This restriction is also valid for Backprojection algorithm. Therefore the reflectivity functions seen in Figure5-

19 and Figure5-21 do not contain signatures from targets outside the region although they don't utilize spotlight filter.

Target Reflectivity Function Spectrum

In Figure5-22, (k_x,k_y) domain spectrum of reconstruction function is shown.

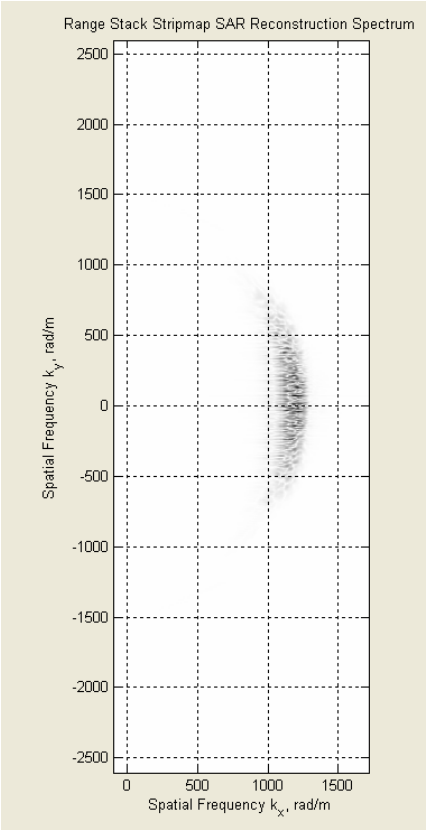

Figure5-22 Range Stacking Reconstruction Spectrum

If the spectrum of Figure5-22 is compared to Figure2-11 which shows theoretical spectral support in (k_x,k_y) domain, it will be seen that obtained spectrum is similar to the theoretical one and the assumption for beam angle is valid ($\varphi_d = \pi/6$).

5.4 FINAL DISPLAY

The graphical user interface designed for SAR processing also includes a method to find the center of mass of the targets from the reflectivity function and to clean the image from noisy background. By using second or third power of the reflectivity function and thresholding the output image, the final display shown in Figure5-23 is obtained. The software can find the exact position of the targets using center of mass of those completely separated target signatures seen in the image. While center of mass is being found, the coordinates obtained from Figure5-23 is used as a mask in the original reflectivity function.

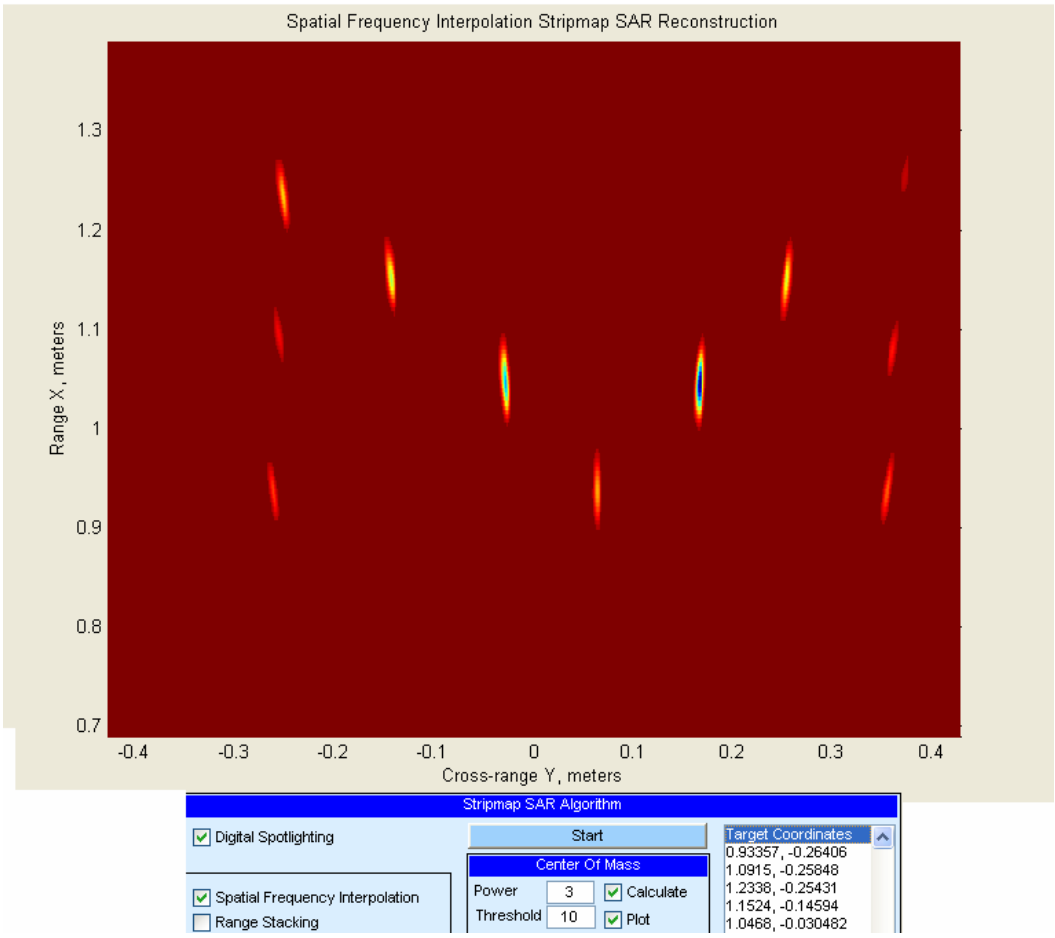

Figure5-23 Final Reflectivity

Spatial Frequency Interpolation Stripmap SAR Reconstruction using Digital Spotlight Filter (Figure5-14) and the actual target region (Figure5-8) are shown together in Figure5-24 to give an idea about the relative accuracy of the founded coordinate values using SAR setup. The center of mass of the signature of the 6th target in the reconstructed target region coincides with the actual position of the same target and this point is taken to be as the (0,0) point of the (x,y) spatial coordinate system. Note that the vertical line in the figure is the range domain (x-axis) while the horizontal line is the cross-range domain (y-axis).

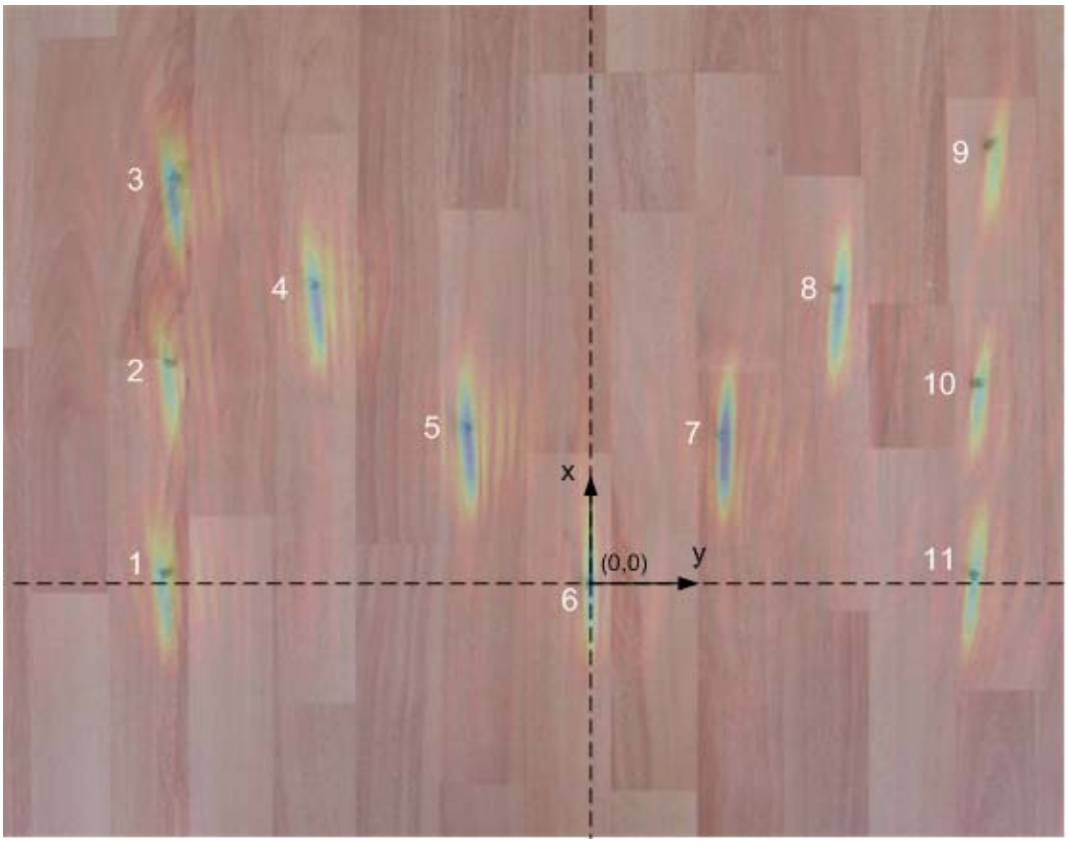

Figure5-24 Obtained Target Reflectivity Function and Actual Target Region with 11 Targets

The center of mass of the target signatures (obtained coordinate) and the actual locations of the targets are given in Table5-1.

Table5-1 Actual and Obtained Coordinates of the Targets

Target No.	Actual Range (x) (cm)	Obtained Range (x) (cm)	Actual Cross-Range (y) (cm)	Obtained Cross-Range (y) (cm)
1	0,85	-0,17	-32,12	-32,66
2	16,68	15,62	-31,70	-32,1
3	30,74	29,85	-31,31	-31,68
4	22,63	21,71	-20,86	-20,84
5	11,79	11,15	-9,37	-9,3
6	0	0	0	0
7	11,26	10,76	10,30	10,37
8	22,36	21,07	18,98	19,09
9	33,31	31,76	30,47	31,02
10	15,18	14,09	29,66	29,75
11	0,69	0,16	29,28	29,25

It seems that the obtained results for y-axis are very close to the actual locations while results for x-axis deviate. The reconstructed target area is distorted more for distant range points.

5.5 RESOLUTION

Range and cross range resolution of targets are examined in order to compare with the theoretical values. The algorithms in this work do not differ in the resolution

because they all used the same principle which is known as Wavefront Reconstruction.

Range and Cross-Range Resolution

Theoretical values for range and cross-range resolution are found before as $\Delta_x = 5.3cm,\ \ \Delta_y = 4.3mm$ for 4 kHz bandwidth signal.

The practical resolutions for x and y axis are found by taking the distance between the central maximum and first local minimum which is shown in Figure5-25.

$\Delta_{x\_practical} = 7.35cm,\ \ \Delta_{y\_practical} = 9.2mm$

For y-axis resolution; the target used in this study having a 0.6cm width is expected to form a $2\Delta_y +$ target width = $1.46\,cm$ signature. Therefore y-axis resolution can be revised to be equal to;

$$\Delta_{y\_practical} = \frac{1.84cm - 0.6cm}{2} = 6.2mm\,.$$

Similarly for x-axis resolution;

$$\Delta_{x\_practical} = \frac{14.7cm - 0.6cm}{2} = 7.05cm\,.$$

The practical resolution is approximately 33% worse than the theoretical resolution for range (x) axis and 45% worse than the theoretical resolution for cross-range (y) axis. Most important reason of this result is because of the assumption made in Multidimensional SAR Problem section. The shaded region in Figure2-11 showing the spectral support of the SAR signal in (k_x, k_y) domain is assumed to be a perfect rectangle while inverse Fourier transform of the same signal is assumed to be a perfect sinc function which is not valid in real case.

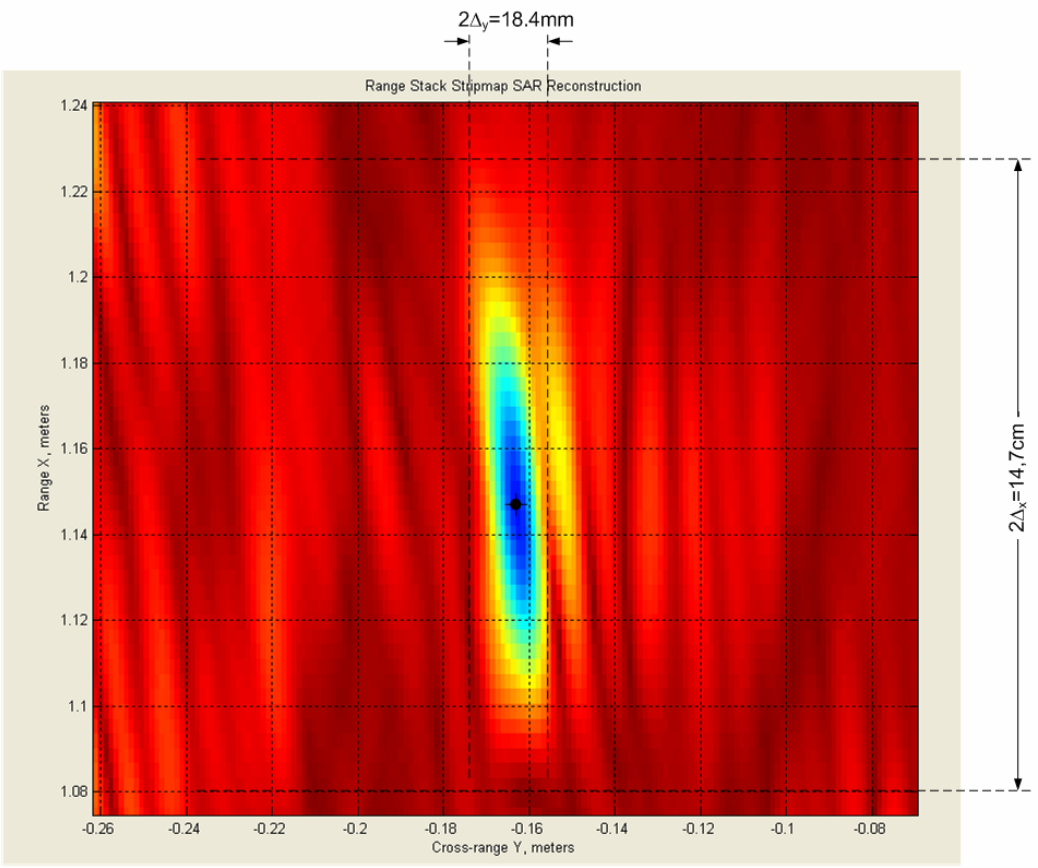

Figure5-25 Practical Resolution Values (4 kHz bandwidth chirp is used)

Following figures are output of some resolution experiments to find the minimum required interval to observe separated target signatures.

Cross-Range (Y) Resolution experiments are shown in Figure5-26 and Figure5-27. In Figure5-26, two groups of targets are placed in the target area. Each group is composed of two targets. Right group has an interval of 1cm between the centers of two targets. This means the space between two targets is 1-0.3-0.3=0.4 cm. It is seen that 0.4 cm-length-interval does not result separable target signatures in the scene. However, the left group of targets has 1.2 cm center distance which ensures to observe separable target signatures. The space between targets in the separable case is 1.2-0.3-0.3=0.6 cm.

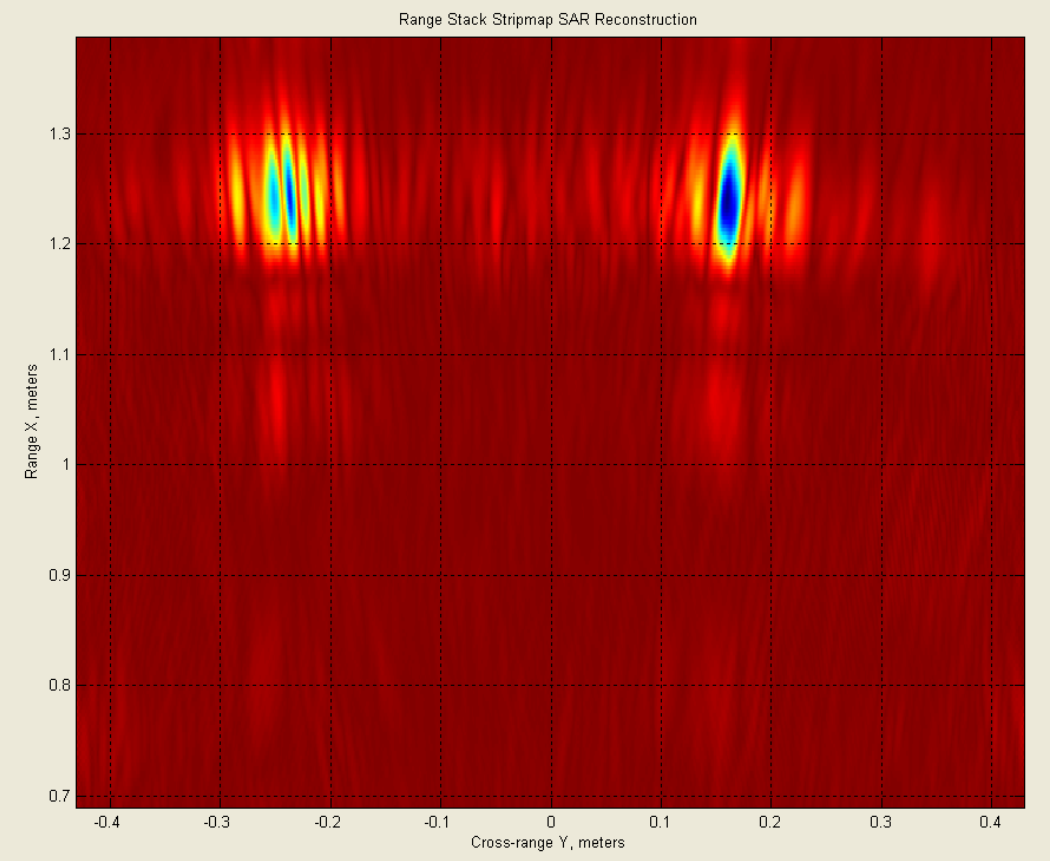

Figure5-26 Y-Resolution Experiment (1.2 cm and 1 cm center distance; 4 kHz bandwidth chirp is used)

The only difference of Figure5-27 from Figure5-26 is that the left group of targets is placed with 1.5 cm center distance which increases the separation of target signatures. In this case the length of the interval between targets is, 1.5cm-0.6cm=0.9cm.

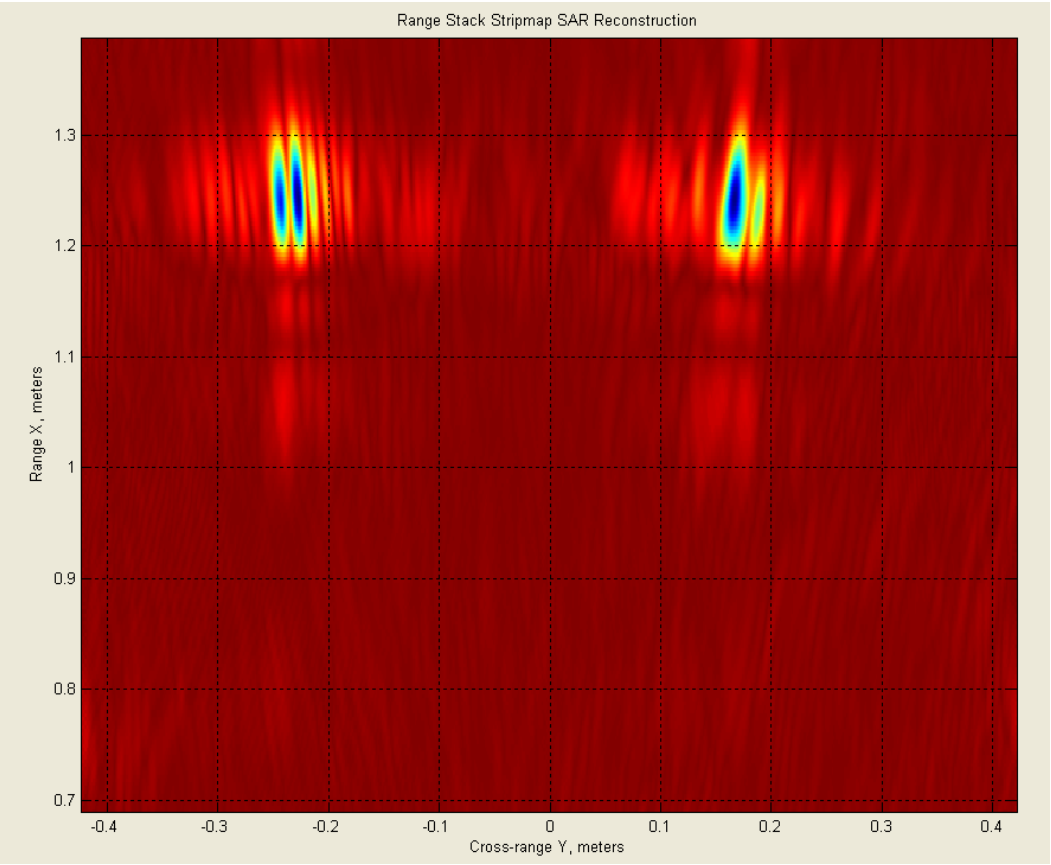

Figure5-27 Y-Resolution Experiment (1.5 cm and 1 cm center distance; 4 kHz bandwidth chirp is used)

Range (X) Resolution experiment is shown in Figure5-28. There are two groups of targets; each group is composed of two targets. The left separated group has a center distance of 10.5 cm while right one has 8 cm which is not enough to observe completely distinguishable target signatures.

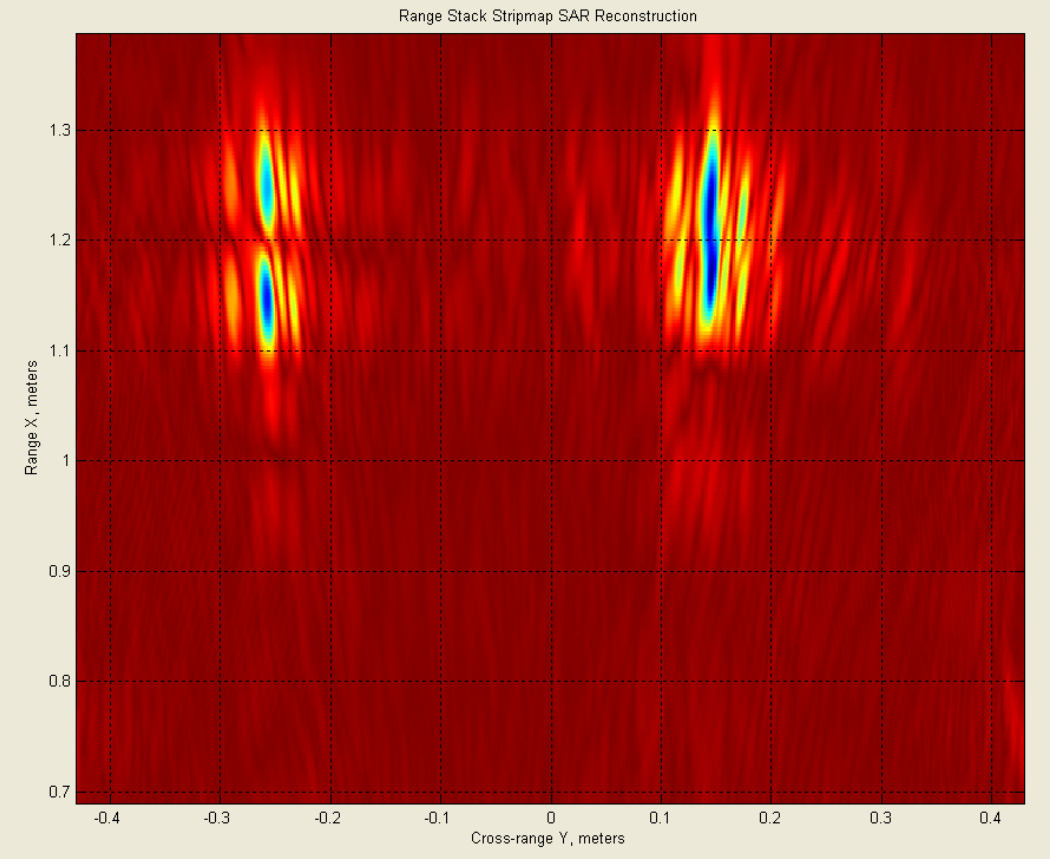

Figure5-28 X-Resolution Experiment (10.5 cm and 8 cm center distance; 4 kHz bandwidth chirp is used)

Effect of Bandwidth on the range resolution will be examined in the following experiment. The theoretical spatial resolution in x-axis is found before as (expression 2.79);

$$\Delta_x = \frac{\pi c \sqrt{X_c^2 + Z_s^2}}{2\omega_0 X_c}$$

where

$\omega_0 = 2\pi f_0$ and f_0 is the half-bandwidth of the transmitted chirp signal.

In Figure5-29, the resolution characteristics of SAR system is shown for a 2 kHz bandwidth transmitted signal (f_0=1 kHz). When this figure is compared with

Figure5-25, it can be easily seen that the resolution in x is worse than the resolution in Figure5-25 where a 4 kHz bandwidth signal is used. Therefore the resolution in x axis can be improved by increasing the bandwidth which is in accordance with the theoretical results.

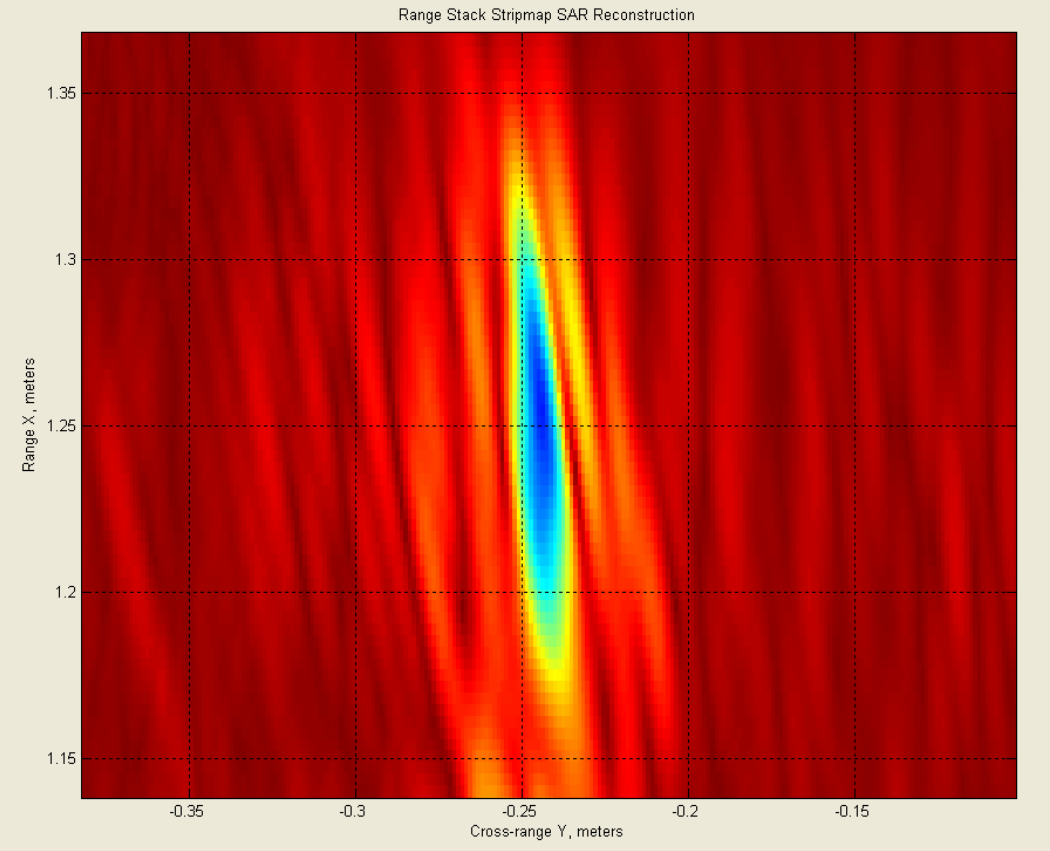

Figure5-29 X-Resolution Experiment (2 kHz bandwidth chirp is used)

CHAPTER 6

DISCUSSION AND CONCLUSION

Radar has been used for electronic observing since 1940s and ever since has experienced a considerable technical boost. Conventional radar is mainly used for both locating an object and measuring its distance and speed [14]. The progressing technical development over many years soon provided the opportunity to form planar images of Earth's surface using a Synthetic Aperture Radar located on an aircraft. Raw SAR data, which is composed of coherent echoed signals, is processed to reconstruct the planar image of the ground. Primary SAR researchers used some approximation based reconstruction algorithms to reduce the computational cost. But today using powerful digital computers and developed digital signal processing algorithms, the basic principles of SAR theory can be applied easily.

In this thesis, a low cost ultrasound experimental setup is designed to evaluate many SAR techniques in response to the necessity of an experimental platform for the performance test of the reconstruction algorithms. The reconstruction algorithms utilizing SAR Wavefront Reconstruction [10] method, namely Spatial Frequency Interpolation, Range Stacking, Time Domain Correlation and Backprojection, are implemented in the study. Spatial Frequency Interpolation, also known as omega-K algorithm [13], performs reconstruction using an accurate interpolator (Stolt Interpolation)[13]. The other three algorithms were developed in order to remove the requirement of mapping (ω,k_u) domain to (k_x,k_y) domain. Also Digital Spotlighting technique is implemented in order to

focus on the target area. The practical differences of the implemented algorithms are considered in terms of computational cost and the clarity of the reconstructed target area.

The clarity of the reconstructed target area is found to be similar for all reconstruction algorithms recommended at [1] as expected. This result verifies the implementation of these algorithms. The resolution values that we work in this study are not good enough to recognize the slight differences due to interpolation, upsampling, (inverse) discrete fourier transform, convolution, phase multiplication e.g. steps in the algorithms. But the computational complexities of the algorithms are different. The first algorithm, Spatial Frequency Interpolation, is the fastest one and gives satisfactorily good result when applied to the Digitally Spotlighted target region. Although it requires an accurate interpolator, the obtained result using Spatial Frequency Interpolation seems to be as good as Range Stacking Algorithm which does not need an interpolator. Time Domain Correlation and Backprojection algorithms are computationally very complex and do not promise any benefit for this system. These two algorithms have a property that they can find the reflectivity of a spatial grid located in the target region. Therefore when it is enough to image a restricted small area, we can make use of this property of Time Domain Correlation and Backprojection to obtain the result rapidly.

The design of the experimental SAR setup is based on two main assumptions. While the radar carrying platform moves, it is assumed that the vehicle stops, the data transmission and reception process are performed and the vehicle moves to the next transceiving position. This stop-and-go assumption simplifies the theory by allowing us to separate the Doppler processing from range processing. The second assumption comes from the theory. SAR imaging is based on a rectangularity approximation given in Figure2-11. The shaded are on the ring is approximated as a perfect rectangle which results a two dimensional sinc function in the spatial domain.

The error sources in the practical system causes distortions in the final reconstructed image. The varying speed of radar carrying platform is an error source. In theory the path of the radar is supposed to be linear while the speed of the platform is assumed to be fixed. In this application the nonuniform acceleration and deceleration of the vehicle leads to imperfect position determination which may result some deterioration in the final image. In Monostatic Stripmap SAR theory that this thesis work is based on, the receiver is assumed to be at approximately the same location as the transmitter. But in the experimental SAR setup, the transmitter is located at 3.5 cm from the receiver resulting slight deterioration in the final image. The analog filters and the narrowband ultrasound transmitter and receiver used in the setup generate phase distortions which certainly affect the SAR system response.

The practical resolution of the experimental SAR setup is found to be 33% worse in x-axis and 45% worse in y axis than the theoretical resolution due to both theoretical assumptions and practical approximations. The founded resolution values will vary according to the position of the target and the deviations in the speed of the vehicle during data acquisition.

The range and cross-range (azimuth) resolutions are found to be;

$$\Delta_x = \frac{\pi c}{2\omega_0}\frac{1}{\cos\alpha}, \qquad \Delta_y = \frac{\pi c}{2\omega_c \sin\varphi_d}.$$

Range resolution is inversely proportional to the bandwidth (ω_0) of the transmitted signal. In order to improve range resolution (decrease Δ_x), bandwidth of the transmitted signal should be increased. The narrow-band ultrasound transducers used in the setup should be replaced with wideband transducers which can work with larger bandwidth signals.

Cross-range resolution depends on the carrier frequency (ω_c) of the transmitted signal and the transducer beam-width (φ_d). It is possible to improve the cross-range resolution (decrease Δ_y) of the system by increasing the carrier frequency of the transmitted signal and increasing the beam-width of the transducers. Therefore the used transducers should be replaced with wider beam-width, higher center frequency valued ones in order to improve the cross-range resolution.

In this study many experiments were done using the designed experimental ultrasound SAR setup. The system was shown to be capable of reconstructing the target area with a satisfactorily good resolution. It can be used to examine the performance of many other reconstruction algorithms, or detect the route of the moving targets.

APPENDIX A

ADDITIONAL STEP FOR THE EXPERIMENTAL SAR SETUP

In our implementation, there is an up and down conversion operation in order to work with the ultrasound transducer. These operations require an additional step to apply the SAR theory given Section 2.2. This additional step is explained in this appendix.

Multidimensional SAR theory discussed in Section 2.2 requires the baseband received signal spectrum to be in the form of (expression 2.54),

$$S_b(\omega,u) = P(\omega+\omega_c)\sum_n \sigma_n \exp\left(-j(\omega+\omega_c)t_n\right)$$

where

$P(\omega+\omega_c)$ is the baseband transmitted signal spectrum.

In time domain,

$p(t) = a(t)\exp(j\beta t + j\alpha t^2)$,

where $a(t) = 1$ for $0 \le t \le T_p$ and zero otherwise,

$\omega_c = \beta + \omega_0$ and $\omega_0 = \alpha T_p$.

The values of the parameters are,

$\omega_c = 2\pi f_c$, $\omega_0 = 2\pi f_0$,

$f_c = 40k\ Hz$, $f_0 = 2k\ Hz$, $T_p = 3m\sec$.

In real application, we only use real (in-phase) signals. Also the SAR setup analog circuitry contains a pure sinusoid (50 kHz) which should be taken into consideration in the calculations. In real application, the data transmission and reception is performed using the analog module. The data transmission and reception structure is given in Figure7-1.

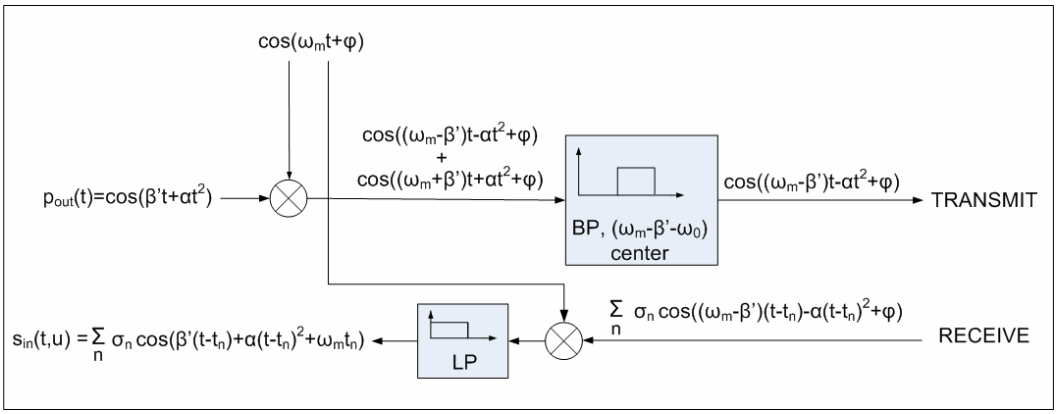

Figure7-1 Data Transceiving Structure

The transmitted signal created in PC is;

$$p_{out}(t) = \cos\left(\beta' t + \alpha t^2\right) \tag{7.1}$$

where

$$\beta' = \omega_c' - \omega_0, \tag{7.2}$$

and

$\omega_c' = 2\pi f_c'$, $f_c' = 10kHz$.

This relatively low frequency signal with center frequency of f_c' is up-converted to the system frequency f_c before transmitting to the target region.

The received echo from the target region comes into the PC analog front end after being down-converted to f_c' centered signal given below,

$$s_{in}(t,u) = \sum_n \sigma_n \cos\left(\beta'(t-t_n) + \alpha(t-t_n)^2 + \omega_m t_n\right), \tag{7.3}$$

where

$\omega_m = 2\pi f_m$, $f_m = 50kHz$.

The following assumptions are made to write expression (7.3):

- The analog filters have no impact on the frequency characteristics of the signal.
- Transmitter and receiver have no impact on the frequency characteristics of the signal.

$p_{out}(t)$ and $s_{in}(t,u)$ are real signals having $-$10kHz and +10kHz centered spectral supports on Fourier domain. We will choose one side of the support (e.g. take $-$10kHz component) and transform into baseband.

Therefore using the negative frequency support, $-$10kHz, the filtered signals are defined as;

$$p_{out\_f}(t) = \exp\left(-j\beta' t - j\alpha t^2\right) \tag{7.4}$$

$$s_{in\_f}(t,u) = \sum_n \sigma_n \exp\left(-j\beta'(t-t_n) - j\alpha(t-t_n)^2 - j\omega_m t_n\right) \tag{7.5}$$

The subscript '_f' stands to distinguish one sided filtered signals to the recorded real signals.

If we translate the signal in expression 7.5 into baseband;

$$\begin{aligned} s_{in\_f\_b}(t,u) &= s_{in\_f}(t,u)\exp(j\omega_c' t) \\ &= \sum_n \sigma_n \exp\left(-j\beta'(t-t_n) - j\alpha(t-t_n)^2 - j\omega_m t_n + j\omega_c' t\right) \\ &= \sum_n \sigma_n \exp\left(j\omega_0(t-t_n) - j\alpha(t-t_n)^2\right)\exp\left(-j(\omega_m - \omega_c')t_n\right) \\ &= \sum_n \sigma_n \exp\left(j\omega_0(t-t_n) - j\alpha(t-t_n)^2\right)\exp\left(-j\omega_c t_n\right) \end{aligned} \tag{7.6}$$

where $\omega_c' = \beta' + \omega_0 = \omega_m - \omega_c$. (7.7)

If $s_{in\_f\_b}(t,u)$ is expressed in terms of $p_{out\_f}(t)$ using (7.4) and (7.6), then;

$$s_{in\_f\_b}(t,u) = \sum_n \sigma_n p_{out\_f}(t) \exp\left(j\omega_0 (t - t_n) - j\alpha (t - t_n)^2\right) \exp(-j\omega_c t_n) . \quad (7.8)$$

Fast time Fourier domain representation of $s_{in\_f\_b}(t,u)$ in terms of $P_{out\_f}(\omega)$ is;

$$S_{in\_f\_b}(\omega,u) = F_t\left\{s_{in\_f\_b}(t,u)\right\} = \sum_n \sigma_n P_{out\_f}(\omega - \omega_c') \exp(-j(\omega + \omega_c) t_n) \quad (7.9)$$

Define a different transmitted signal using $p_{out\_f}(t)$ as;

$$p_e(t) = p_{out\_f}(t) \exp(j\omega_m t) . \quad (7.10)$$

The defined signal is represented in the Fourier domain as;

$$P_e(\omega) = P_{out\_f}(\omega - \omega_m) . \quad (7.11)$$

One sided filtered baseband received signal $S_{in\_f\_b}(\omega,u)$ given in expression (7.9) can be written using expression (7.7) and (7.11) in terms of $P_e(\omega)$ as given in the following;

$$\begin{aligned} S_{in\_f\_b}(\omega,u) &= \sum_n \sigma_n P_e(\omega + \omega_m - \omega_c') \exp(-j(\omega + \omega_c) t_n) \\ &= P_e(\omega + \omega_c) \sum_n \sigma_n \exp(-j(\omega + \omega_c) t_n) . \end{aligned} \quad (7.12)$$

Finally, similar expression to equation (2.54) for baseband received signal spectrum is obtained. Hence using one side of the spectrum of recorded real signals and defining a different transmitted signal $p_e(t)$, the designed experimental setup can be used in SAR applications. PC side of Data Transceiving Structure given in Figure7-1 is shown in Figure7-2.

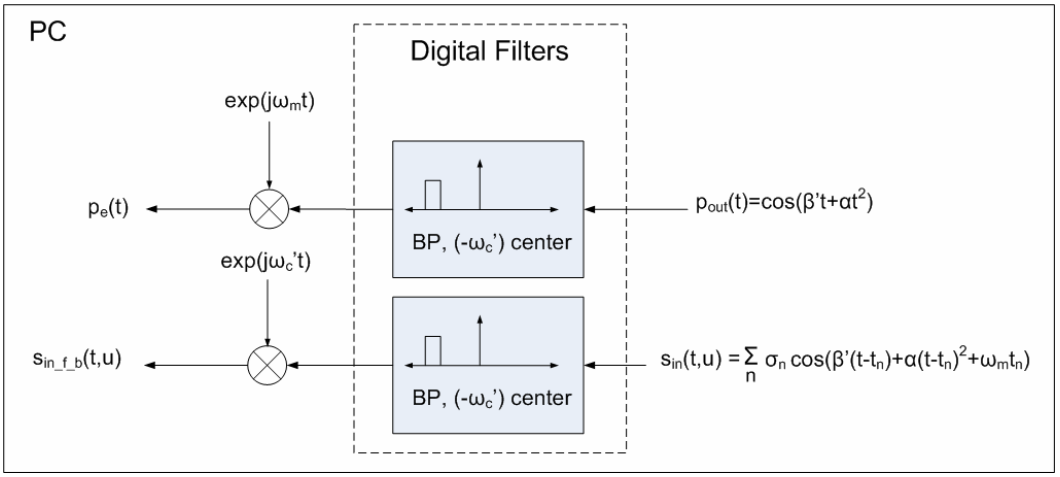

Figure7-2 Digital Signal Process in PC to Adapt the Output of the Analog Module to the Theory

REFERENCES

1. M. Soumekh, "Synthetic Aperture Radar Signal Processing with MATLAB Algorithms", John Wiley & Sons, 1999.

2. F. Vincent, B. Mouton, E. Chaumette, C. Nouals, O. Besson, "Synthetic Aperture Radar Demonstration Kit For Signal Processing Education", IEEE International Conference on Volume 3, Issue, 15-20 April 2007 pp. III-709 - III-712

3. J. C. Curlander, R. N. McDonough, "Synthetic Aperture Radar: Systems and Signal Processing", JohnWiley & Sons, 1991.

4. Microbric, "The Viper Manual v1.3", October 2005.

5. Prowave Electronic Corp, "Air Ultrasonic Ceramic Transducers 400ST/R160 Datasheet"

6. D. Gabor, "A new microscope principle," Nature, 161:777, 1948

7. E. Leith and J. Upatnieks, "Reconstructed wavefronts and communication theory," J. Optical Soc. Am., 52: 1123-1130, 1962.

8. E. Leith and J. Upatnieks, "Wavefront reconstruct with diffused illumination and three dimensional objects, theory," J. Optical Soc. Am., 54: 1295-1301, 1964.

9. M. Soumekh, "Band-limited interpolation from unevenly spaced sampled data," IEEE Trans. Acoust. Speech Signal Process., 36: 110-122, 1988

10. J. Goodman, Introduction to Fourier Optics, New York: McGraw-Hill, 1968

11. M. Soumekh, "Fourier Array Imaging, Englewood Cliffs, NJ:Printice Hall, 1994.

12. Bassem R. Mahafza, "Radar System Analysis and Design Using MATLAB" Chapman and Hall/CRC, 2000

13. Ian G. Cumming, Frank H. Wong, "Digital Processing of Synthetic Aperture Radar Data" Artech House, 2005

14. A. Hein, "Processing of SAR Data, Fundamentals, Signal Processing, Interferometry" Springer, 2003

15. James D. Taylor, “Introduction to Ultra-Wideband Radar Systems” CRC Press, 1994